University of Kentucky
UKnowledge

Theses and Dissertations--Pharmacy College of Pharmacy

2023

Self-Assembled Ternary Polypeptide Nanoparticles With Improved Biostability For Drug Delivery In Cancer Therapy

Preye Mike Agbana
University of Kentucky, preye.agbana@gmail.com
Author ORCID Identifier:
https://orcid.org/0000-0002-9303-1740
Digital Object Identifier: https://doi.org/10.13023/etd.2023.211

Right click to open a feedback form in a new tab to let us know how this document benefits you.

Recommended Citation

Agbana, Preye Mike, "Self-Assembled Ternary Polypeptide Nanoparticles With Improved Biostability For Drug Delivery In Cancer Therapy" (2023). *Theses and Dissertations--Pharmacy*. 145.
https://uknowledge.uky.edu/pharmacy_etds/145

This Doctoral Dissertation is brought to you for free and open access by the College of Pharmacy at UKnowledge. It has been accepted for inclusion in Theses and Dissertations--Pharmacy by an authorized administrator of UKnowledge. For more information, please contact UKnowledge@lsv.uky.edu.

STUDENT AGREEMENT:

I represent that my thesis or dissertation and abstract are my original work. Proper attribution has been given to all outside sources. I understand that I am solely responsible for obtaining any needed copyright permissions. I have obtained needed written permission statement(s) from the owner(s) of each third-party copyrighted matter to be included in my work, allowing electronic distribution (if such use is not permitted by the fair use doctrine) which will be submitted to UKnowledge as Additional File.

I hereby grant to The University of Kentucky and its agents the irrevocable, non-exclusive, and royalty-free license to archive and make accessible my work in whole or in part in all forms of media, now or hereafter known. I agree that the document mentioned above may be made available immediately for worldwide access unless an embargo applies.

I retain all other ownership rights to the copyright of my work. I also retain the right to use in future works (such as articles or books) all or part of my work. I understand that I am free to register the copyright to my work.

REVIEW, APPROVAL AND ACCEPTANCE

The document mentioned above has been reviewed and accepted by the student's advisor, on behalf of the advisory committee, and by the Director of Graduate Studies (DGS), on behalf of the program; we verify that this is the final, approved version of the student's thesis including all changes required by the advisory committee. The undersigned agree to abide by the statements above.

Preye Mike Agbana, Student

Dr. Younsoo Bae, Major Professor

Dr. David Feola, Director of Graduate Studies

SELF-ASSEMBLED TERNARY POLYPEPTIDE NANOPARTICLES WITH IMPROVED BIOSTABILITY FOR DRUG DELIVERY IN CANCER THERAPY

DISSERTATION

A dissertation submitted in partial fulfillment of the
requirements for the degree of Doctor of Philosophy in the
College of Pharmacy
at the University of Kentucky

By
Preye Mike Agbana
Lexington, Kentucky
Director: Dr. Younsoo Bae, Associate Professor of Pharmaceutical Sciences
Lexington, Kentucky
2023

Copyright © Preye Mike Agbana 2023
[https://orcid.org/0000-0002-9303-1740]

ABSTRACT OF DISSERTATION

SELF-ASSEMBLED TERNARY POLYPEPTIDE NANOPARTICLES WITH IMPROVED BIOSTABILITY FOR DRUG DELIVERY IN CANCER THERAPY

Cancer remains a real and present threat to global health. In the United States, according to cancer statistics, almost 40% of people will be diagnosed with cancer at some point in their lifetime. Conventional chemotherapy has become the mainstay for cancer treatment option. However, chemotherapeutic agents are plagued with problems such as poor aqueous solubility, chemical degradation, Bio instability, and off-site toxicity due to non-specificity. New drug modalities are needed to tackle the ever-growing burden on cancer. In recent times, the promise of nanotechnology has aided to develop drug delivery vehicles to facilitate the administration of potent chemotherapeutics. Nanoformulations such as liposomes and polymeric micelles have been previously developed to tackle these pharmaceutical limitations, however, these modalities have inherently low drug loading, uncontrolled release and particle instability that ultimately produce sub-par outcomes. This work hypothesizes that the design of novel nanoparticles with attention paid to particle stability and controlled release will improve the performance of potent drugs.

To this end, this work showcases the design and optimization of a novel self-assembled ternary polypeptide nanoparticle. For this study, we used a model drug carfilzomib (CFZ) already approved by the Food and Drug Association (FDA). Carfilzomib (CFZ) is a tetrapeptide epoxyketone proteasome inhibitor approved by the FDA for treatment of relapsed/refractory multiple myeloma (MM). Although it has been successful in treating patients with MM, CFZ has shown limited efficacy against solid tumors in the clinic. One pharmaceutical limitation of CFZ is its poor aqueous solubility. Additionally, CFZ is prone to peptide degradation and epoxyketone ring opening. Clinical limitations include low half-life, rapid clearance and poor targetability. To address these limitations, self-assembled ternary polypeptide nanoparticles (tPNPs) was designed comprising Heptakis(6-amino-6-deoxy)-βCD-heptahydrochloride (HaβCD) and Azido-poly (ethylene glycol)-block-poly (L-glutamic acid sodium salt) (N3-PEG-PLE). CFZ is

entrapped within the core of HaβCD which then ionically interacts with N3-PEG-PLE to form CFZ/tPNPs. For further optimization, small molecule organic acids and polycations were used to enhance particle stability and controlled release. For targeted delivery of CFZ, epithelial cell adhesion molecule (EpCAM) antibody was conjugated to N3-PEG-PLE before drug loading to form (CFZ/EpCAM-tPNPs).

All formulations (tPNPs, CFZ/tPNPs and CFZ/EpCAM-tPNPs) showed a uniform particle size of ~ 50 nm. Addition of cryoprotectants ensured the stability of these formulations after freeze drying. CFZ/tPNPs were also able to achieve high drug loading (>1 mg/mL). These formulations were tested in vitro in DLD-1 CFZ resistant cells. The EpCAM-tPNPs had significantly better cellular uptake than tPNPs and the control. CFZ/tPNPs better sustained proteasome inhibition compared to free CFZ. The optimized formulation prepared with polycation stabilization also showed better proteasome suppression than free CFZ. Finally, CFZ/tPNPs and CFZ/EpCAM-tPNPs showed a greater cytotoxicity against DLD-1 CFZ resistant cells than free CFZ. These results suggest that CFZ/tPNPs and CFZ/EpCAM-tPNPs could be potentially useful for improving the efficacy of CFZ in solid tumors, hence, expanding its clinical utility.

Biodistribution studies show particle accumulation in tumor as well as peripheral organs. This potentiates the development of different tumor models to better assess particle effect and treatment outcomes.

Taken together, this thesis provides the basis for the development and optimization of a novel nanoparticle to tackle some of the limitations of current chemotherapy. It also paves the way for further exploration to expand our knowledge of the effect of such formulation modalities on in vivo systems.

KEYWORDS: Ternary Polypeptide Nanoparticles, Carfilzomib, Drug delivery, Cyclodextrin, Complexation, Targeting.

Preye Mike Agbana

(Name of Student)

4/26/2023

Date

SELF-ASSEMBLED TERNARY POLYPEPTIDE NANOPARTICLES WITH IMPROVED BIOSTABILITY FOR DRUG DELIVERY IN CANCER THERAPY

By
Preye Mike Agbana

Dr. Younsoo Bae
Director of Dissertation

Dr. David Feola
Director of Graduate Studies

4/26/2023
Date

DEDICATION

To God my father, Jesus Christ my savior and the Holy Spirit, my comforter and advocate, I give all the glory for the gift of salvation, the unconditional love, and the strength to persevere through the difficulties of life. I dedicate this work to my wife, Miranda Agbana, thank you for being my support and constant source of joy and encouragement throughout this Journey. Your love for me inspires me every day. And to the rest of my family, I could not have made it this far without you. Thank you. A special thank you, to my parents, Comrade Mike Agbana and Mrs. Timi Agbana. You have always believed in me and pushed me to be the best I can. Thank you.

ACKNOWLEDGMENTS

I would like to express my appreciation to my mentor and advisor, Dr. Younsoo Bae. His dedication to my well-being and growth was evident from my first day in the lab in August 2018. Under Dr. Bae's tutelage, I learned facts I would not have known otherwise, I acquired skills that would propel me, and I gained enthusiasm for our subject matter. Dr. Bae instilled in me the importance of the right philosophy in the pursuit of a doctorate. I have learned so much from Dr. Bae about how to be a scientist. My successes would not be if not for the guidance, support, and encouragement of Dr. Bae, and for that I want to relay my sincerest gratitude.

My graduate committee members each played significant roles in my graduate story. Dr. Piotr Rychahou trained me in mastering animal work. His knowledge and experience helped me to create experimental design with the mindset of producing efficient and biologically useful formulations. Outside of the details of lab work, Dr. Rychahou was beyond supportive of my endeavors. He encouraged me to persevere through the difficult moments. Secondly, I would like to express my gratitude to Dr. Kyung-Bo Kim. Most of my collaborative work was done with Dr. Kim. He is a cheerful and optimistic scientist that taught me to have a positive outlook. Dr. Kim fostered in me the desire to learn about the mechanisms of drug action in cells and how that can be used in drug development. I am grateful for Dr. Kim's influence on my interest in learning beyond the scope of my lab bench. Finally, I would like to thank Dr. Dan Pack whose expertise in drug and gene formulation was key in my design of formulation. I was also fortunate to have learned in class from Dr. Pack. Especially during the initial lockdowns of the COVID-19 pandemic,

Dr. Pack was gracious and kind in making himself available to teach but also was cognizant of the new struggles of at home learning for students. My committee members are my heroes of science that I aspire to be like.

During my time at the College of Pharmacy, I have been fortunate to have wonderful lab mates. My first lab mate was Sharonda Jackson. We worked very closely in developing and advancing projects. It was also a breath a fresh air to have someone else to bounce ideas off. I would like to thank Kaysi M. Lee, my other lab mate. She brought cheer and a smile to work every day. I am grateful that our paths crossed. Other past graduate students and postdocs were also influential in my journey. Dr. Min Jae Lee a graduate student at the time taught me how to perform a lot of the in vitro assays in this dissertation. Dr. Ji Eun Park also worked with me in formulation testing. Dr. Park's patience and kindness with me was the boost I needed to see this journey to this end. Thank you to all the students and colleagues that I have had meaningful conversations about my projects and science in general.

I would be remiss to not mention the valuable support I received from other members of the College of Pharmacy and our graduate support teams. Catina Rossoll is the engine that propels our program forward. I am so thankful for Catina's guidance, she made sure I was on track with due dates and deadlines. Catina understands the plight of the graduate student and she looked out for me. Thank you, Catina, for answering all the questions I had and helping me to be successful as a graduate student. One of my first encounters as a graduate student was with Kristi Moore. I could tell immediately the care she took in her work. Her thoroughness was contagious for me as I grew into my own. Kristi helped me to learn safe practices. I was especially thrilled about our lab safety

successes, and it would not have been possible without Kristi. My first teaching assistant supervisor was Dr. Trenika Mitchell. I had no previous experience being a TA, but Dr. Mitchell took me under wings and gave me the confidence to help other students. Dr. Mitchell has always looked out for me and checked up on me through the difficulties of the COVID-19 pandemic and even the challenges of being different, and for that I say thank you. I am also grateful for the support from Chris Porter, our IT specialist at the College of Pharmacy. Chris is ever present and willing to help. Thank you, Chris, for making my work go as smooth as possible. Finally, I want to recognize the many members of the house keeping staff at the College of Pharmacy. Their work allows our work to go on unhindered, as such, I am grateful for their efforts.

Thank you to everyone too numerous to mention that has been a part of my journey. Through your support, prayer, thought and encouragement, I have walked this challenging and adventurous path. For that, you have my sincere gratitude.

TABLE OF CONTENTS

ACKNOWLEDGMENTS iii

LIST OF TABLES xi

LIST OF FIGURES xii

CHAPTER 1. Background 1

1.1 Cancer Treatment Using Chemotherapy 1

1.2 Nanotherapeutics as Alternative to Conventional Chemotherapy 2

1.3 Polypeptide Nanoparticles 3

1.4 Carfilzomib as a Model Drug for Polypeptide Nanoparticles 5

CHAPTER 2. Development of Ternary Polypeptide Nanoparticles 10

2.1 Introduction 10

2.2 Materials and Methods 14

2.2.1 Materials 14

2.2.2 Preparation of tPNPs 14

2.2.3 Particle size and surface charge measurement 19

2.2.4 Drug loading determination 19

2.2.5 Stability assessment of lyophilized tPNPs 19

2.2.6 Confirmation of particle integrity for tPNPs in the presence of serum proteins 20
2.2.7 Drug release study 20
2.2.8 Proteasome activity assessment 21
2.2.9 Cellular uptake of tPNPs 21
2.2.10 Cell viability 22
2.3 Results 23
2.3.1 Preparation of tPNPs 23
2.3.2 Stability of CFZ/tPNPs 27
2.3.3 Confirmation of particle integrity for tPNPs in serum-containing cell culture media 29
2.3.4 Drug release studies 31
2.3.5 Proteasome activity inhibition 34
2.3.6 Cellular uptake of tPNPs 36
2.3.7 Cell viability 39
2.4 Discussion 42
2.5 Conclusion 46
CHAPTER 3. Effects of organic acids on drug release from ternary polypeptide nanoparticles entrapping carfilzomib 47
3.1 Introduction 47
3.2 Materials and Methods 52
3.2.1 Materials 52

3.2.2 Nanoparticle preparation 52

3.2.3 Particle size measurement 53

3.2.4 Drug loading quantification 54

3.2.5 Effects of buffers on particle stability and drug release kinetics 55

3.3 Results 56

3.3.1 Preparation of CFZ/tPNPs using organic acids 56

3.3.2 Effect of buffers on particle stability 58

3.3.3 Drug loading quantification 58

3.3.4 Drug release 61

3.3.5 Effect of mixing ratio on drug remaining after 24 h post incubation 61

3.4 Discussion 66

3.5 Conclusion 70

CHAPTER 4. Carfilzomib-loaded ternary polypeptide nanoparticles stabilized by polycationic complexation 71

4.1 Introduction 71

4.2 Materials and Methods 75

4.2.1 Materials 75

4.2.2 Cell culture 75

4.2.3 Preparation of tPNPs 76

4.2.4 Particle size and zeta potential determination 76

4.2.5 Drug loading and encapsulation efficiency 77

4.2.6 Drug release confirmation 77

4.2.7 Cell viability determination 78

4.2.8 Proteasome activity assay 78

4.3 Results 80

4.3.1 Physiochemical characterization of tPNPs 80

4.3.2 Drug loading and entrapment efficiency 80

4.3.3 Drug release of CFZ from tPNPs 83

4.3.4 Cell viability 86

4.3.5 Proteasome activity 86

4.4 Discussion 90

4.5 Conclusions 94

CHAPTER 5. Biodistribution of ternary polypeptide nanoparticles using fluorescence imaging: A qualitative and quantitative method 95

5.1 Introduction 95

5.2 Materials and Methods 97

5.2.1 Materials 97

5.2.2 Preparation of fluorescent tPNPs 97

5.2.3 Subcutaneous tumor model development 98

5.2.4 In vivo and ex vivo imaging 99

5.3 Results 100

5.3.1 In vivo imaging 100

5.3.2 Ex vivo imaging 100

5.4 Discussion 108

5.5 Conclusions 110

CHAPTER 6. Summary and future direction 111

References 115

VITA 139

LIST OF TABLES

Table 2.1. Particle properties of tPNPs. Data is shown as Mean ± SD except polydispersity index (PDI). All drug loading shown in the last column were measured for freeze-dried formulations. 26

Table 2.2. Kinetic parameters for CFZ release from tPNPs in comparison to βCD. Values were determined by dynamic dialysis 33

Table 2.3. The half maximal inhibitory concentration (IC_{50}) values of CFZ, CFZ/tPNP, and CFZ/EpCAM-tPNP against CFZ-resistant DLD-1 colorectal cancer cells after 48, 72 and 96 h of treatment. 41

Table 3.1. Physiochemical properties of CFZ/tPNPs prepared by using different combinations of citric acid and lactic acid. 60

Table 3.2. Kinetic parameters for CFZ release from tPNPs with organic acids at various mixing ratios. 65

Table 4.1. Physiochemical properties of polyion stabilized tPNPs 82

Table 4.2. Kinetic parameters of polyion stabilized tPNPs at different pH values. 85

LIST OF FIGURES

Figure 1.1. Chemical structure of carfilzomib. 6

Figure 1.2. Mechanism of carfilzomib inhibition. The 26S proteasome consists of the 20S core and two 19S caps at either end. There are 7 subunits of the 20S core of which carfilzomib binds irreversibly toe the β5 chymotrypsin-like subunit leading to cell apoptosis. With permission from Chari A, Mazumder A, Jagannath S. Proteasome inhibition and its therapeutic potential in multiple myeloma. *Biologics*. 2010; 4:273-87.. 8

Figure 2.1. Structure and conformation of natural cyclodextrins. With permission from Gidwani B, Vyas A. A comprehensive review on cyclodextrin-based carriers for delivery of chemotherapeutic cytotoxic anticancer drugs. *BioMed research international*. 2015 Oct 25;2015. 12

Figure 2.2. Schematic for preparation of ternary polypeptide nanoparticles..... 17

Figure 2.3. [3+2] cycloaddition click chemistry reaction for the synthesis of fluorescent polymer used for preparation of fluorescently labelled ternary polypeptide nanoparticles. 18

Figure 2.4. Particle size distribution of (a) Empty tPNP, (b) CFZ/tPNP, and (c) CFZ/EpCAM-tPNP 24

Figure 2.5. SDS-PAGE to confirm the conjugation of EpCAM to N_3-PEG-PLE. Lane 1 shows molecular weight markers, lane 2 shows EpCAM antibody modified with alkyne, and lane 3 shows EpCAM conjugated to N_3-PEG-PLE by copper-catalyzed [3 + 2] cycloaddition reaction. 25

Figure 2.6. Particle size comparison among CFZ/tPNPs before and after freeze drying in the presence of cryoprotectants (*: p = 0.0275; **: p = 0.0028). 28

Figure 2.7. Confirmation of particle integrity for tPNPs incubated in cell culture media with 10% FBS at 37°C. βCD was used as a control. (*: p = 0.0014; **: p < 0.0001)..... 30

Figure 2.8. In vitro drug release curves of CFZ/tPNP and CFZ/βCD 32

Figure 2.9. Changes in proteasome activity of DLD-1/ABCB1 cells treated with free CFZ or CFZ/tPNPs for 6, 24, 48 and 72 h. The values from experiments in triplicate and normalized to untreated proteasome activity and presented as mean ± S.D. (*: p < 0.0001). 35

Figure 2.10. Cellular uptake of fluorescent tPNPs with and without EpCAM conjugation. Free dye (AFDye 647) was used as a control. 37

Figure 2.11. Quantitative analysis of fluorescence integrity for tPNPs internalizing in DLD-1 CFZ resistant cells. Results are as percentage relative to free dye fluorescence at 24 h. The area under the curve (AUC) was in order of FL-EpCAM-tPNP (3418) > FL-tPNP (2409) > AFDye 647 (1842). (*: p = 0.0032; **: p = 0.0063)..... 38

Figure 2.12. Effect of tPNPs on the viability of CFZ-resistant DLD-1 colorectal cell line compared to free CFZ after (a) 48 h (b) 72 h and (c) 96 h incubation..... 40

Figure 3.1. Solubility of βCD in solutions of hydroxy acids and HCL as a function of acid concentration. With permission from Fenyvesi E, Vikmon M, Szeman J, Redenti E, Delcanale M, Ventura P, Szejtli J. Interaction of hydroxy acids with β-cyclodextrin. *Journal of inclusion phenomena and macrocyclic chemistry*. 1999 Mar;33(3):339-44… 50

Figure 3.2. Preparation of organic acid stabilized tPNPs for improved particle stability and drug retention. 51

Figure 3.3. Particle size distribution of nanoparticles prepared using various combination of citric acid and lactic acid. 57

Figure 3.4. Particle stability in various buffers such as tris buffered saline (TBS), phosphate buffered saline (PBS), normal saline (NS) and citrate buffer (CB). 59

Figure 3.5. Drug release profiles for tPNPs with organic acids at various mixing ratios (enlarged view of inset for initial 6 h post incubation). 63

Figure 3.6. Drug entrapment assessment (% of CFZ remaining at t = 24 h) 64

Figure 4.1. Design of CFZ-loaded tPNPs stabilized by polyion complexation 74

Figure 4.2. Histogram showing size distribution of polyion stabilized empty and CFZ/tPNPs 81

Figure 4.3. Effect of pH on the release of CFZ from polyion stabilized tPNPs 84

Figure 4.4. Cell Viability of DLD 1 CFZ resistant cells treated with CFZ or polyion stabilized CFZ/tPNPs 88

Figure 4.5. Proteasome activity of DLD 1 CFZ resistant cells treated with CFZ or polyion stabilized CFZ/tPNPs 89

Figure 5.1. In vivo full body images of mice bearing 100 mm3 tumors treated with saline, FL-PLL/tPNPs or FL-PLL/EpCAM-tPNPs. 102

Figure 5.2. In vivo full body images of mice bearing 100 mm3 tumors treated with saline, FL-PLL/tPNPs or FL-PLL/EpCAM-tPNPs. 103

Figure 5.3. Ex vivo fluorescence images of organs and tumors obtained at 24 h post injection into 100 mm^3 tumor bearing mice 104

Figure 5.4. Semiquantitative analysis of fluorescence intensity for 100 mm^3 tumor bearing mice 105

Figure 5.5. Ex vivo fluorescence images of organs and tumors obtained at 24 h post injection into 100 mm^3 tumor bearing mice 106

Figure 5.6. Semiquantitative analysis of fluorescence intensity for 100 mm^3 tumor bearing mice..... 107

CHAPTER 1. BACKGROUND

1.1 Cancer Treatment Using Chemotherapy

Cancer remains the second leading cause of death among Americans after heart disease. The American Cancer Society estimates that there will be a whooping 1.9 million new cases of cancer in 2022 with 32% of these cases leading to death [1]. It is characterized by rapid and uncontrollable proliferation of cells due to mutations that hijack the normal cellular activities.

One of the tools developed over the years to tackle cancer is conventional chemotherapy. This form of treatment is used where traditional surgical resection or radiotherapy is inadequate due to the development of secondary metastatic disease [2]. However, even with the progress of cancer diagnosis and chemotherapeutic options in recent times, chemotherapy is often plagued with life-threatening or life-altering side effects such as acute toxicity, white and red blood cell loss, vomiting, nausea and hair loss [3, 4]. Although most patients become originally responsive, with frequent and recurrent chemotherapy, patients develop drug resistance [5]. Toxicity and drug resistance associated with chemotherapy pose two major challenges for new drug delivery systems: improve drug delivery selectivity and overcome resistance in other to maximize therapeutic efficacy while minimizing toxic side effects. Additionally, the advent of high throughput screening and combinatorial chemistry methods yield compounds that have poor aqueous solubility [6, 7]. Many chemotherapeutics fall into the class II or IV of the biopharmaceutical classification system which comprises drugs that have a combination of poor solubility

and/or poor permeability [8]. There are limited options available to simultaneously resolve these issues, hence, a need for novel therapies.

1.2 Nanotherapeutics as Alternative to Conventional Chemotherapy

Nanotherapeutic drug delivery systems (NDDS) have emerged as tools to overcome the limitations of conventional chemotherapy. This allows for, intracellular uptake, and tumor specific delivery of these vehicles [9]. In addition, NDDS have advantages over conventional chemotherapy owing their size. Tumor development requires rapid angiogenesis to supply essential nutrients and oxygen to defective cells. This rapid development of blood vessels leads to the formation of leaky vasculature that allows sub-200 nm nanoparticles to extravasate into tumors. Additionally, the poor lymphatic drainage associated with these tumors allows such nanoparticles to accumulate within tumors with slow clearance rates. The leaky vasculature and poor lymphatic drainage taken together is termed the enhanced permeation and retention (EPR) effect [10]. Furthermore, NDDS such as liposomes, polymeric micelles, and polymeric nanoparticles provide higher solubility and bioavailability over free drugs. Nanoparticles typically have a hydrophobic core and a hydrophilic shell. Lipophilic drugs can be loaded into the core of nanoparticles by hydrophobic interactions while the shell is exposed to the surrounding aqueous environment, enhancing the overall solubility of drugs [11]. Surface properties of nanoparticle shell can be tuned to secure the fate of nanoparticles in vivo. For example, PEGylated nanoparticles have antibiofouling properties which significantly reduce their clearance by macrophages of the reticuloendothelial system [12]. Cell membranes are negatively charged so, surface charge of NDDS have a role to play in cellular uptake as well as affect their interaction with plasma protein.

1.3 Polypeptide Nanoparticles

Recently, polypeptides have received significant attention due to their bio activity, controlled synthesis, and structure-property relationships [13-15]. Polypeptide copolymers can self-assemble into a variety of nano and microstructures with interesting properties. Based on the surrounding solvents, some of these structures include micelles, vesicles, polymersomes and nanoassemblies [16-18]. Polypeptides are synthetic polymers derived from natural amino acids. Although polypeptides have molecular weight smaller than proteins, they adopt conformations like natural proteins such as a random coil, α-helix, or β-sheet. The conformation and molecular architecture of polypeptides often relates to their solubility and stability of their linkages which together have an effect on self-assembly properties [19]

Early development of synthetic polypeptides focused on easily produced water soluble homo-polypeptides such as poly(L-lysine), poly(L-aspartic acid) and poly(L-glutamic acid) [20]. These polypeptides are highly charged and water soluble at neutral pH, and although they mimic natural proteins, they are limited in function and are susceptible to precipitation due to charge interactions when in contact with in vivo fluids [21]. As a drug delivery vehicle, drug molecules were attached to these polypeptides by chemical conjugation to their side chains. With this modality, drug release involved chemical disruption of bonds typically by acidic cleavage [22]. With advancement in synthetic technologies, polypeptide copolymers can be synthesized to have various topologies such as graft, block, and dendrimer-like structures [23-25]. They can also be linked with other polymers such as polyethylene glycol (PEG) that confer properties needed for effective drug delivery [12]. Additionally, their diversity in functionality allows

polypeptides to partake in facile modifications to possess targeting ligands. Small peptides or large proteins can be substituted onto their side chains or end group to confer additional targeting for treating cancer [26].

Biocompatibility and biodegradability are paramount for drug delivery vehicles, hence the attractiveness of polypeptides in nanotechnology. Structures comprised of polypeptides have secondary structures like proteins as well as amide linkages that confer degradability [27]. Due to their highly charged state, polypeptide copolymers can self-associate with oligomers or polypeptides of opposite charge. This association leads to the formation of a class of organized nanoassemblies termed polypeptide nanoparticles (PNPs) that have a core-shell structure by electrostatic interactions [28, 29]. PNPs consist of a hydrophobic core and a hydrophilic shell. The core allows for physical entrapment of lipophilic drugs by hydrophobic or ionic interactions while the hydrophilic shell allows for solubilization in aqueous environment. With physical entrapment, a major concern is burst drug release [30]. However, core stabilizers have been used to mitigate burst drug release. Another advantage of the core-shell structure of PNPs is their size. PNPs typically have particle size below 100 nm. This is advantageous for drug delivery because these PNPs have been shown to evade the body's natural defense system, and in so doing prolong the blood circulation time. Additionally, the sub-100 nm particle size of PNPs allows them to take advantage of a phenomena known as the enhanced permeation and retention (EPR) effect. Most solid tumors have a unique physiology different from healthy tissues and organs. To facilitate growth, tumor cells hijack neovasculature to induce angiogenesis for adequate supply of oxygen and nutrients. As the tumor increase in size, they recruit more blood vessels or engulf existing vessels. However, unlike healthy organ vessels, the

endothelial lining of tumor vessels is incomplete which makes them have large pores. This leads to significantly higher vascular permeability. Additionally, these tumor microenvironments are associated with poor lymphatic drainage [31-33]. Due to the combination of leaky vasculature and poor lymphatic drainage, nanoparticles can extravasate and preferentially accumulate and reside in tumors longer than in normal organs [34].

1.4 Carfilzomib as a Model Drug for Polypeptide Nanoparticles

Carfilzomib (CFZ) was used as our model drug because it exhibits most of the developability concerns associated with conventional chemotherapy. CFZ is the second-generation proteasome inhibitor approved by the FDA for the treatment of multiple myeloma [35]. Structurally, it is a tetrapeptide with an epoxyketone pharmacophore (Figure 1.1) derived from the natural product epoxomicin [36, 37]. With a molecular formula of $C_{40}H_{57}N_5O_7$ and a molecular weight of 719.91 g/mol, CFZ is a BCS class II drug.

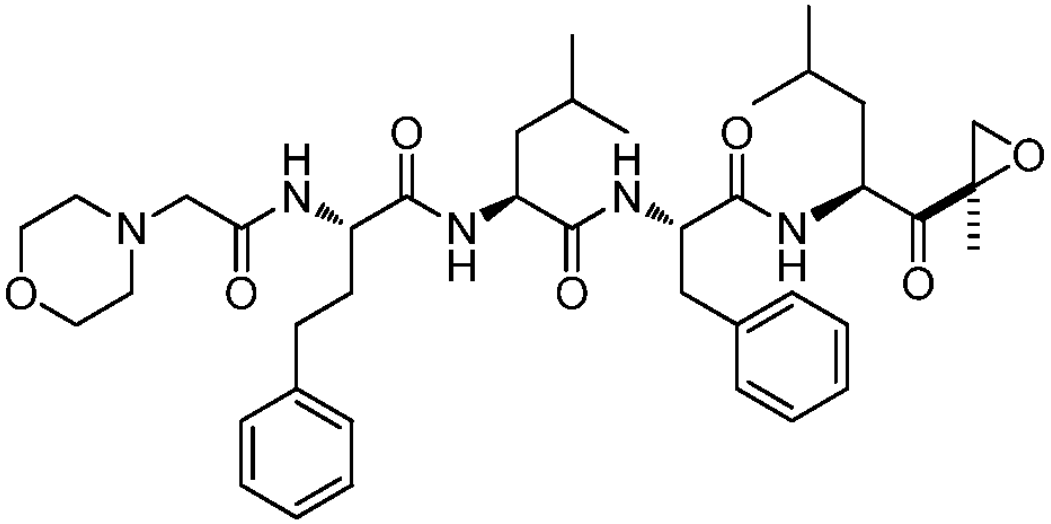

Figure 1.1. Chemical structure of carfilzomib.

The approval of the Bortezomib (BTZ) in 2003 paved the way for proteasome inhibition as a viable route for multiple myeloma cancer therapy. However, some patients become unresponsive to BTZ due to resistance, leading to relapse [38]. CFZ has shown great efficacy in treating patients with relapsed/refractory multiple myeloma that are often resistant to the first-generation proteasome inhibitor BTZ [39-41]. It does this by binding selectively and irreversibly to the 20S proteasome to inhibit the chymotrypsin-like activity (Figure 1.2) [42]. The inhibition prevents the proteasome from degrading ubiquitinated proteins and leads to cell cycle arrest and apoptosis [43]

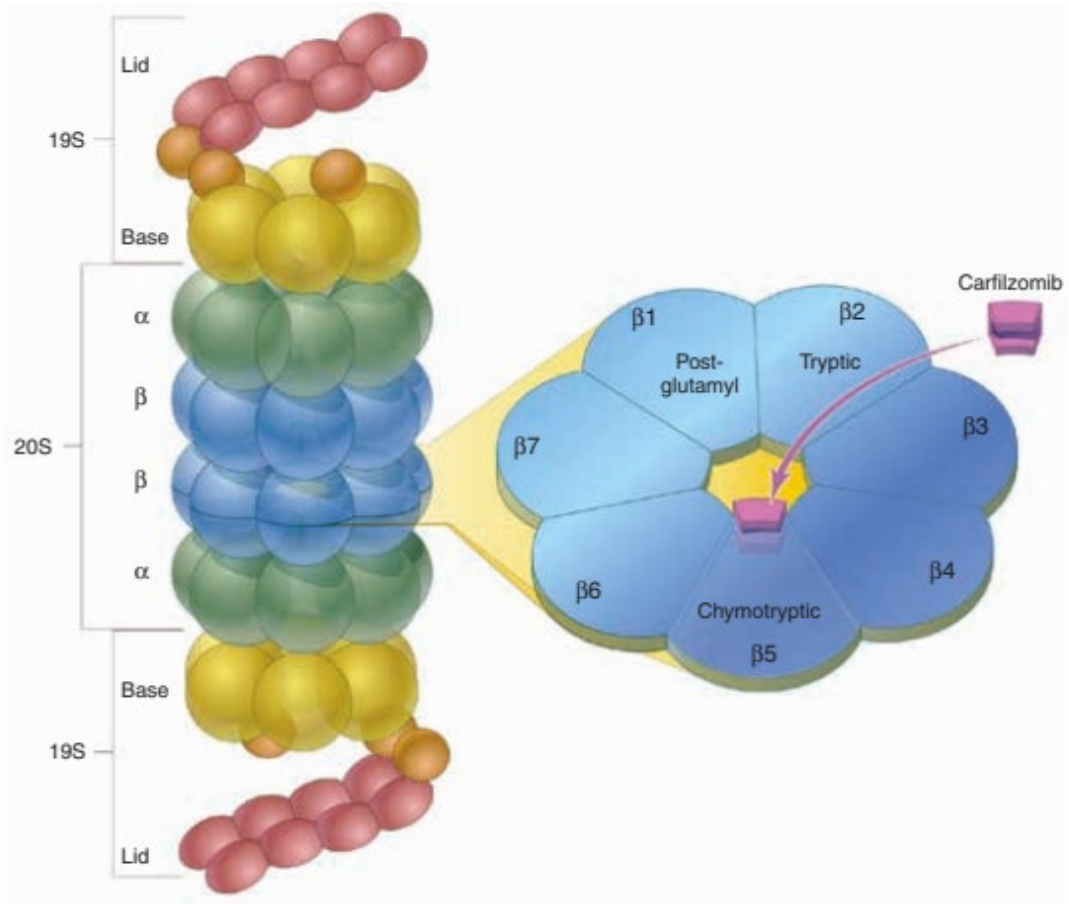

Figure 1.2. Mechanism of carfilzomib inhibition. The 26S proteasome consists of the 20S core and two 19S caps at either end. There are 7 subunits of the 20S core of which carfilzomib binds irreversibly toe the β5 chymotrypsin-like subunit leading to cell apoptosis. With permission from Chari A, Mazumder A, Jagannath S. Proteasome inhibition and its therapeutic potential in multiple myeloma. *Biologics*. 2010; 4:273-87.

Due to its success in treating relapsed/refractory multiple myeloma, CFZ has been explored as a therapeutic for treating other solid cancers (NCI clinical trial identifiers: NCT00531284). However, CFZ has achieved modest success in treating solid cancers due to several pharmaceutical and clinical limitations such as, short blood retention time, inefficient tumor accumulation, and poor biostability [44-46]. The unique chemical structure and mode of drug action, do not hold long in the body because CFZ undergoes enzymatic cleavage of its peptide chains and epoxyketone ring opening [47]. CFZ is also a substrate of the efflux transporter P-gp that significantly reduces its cellular uptake and induces drug resistance [48-50]. CFZ has a solubility of less than 10 μM in most pharmaceutically relevant solvents, which further hinders its clinical utility [51]. Currently, few injection formulations have been developed for CFZ to address these problems.

The only injection formulation that FDA has yet approved for CFZ is Captisol®, which is sulfobutyl ether β-cyclodextrin acting as a solubilizer of the proteasome inhibitor [52]. Although this cyclodextrin-based formulation has improved water solubility of CFZ, it requires a large amount of cyclodextrin with respect to CFZ (> 50 fold by mass) and shows little protective effect against in vivo degradation of CFZ [53]. Cyclodextrins have a short blood circulation time with a half-life of < 30 minutes due to extra-hepatic clearance [46]. Nanoparticle formulations such as polymer micelles, nanocrystals, and liposomes have been also developed as injection formulations of CFZ, but none of them has significantly improved in vivo efficacy of the proteasome inhibitor for solid cancer treatment [54-59]. Thus, the development of new injection formulations addressing these issues will greatly expand therapeutic benefits of CFZ to other cancers.

CHAPTER 2. DEVELOPMENT OF TERNARY POLYPEPTIDE NANOPARTICLES

Portions of this chapter is a modified adaptation from the manuscript previously published in [32]. Reproduced with permission from Springer Nature. Copyright © (2020) Springer Science Business Media, LLC.

2.1 Introduction

This work focuses on the design and development of ternary polypeptide nanoparticles (tPNPs) as a new injection formulation for CFZ. The core of tPNPs take advantage of the solubilizing effect of cyclodextrins CDs

CDs are a class of cyclic oligosaccharides made up of glucose molecules linked by α-1,4-glycosidic linkages. Natural CDs have either 6,7 or 8 glucose molecules and are called α-CD, β-CD, or γ-CD, respectively. Spatially, CDs take the shape of a truncated cone or a toroid having a cavity. (Figure 2.1). Because of the prevalence of hydroxyl groups, CDs are water soluble. However, their cavity is relatively apolar which creates a hydrophobic environment. Therefore, CDs can interact with lipophilic molecules in a host-guest manner while maintaining its overall water solubility. This interaction between lipophilic molecules and the cavity of CDs is referred to as inclusion complexation and it is driven by exclusion of water from the interior of CD. An equilibrium is then established between CD and the guest molecule.

tPNPs entrap CFZ through ternary (hydrophobic, ionic, and supramolecular) interactions in three steps. First, CFZ was entrapped in the cavity of heptakis(6-amino-6-deoxy)-β-cyclodextrin(hepta-hydrochloride) (HaβCD) through hydrophobic interaction.

HaβCD is a modified β-CD where the exterior hydroxyl groups have been replaced with amines which render it positively charged. Secondly, the drug-cyclodextrin inclusion complexes were mixed with the polypeptide azido-poly (ethylene glycol)-block-poly (L-glutamic acid sodium salt) (N_3-PEG-PLE) to form polyionic complex nanoparticles, and finally, the nanoparticles were modified with fluorescent dyes (AFDye 647) for imaging and/or epithelial cell adhesion molecule (EpCAM) antibodies for cell targeting. The hydrophobic interaction between cyclodextrin and drug molecules ensures the entrapment of CFZ and potentially its derivatives without having to alter the compositions of tPNPs.

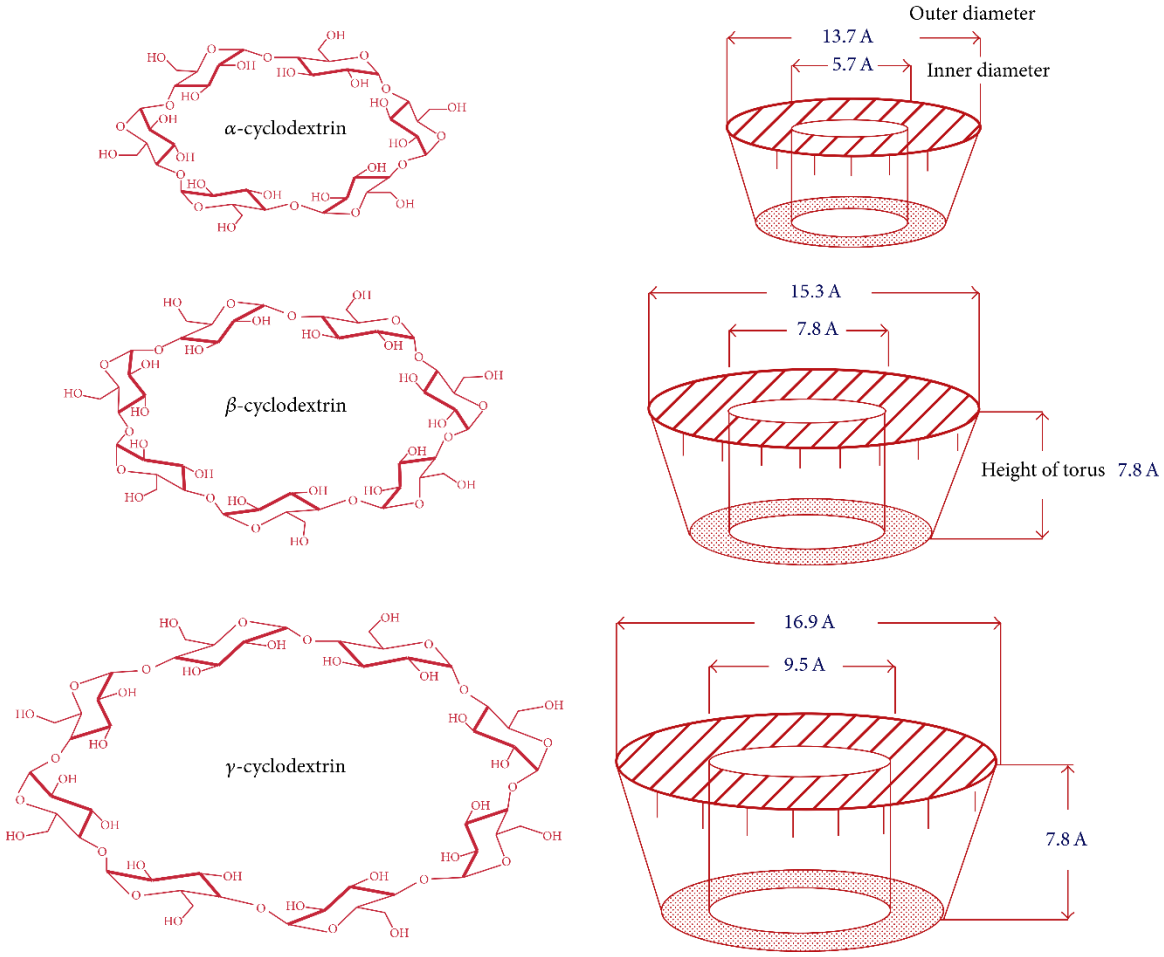

Figure 2.1. Structure and conformation of natural cyclodextrins. With permission from Gidwani B, Vyas A. A comprehensive review on cyclodextrin-based carriers for delivery of chemotherapeutic cytotoxic anticancer drugs. *BioMed research international*. 2015 Oct 25;2015.

The ionic interaction between CFZ-loaded CDs with positive amines and anionic carboxylates on N_3-PEG-PLE polymers significantly reduces the amount of CD used to solubilize and protect the drug in an aqueous solution. The supramolecular interactions among drug, CD, and polymers are beneficial to control the shape, size, and other physicochemical properties of tPNPs by minimizing the variations in nanoparticle batches and drug payloads. The EpCAM antibody was used to improve cell targeting efficiency for the nanoparticles. EpCAM is a 314 amino acid transmembrane protein that is found almost exclusively on epithelial cells [60]. While its main function is cell adhesion in normal cells, EpCAM is overexpressed in many malignant tumors [61], making it a useful target for new drug therapies [62].

We hypothesize that tPNPs will maintain uniform particle size and high drug entrapment to improve stability, intracellular accumulation, and thus efficacy of CFZ. Our expectation is that EpCAM will further enhance cytotoxicity of the proteasome inhibitor against drug-resistant cancer cells overexpressing P-gp on the cell surface [63-65]. To answer these questions, CFZ-loaded tPNPs (CFZ/tPNPs) were characterized for their physicochemical properties, drug entrapment/release profiles, proteasome inhibition activity, EpCAM-mediated cell targeting efficiency, and in vitro cytotoxicity against CFZ-resistant DLD-1 colorectal cancer cells.

2.2 Materials and Methods

2.2.1 Materials

Heptakis (6-amino-6-deoxy)-βCD heptahydrochloride (HaβCD) was purchased from Cyclolab R&D Laboratory Ltd. (Budapest, Hungary). Azido-poly(ethylene glycol)-block-poly(L-glutamic acid sodium salt) (N_3-PEG-PLE, 20 kDa with 5 kDa PEG and 100 repeating units of glutamate) was purchased from Alamanda Polymers (Huntsville, AL). Citric acid was obtained from EM Science (Gibbstown, NJ). CFZ was purchased from LC laboratories (Woburn, MA). Potassium biphthalate sodium hydroxide buffer, formic acid, and HPLC grade water were obtained from Fisher Scientific (Fair-lawn, NJ). Slide-A-Lyzer G2 dialysis cassettes (10,000 MWCO) and alkyne-PEG-NHS (4 units of PEG modified with alkyne and N-hydroxysuccinimide at each end, 401.41 g/mol) were obtained from Thermo Fisher Scientific (Rockford, IL). Alexa-fluor 647-Dibenzocyclooctyne (AFDye 647 DBCO) was purchased from Click Chemistry Tools (Scottsdale, AZ). EpCAM antibody was purchased from Santa Cruz Biotechnology (Dallas, TX).

CFZ resistant DLD-1 cells were cultured as reported previously [45]. Briefly, DLD-1 cells were sub-cultured in RPMI 1640 media supplemented with 10% fetal bovine serum (FBS). Cells were incubated at 37°C in a humidified incubator with 5% CO_2. The cells were maintained in the log growth phase by periodic sub-culturing.

2.2.2 Preparation of tPNPs

Ternary polypeptide nanoparticles (tPNPs) were prepared by mixing HaβCD and N_3-PEG-PLE to form polyion complexes. The net charge between amino groups of HaβCD and carboxylate groups of N_3-PEG-PLE was adjusted to zero by using citric acid. To

prepare CFZ/tPNPs, drug and HaβCD were mixed at a 1:4 mass ratio, which appeared best to prepare most stable inclusion complexes in preliminary studies. CFZ and HaβCD were mixed at different mass ratios ranging from 1:1 to 1:10 to determine the optimum combination. We observed no noticeable increase in drug loading above a 1:2 mixing ratio. However, mixtures below a 1:4 ratio exhibited rapid precipitation of CFZ and aggregation of nanoparticle. In addition, we also aimed to reduce the CD-drug ratio, given that highly excessive CD content in carfilzomib formulation currently used in the clinic causes patient discontent due to a long injection time. A mixing ratio of 1:4 was chosen for further studies to minimize the amount of HaβCD used in preparation of tPNPs. Briefly, 1 mg of CFZ dissolved in ethanol and 4 mg of HaβCD in water were mixed in a round bottom flask to which citric acid was added to facilitate complexation. The mixed solution was evaporated under reduced pressure to remove organic solvent. 2 mg of N_3-PEG-PLE in water was then added to the flask followed by sonication for 2 minutes to prepare self-assembled polyion complexes of CFZ/tPNPs. Figure 2.2 shows the schematic for preparation of CFZ/tPNPs.

For the preparation of fluorescent tPNPs (Fl-tPNPs), copper-free [3+2] cycloaddition was used to label N_3-PEG-PLE with AFDye 647 DBCO. N_3-PEG-PLE in water was added to AFDye 647 DBCO dissolved in DMSO, and the mixture was left to react in the dark for 1 h (Figure 2.3). Unreacted dye and DMSO were removed by dialyzing the mixture against deionized water. Dye-labeled polymers were collected by freeze drying. Empty FL-tPNPs were prepared as described above, yet slight modification was made to prevent fluorescence quenching by mixing dye-labeled and dye-free polymers at 1:1 ratio.

To prepare EpCAM-conjugated tPNPs (EpCAM-tPNPs), EpCAM antibody was modified with alkyne prior to complexation. Briefly, alkyne-PEG-NHS in DMSO was added at a 1.5 molar excess to an EpCAM antibody solution in PBS. The reaction was allowed to proceed for 1 h and DMSO was removed by dialysis in PBS. The alkyne-modified EpCAM was reacted with N_3-PEG-PLE in PBS by copper-catalyzed [3+2] cycloaddition. The mixture was dialyzed in deionized water to remove free copper and other small molecule impurities. EpCAM conjugation was confirmed by SDS-PAGE. 5 μg of EpCAM standard and EpCAM conjugated polymer were added to a gradient gel (4-15% agarose gel). The gel was run at 80 V for 1 h. A silver stain was used to visualize bands.

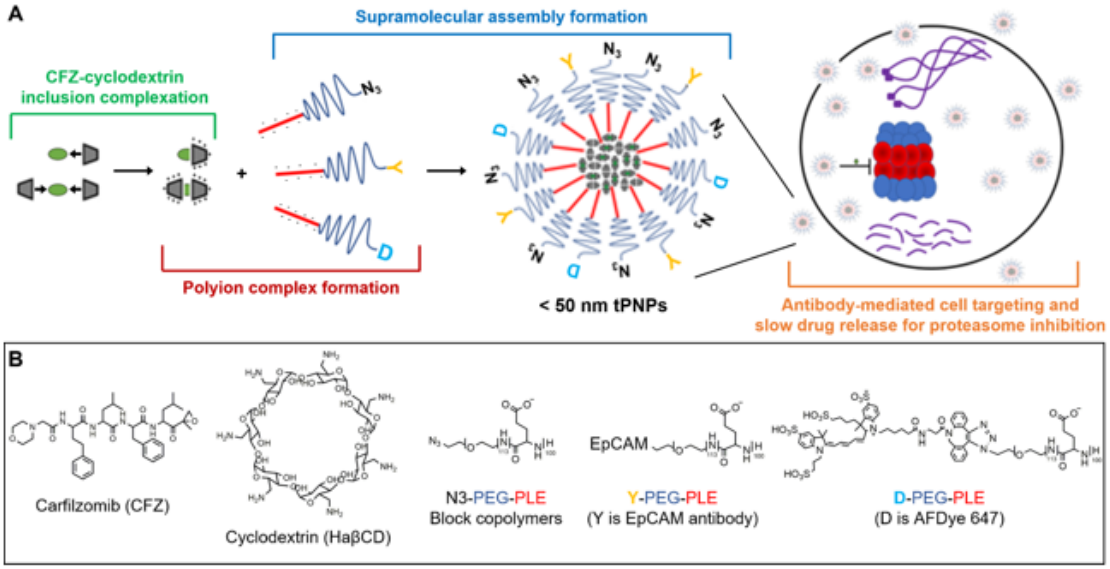

Figure 2.2. Schematic for preparation of ternary polypeptide nanoparticles

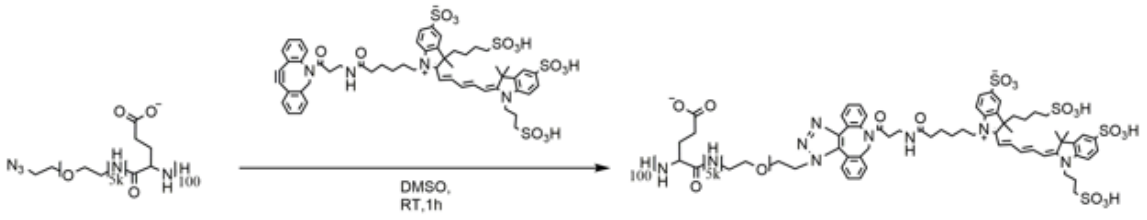

Figure 2.3. [3+2] cycloaddition click chemistry reaction for the synthesis of fluorescent polymer used for preparation of fluorescently labelled ternary polypeptide nanoparticles.

2.2.3 Particle size and surface charge measurement

Particle size and surface charge of tPNPs were measured by dynamic light scattering (DLS, Zetasizer Nano ZS, Malvern, UK). Folded capillary cuvettes were used for the measurement. A measurement angle and temperature were set 173° backscatter and 25°C, respectively. The measurement was repeated for freeze-dried tPNPs that were reconstituted in PBS (10 mM, pH 7.4, 2 mg/mL). Data obtained from triplicate measurements are reported as mean ± S.D.

2.2.4 Drug loading determination

CFZ entrapment in tPNPs was determined by high performance liquid chromatography (HPLC, Agilent Eclipse XDB-C18 column). The mobile phase consisted of acetonitrile (ACN) and HPLC grade water containing 1% formic acid. An isocratic method (55:45 = ACN;water) with a flow rate of 0.5 mL/min was used to elute CFZ (3.64 min elution). Drug peaks were integrated at a wavelength of 210 nm to draw a calibration curve for CFZ concentration determination. Drug concentrations are reported as mean ± S.D.

2.2.5 Stability assessment of lyophilized tPNPs

Lyophilization conditions were optimized for tPNPs by testing mannitol and trehalose as cryoprotectants. The cryoprotectants were added at 2 or 5% (w/v) to tPNP solutions in deionized water and the mixed solutions were flash frozen in dry ice. A Labconco FreeZone® freeze drying system was used for lyophilization. Freeze dried

samples were tested for particle stability during storage and after reconstitution (e.g., aggregation, particle size and drug entrapment).

2.2.6 Confirmation of particle integrity for tPNPs in the presence of serum proteins

Particle integrity of tPNPs was monitored by a solvato-fluorochromic method as we reported [66, 67]. Briefly, tPNPs were entrapped with Nile Blue (NB), which is a dye that fluoresces strongly in a hydrophobic core of a nanoparticle yet quenches its fluorescence in water as the nanoparticle breaks down. NB-loaded tPNPs were incubated in RPMI 1640 cell culture media containing 10% FBS at 37°C for 72 h. The incubation condition mimics an in vivo environment following intravenous injection of tPNPs. NB fluorescence was measured at 0, 1, 3, 6, 24, 48 and 72 h with 580 nm excitation and 630 nm emission using a microplate reader (SpectraMax M5, Sunnyvale, CA). The βCD formulation was used as a control. Data was collected in triplicate and reported as mean ± S.D.

2.2.7 Drug release study

Drug release profiles were investigated for CFZ/tPNPs by the dialysis method as previously reported [67]. Freshly prepared freeze-dried CFZ/tPNPs were dissolved in a potassium biphthalate sodium hydroxide buffer solution (pH 7.4, 10mM). CFZ/tPNPs at 10 mg/mL were transferred to dialysis cassettes (10,000 MWCO), which were dialyzed under sink conditions. Drug concentrations were determined at 0, 1, 3, 6, 24, 48 and 72 h by HPLC as described above. CFZ-loaded βCD complexes were used as a control. Drug

release profiles were obtained by fitting the drug concentration-time curves to an exponential decay using GraphPad Prism 8 software. All experiments were performed in triplicates. Results are reported as mean ± S.D.

2.2.8 Proteasome activity assessment

CFZ resistant DLD-1 cells were seeded at a density of 150,000 per well in 12 well plates and allowed to attach overnight. The cells were treated with 500 nM free CFZ or CFZ/tPNPs for 6, 24, 48, or 72 h. After washing twice with Hank's balanced salt solution (HBSS), the cells were harvested and lysed in a passive lysis buffer. Protein lysates were quantified using the Bradford assay and diluted in a 20S proteasome assay buffer (20 mM Tris-HCl, 0.5 mM EDTA, 0.035% SDS, pH 8.0). Diluted protein lysates (5 µg) were added to a 96-well plate, and enzyme reactions were initiated by a Suc-LLMY-AMC substrate solution (100 µM). Fluorescence from each well was measured for 1 h at one reading per minute using a SpectraMax M5 plate reader (excitation 360 nm/emission 460 nm). Proteasome activity of CFZ resistant DLD-1 cells treated with free CFZ or CFZ/tPNP was determined as a percentage of proteasome activity in untreated CFZ resistant DLD-1 cells.

2.2.9 Cellular uptake of tPNPs

Cells were seeded on a P-35mm glass plate at 150,000 cells/mL. Next day, the cells were incubated with AFDye 647 DBCO, FL-tPNP, or FL-EpCAM-tPNP at 37°C and 5% CO_2 atmosphere. At 1h, 3h and 24h post incubation, the cells were washed three times with PBS to remove free dyes and fluorescent nanoparticles in the cell culture

media. Fluorescent microscopy was then performed to image internalized dyes and nanoparticles by using an EVOS fluorescence microscope equipped with a Cy5 filter. ImageJ software was used for quantitative image analysis. Briefly, images were converted to an 8-bit format, subsequently changed to binary. Mean gray values for regions of interests (ROIs) were determined in each image, and relative fluorescence unit per cell was calculated as the average of the total mean gray value.

2.2.10 Cell viability

Before starting the cell viability assay, CFZ resistant DLD-1 cells were cultured in the absence of CFZ for seven days. The cells were seeded at 5,000 cells per well in a 96 well plate. After overnight incubation, the cells were treated with serial dilutions of free CFZ, CFZ/tPNPs, and CFZ/EpCAM-tPNPs. Cell viability was measured at 48, 72, and 96 h post incubation by using the MTS method [68]. Cell viability was calculated as a percentage of viable cells compared to the control of untreated cells. The half maximal inhibitory concentration (IC_{50}) values were determined by a non-linear regression using GraphPad Prism 8 software.

2.3 Results

2.3.1 Preparation of tPNPs

DLS analysis revealed that all tPNPs had a sub-50 nm particle size and neutral charge, which are suitable for drug delivery to solid tumors [69]. Figure 2.4 shows particle size distributions for empty tPNP, CFZ/tPNP, and CFZ/EpCAM-tPNP. Empty tPNPs had an average diameter of 46.1 nm (PDI = 0.043), and the particle size remained unchanged even after drug loading or EpCAM conjugation. CFZ/tPNPs showed a 53.4 nm particle size in average (PDI = 0.182) while CFZ/EpCAM-tPNPs were 56.5 nm in diameter (PDI = 0.151). Physiochemical properties of tPNPs are summarized in Table 2.1.

Successful antibody conjugation was confirmed by SDS-PAGE gel as shown in Figure 2.5. A single band showing an upward shift in molecular weight indicates that the polymer chains are covalently bonded to EpCAM with no free antibody remained. Table 2.1 shows that CFZ was successfully entrapped in tPNPs at a high yield with a reduced amount of cyclodextrin. An optimal molar ratio between drug and cyclodextrin appeared 1:1 because a molar ratio above 1:1 showed no observable difference in drug loading.

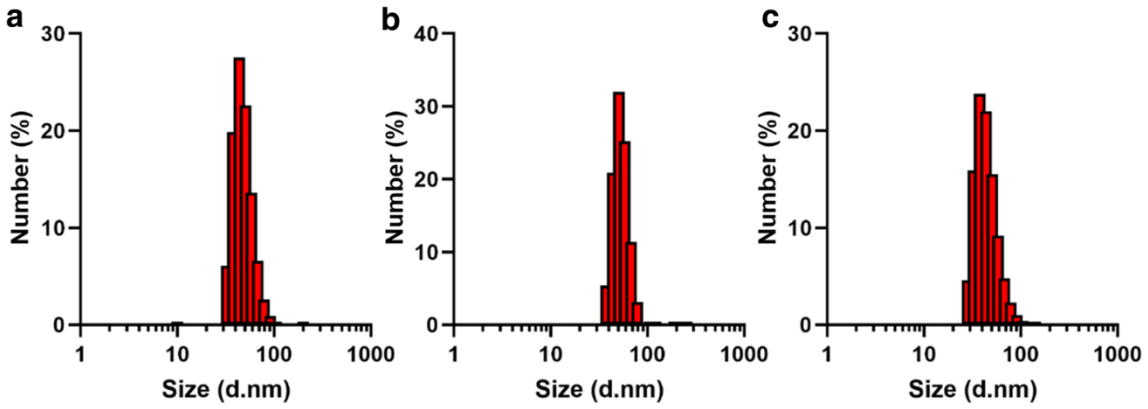

Figure 2.4. Particle size distribution of (a) Empty tPNP, (b) CFZ/tPNP, and (c) CFZ/EpCAM-tPNP

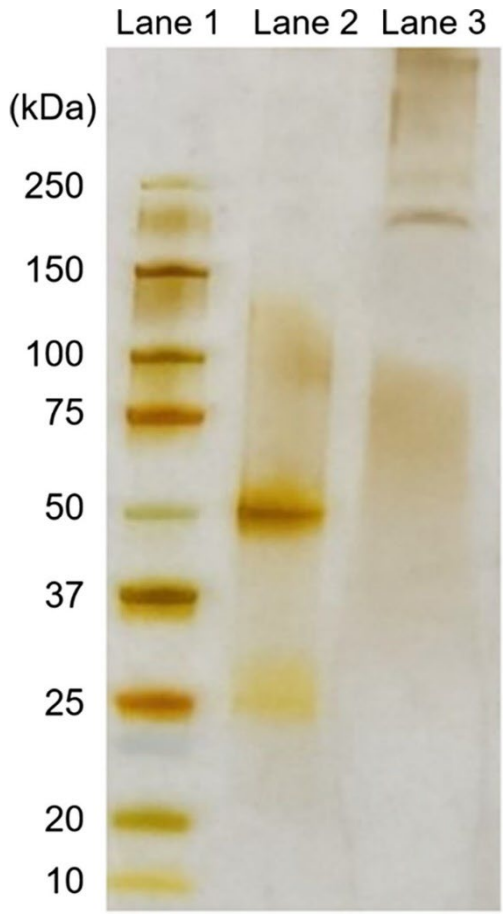

Figure 2.5. SDS-PAGE to confirm the conjugation of EpCAM to N_3-PEG-PLE. Lane 1 shows molecular weight markers, lane 2 shows EpCAM antibody modified with alkyne, and lane 3 shows EpCAM conjugated to N_3-PEG-PLE by copper-catalyzed [3 + 2] cycloaddition reaction.

Table 2.1. Particle properties of tPNPs. Data is shown as Mean ± SD except polydispersity index (PDI). All drug loading shown in the last column were measured for freeze-dried formulations.

Formulation	Particle size (nm)	PDI	Zeta potential (mV)	Drug loading (mg/mL)
Empty tPNP	46.1 ± 4.0	0.043	0.47 ± 0.12	-
CFZ/tPNP	53.4 ± 4.6	0.182	1.12 ± 0.30	1.16 ± 0.23
CFZ/EpCAM-tPNP	56.5 ± 9.9	0.151	1.16 ± 0.29	1.01 ± 0.13

2.3.2 Stability of CFZ/tPNPs

Drug-loaded tPNPs remain stable during storage in aqueous solutions or after lyophilization. In preliminary studies, CFZ/tPNPs were difficult to dissolve in PBS and required sonication for a long time. The particle size of CFZ/tPNPs significantly changed before and after freeze-drying and large aggregates were also visible even after 1 h sonication. These issues were resolved by using cryoprotectants such as mannitol and trehalose. Freeze-dried CFZ/tPNPs were readily reconstituted in the presence of these cryoprotectants. The effects of cryoprotectants on particle size is shown in Figure 2.6. For both 2% mannitol and trehalose, vigorous shaking was required to fully disperse tPNPs and they showed a particle size >3 fold greater than the initial particle size before freeze-drying. With a 5% of both cryoprotectants, particle size remained the same before and after freeze-drying. Mild shaking was still required to disperse tPNPs with 5% mannitol yet tPNPs dispersed readily with 5% trehalose.

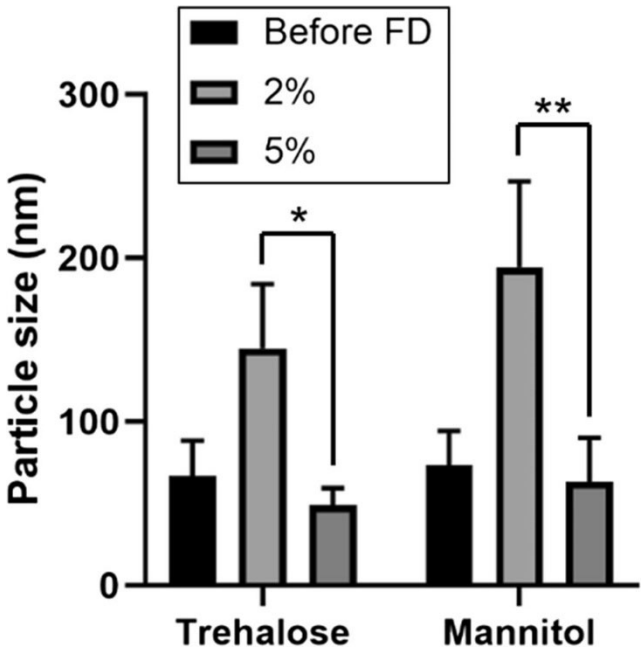

Figure 2.6. Particle size comparison among CFZ/tPNPs before and after freeze drying in the presence of cryoprotectants (*: p = 0.0275; **: p = 0.0028).

2.3.3 Confirmation of particle integrity for tPNPs in serum-containing cell culture media

tPNPs maintained particle integrity in the presence of serum proteins for a prolonged time with more than 50% of initial NB fluorescence remaining during incubation in cell culture media at 37ºC for 72 h (Figure 2.7). tPNPs were more stable than βCDs to entrap NB up to 24 h prior to slow particle dissociation. Both tPNPs and βCDs performed similarly between 24 and 72 h although tPNPs retained NB fluorescence approximately 20% greater than βCDs. These results confirmed that tPNPs suppressed interactions with serum proteins more effectively than CD formulations to maintain particle integrity as drug carriers.

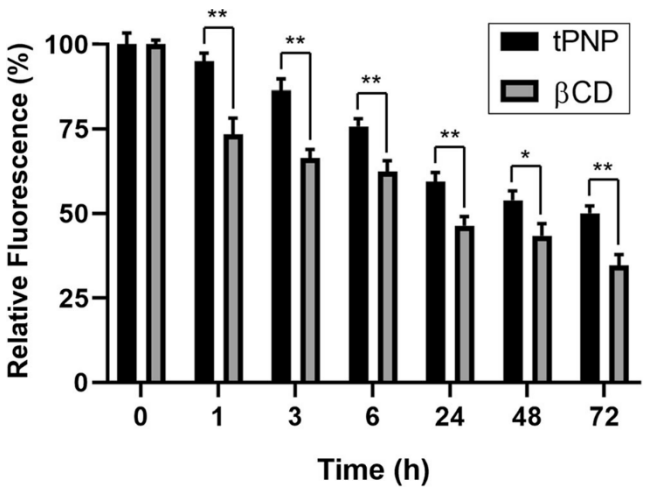

Figure 2.7. Confirmation of particle integrity for tPNPs incubated in cell culture media with 10% FBS at 37°C. βCD was used as a control. (*: $p = 0.0014$; **: $p < 0.0001$).

2.3.4 Drug release studies

tPNPs achieved sustained release of CFZ as opposed to βCD inclusion complexes used as a control. Both tPNPs and control showed biphasic drug release profiles with initial burst drug release as shown in Figure 2.8. However, tPNPs slowed down drug release after the initial burst with a drug release half-life of > 20 h. Kinetic parameters for drug release profiles are summarized in Table 2.2.

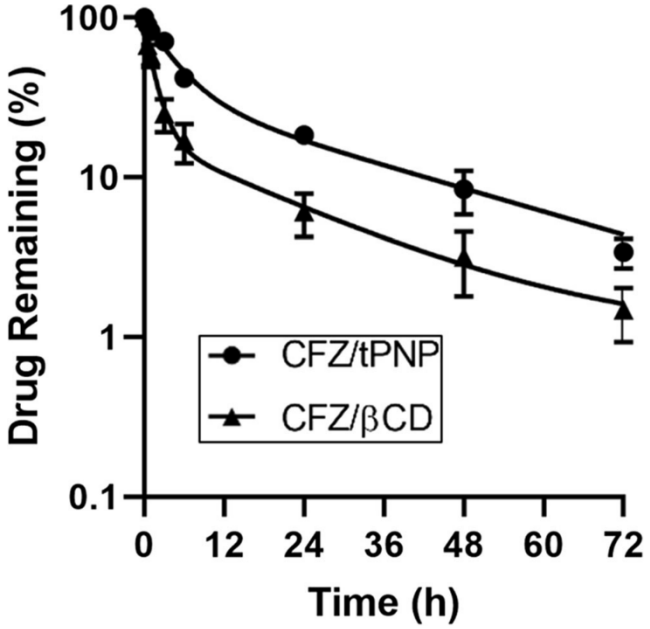

Figure 2.8. In vitro drug release curves of CFZ/tPNP and CFZ/βCD

Table 2.2. Kinetic parameters for CFZ release from tPNPs in comparison to βCD. Values were determined by dynamic dialysis

Formulation	$T_{1/2av}$ (h)	$T_{1/2fast}$ (h)	$T_{1/2slow}$ (h)	$K_{av}(h^{-1})$	$K_{fast}(h^{-1})$	$K_{slow}(h^{-1})$
CFZ/tPNP	6.46	3.273	24.36	0.0115	0.2118	0.0285
CFZ/βCD	1.59	0.8413	14.2	0.0453	0.8239	0.0477

2.3.5 Proteasome activity inhibition

CFZ/tPNPs suppressed proteasome activity in CFZ-resistant DLD-1 cells for a longer period than free CFZ (Figure 2.9). Both free CFZ and CFZ/tPNPs suppressed proteasome activity over 6 h in DLD1 cells, but only CFZ/tPNPs showed prolonged inhibition of proteasome activity up to 72 h. In contrast, free CFZ shows proteasome activity recovering after 24 h. These results suggest that initial proteasome inhibition was comparable between free CFZ and CFZ/tPNPs, but tPNPs extended the inhibition of proteasome activity for a long time, presumably due to sustained CFZ release.

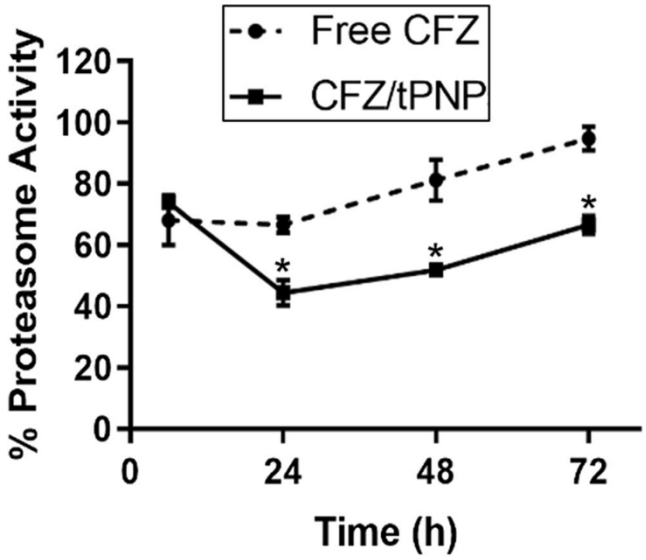

Figure 2.9. Changes in proteasome activity of DLD-1/ABCB1 cells treated with free CFZ or CFZ/tPNPs for 6, 24, 48 and 72 h. The values from experiments in triplicate and normalized to untreated proteasome activity and presented as mean ± S.D. (*: $p < 0.0001$).

2.3.6 Cellular uptake of tPNPs

Microscopy using fluorescent nanoparticles confirmed that tPNPs internalized in cancer cells as early as 1 h while demonstrating the highest intracellular accumulation after 24 h post incubation (Figure 2.10). Quantitative analysis of the images revealed that tPNPs showed greater intracellular accumulation than free dyes and EpCAM enhanced the intracellular uptake of tPNPs (Figure 2.11).

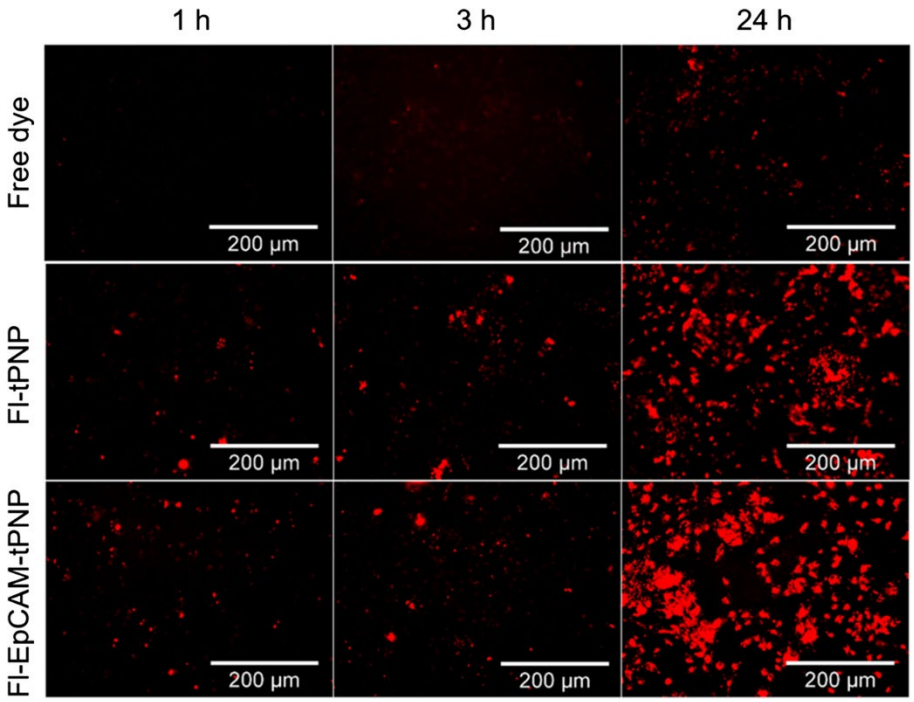

Figure 2.10. Cellular uptake of fluorescent tPNPs with and without EpCAM conjugation. Free dye (AFDye 647) was used as a control.

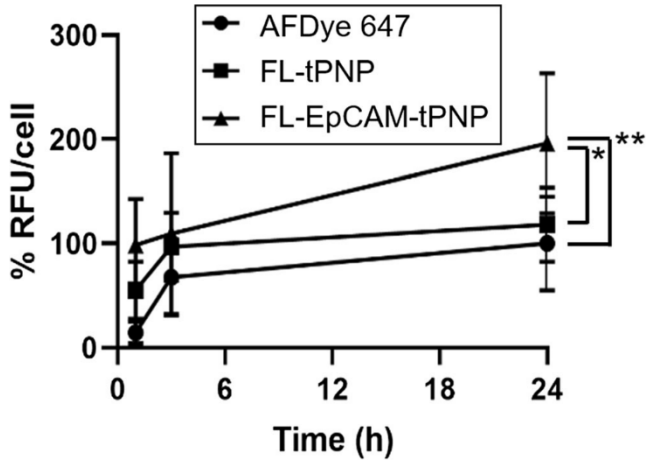

Figure 2.11. Quantitative analysis of fluorescence integrity for tPNPs internalizing in DLD-1 CFZ resistant cells. Results are as percentage relative to free dye fluorescence at 24 h. The area under the curve (AUC) was in order of FL-EpCAM-tPNP (3418) > FL-tPNP (2409) > AFDye 647 (1842). (*: $p = 0.0032$; **: $p = 0.0063$).

2.3.7 Cell viability

CFZ/tPNPs and CFZ/EpCAM-tPNPs time-dependently increased cytotoxicity against CFZ-resistant DLD-1 cells (Figure 2.12). Cell viability decreased as incubation time increased from 48 to 96 h. In all cases, tPNPs showed higher cytotoxicity than free CFZ as summarized in Table 2.3. These results indicate that tPNPs improved in vitro efficacy of CFZ through enhanced cellular uptake and sustained drug release in comparison to free CFZ.

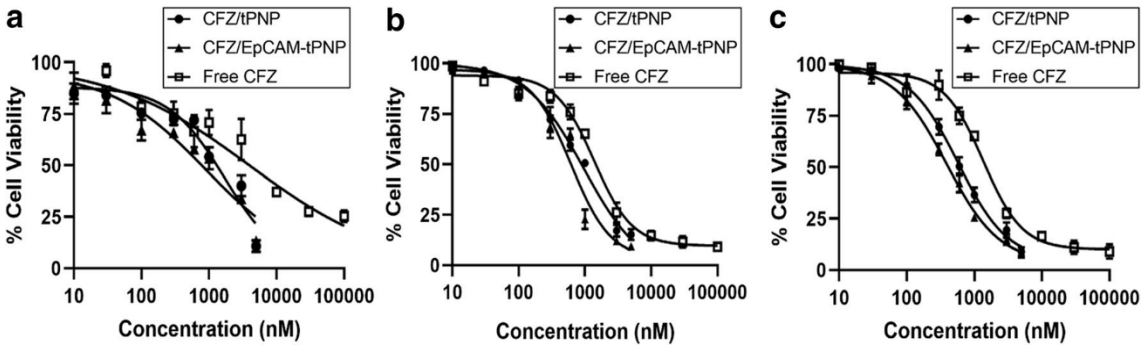

Figure 2.12. Effect of tPNPs on the viability of CFZ-resistant DLD-1 colorectal cell line compared to free CFZ after (a) 48 h (b) 72 h and (c) 96 h incubation.

Table 2.3. The half maximal inhibitory concentration (IC_{50}) values of CFZ, CFZ/tPNP, and CFZ/EpCAM-tPNP against CFZ-resistant DLD-1 colorectal cancer cells after 48, 72 and 96 h of treatment.

Formulation	IC_{50} (μM, mean ± SD)		
	48 h	72 h	96 h
CFZ	3.97 ± 0.87	1.37 ± 0.19	1.64 ± 0.40
CFZ/tPNP	1. 69 ± 0.48	0.97 ± 0.23	0.43 ± 0.16
CFZ/EpCAM-tPNP	0.91 ± 0.32	0.612 ± 0.14	0.36 ± 0.11

2.4 Discussion

There is an urgent need to develop a new injection formulation for proteasome inhibitors to maximize the therapeutic benefits in cancer treatment. The second-generation proteasome inhibitor CFZ received a fast-track FDA approval in 2012 for its combination therapy with immunomodulatory agents to treat patients with relapsed/refractory multiple myeloma [70]. The approval was made due to its greater performance over the first-generation proteasome inhibitor bortezomib (BTZ) as CFZ appeared also efficacious for patients with developed BTZ-resistance [71-73]. The higher efficacy and lower toxicity of CFZ over BTZ has prompted its expansion to non-hematological cancers [74-76]. However, CFZ has shown its own pharmaceutical and clinical limitations, which include poor aqueous solubility, rapid metabolic degradation, epoxide ring opening leading to low half-life, poor targetability and reduced efficacy due to P-gp upregulation in drug resistant cells. All these limitations hamper further utility of CFZ in treating other types of cancers such as solid cancers.

In this study, we develop tPNPs as a new injection formulation of CFZ to address solubility, stability, and delivery issues of the proteasome inhibitor. tPNPs were confirmed to have an average of 50 nm particle size, which remained unchanged after CFZ entrapment or lyophilization. These properties are unique in comparison to other nanoparticle formulations that often alter particle size and stability during storage and use. The uniform size and improved stability of tPNPs appeared beneficial to entrap CFZ with a reduced amount of CD as opposed to a commercially available CFZ formulation Captisol®. Our

results show that tPNPs can enhance drug encapsulation at a far lower ratio of drug:CD (1:1 or 1:2 maximum) than Captisol® that requires > 50 fold CD molecules to dissolve the same amount of drug molecules [52]. Captisol® is administered intravenously into patients for several hours of infusion, minimum 4 days per week. The long drug infusion time is attributed to potential side effects of excipients added in a large amount while maintaining plasma drug concentrations for effective treatment. Thus, the higher drug loading content of tPNPs with a lower amount of excipients such as CD would allow for shorter injection time for a larger amount of drug for rapid therapeutic outcomes.

Nanoparticles stored in aqueous solutions often show reduced stability limiting their clinical use [77]. Long-term storage of nanoparticles generally requires conversion of emulsions, nanosuspensions, and nanoparticle solutions into a solid form [78, 79]. Lyophilization is also widely used to enhance shelf-life and stability of nanoparticles. However, all of these methods do not always guarantee the 'pharmaceutical elegance' of nanoparticles such as particle size, integrity, drug retention, and dispersion in solutions prior to injections. Cryoprotectants are often used to prevent aggregation of powered nanoparticles during lyophilization [80, 81]. When nanoparticles are lyophilized in the absence of cryoprotectants, stress aggregation occurs which prevents proper redispersion in aqueous media and thus increases their particle size during solvent sublimation [82, 83]. With these in mind, we tested two cryoprotectants (Trehalose and Mannitol) at different concentrations for lyophilization of tPNPs.

Consistent with literature, a higher concentration of cryoprotectants maintained the integrity of tPNPs after lyophilization [84, 85]. The cryoprotectant concentrations we tested were well below what is commonly used [86-88]. The small particle size of tPNPs

maintained after EpCAM conjugation was also unique. Surface modification of nanoparticles often results in variations in size and particle stability, which negatively affects in vivo drug delivery performance and therapeutic outcomes of nanoparticle formulations. Whereas, tPNPs may prolong blood circulation with minimum disparity among formulation batches and ensure reduced glomerular filtration from the kidney to potentially increase their residence time in tumors [89].

High drug entrapment in tPNPs may be beneficial to reduce the amount of material injected into the body for the same therapeutic outcomes. tPNPs were designed to entrap CFZ by forming a strong inclusion complex in the lipophilic core of HaβCD that are further enveloped in the core of a polyion complex made from cationic CD and anionic block copolymers. Ionic interactions between the amine groups of HaβCD and carboxylic groups on N_3-PEG-PLE self-assemble into nanoparticles producing the 'ternary' system. tPNPs with the unique structure appeared more effective than βCDs to maintain particle integrity for a prolonged time (> 72 h) in cell culture media with serum proteins at 37°C. The improved particle integrity will be beneficial for in vivo applications of tPNPs [54, 69, 90]. tPNPs showed a bimodal drug release profile with a rapid release followed by a sustained release. The ternary structure of tPNPs seems to play a major role to finely tune drug release profiles, and thus further investigation is warranted to achieve more sophisticated drug release control.

Nanoparticles are widely used for drug delivery to tumors with passive targeting, which is mainly driven by the enhanced permeation and retention (EPR) effect. However, studies have reported variations in the EPR effect due to the heterogeneity of tumors [91, 92]. Active tumor targeting has garnered attention recently as an alternative drug delivery

approach, which is achieved by modifying nanoparticles with cancer cell targeting molecules [93]. The overexpression of certain proteins on cancer cells compared to normal cells allows nanoparticles coated with targeting molecule to be taken up by the cells where drug payloads can then be delivered to induce pharmacologic effect [94]. This targeting molecule increases the specificity of these particles to the specific tumor site, allowing them to preferentially accumulate at the desired site where therapeutic agent is needed, consequently, unwanted side effects can be minimized [95]. In this study, we used EpCAM to investigate the effect of targeted delivery on the accumulation of tPNPs in vitro. As shown in Figures 2.9 and 2.10, EpCAM-tPNPs increased intracellular accumulation in comparison to non-targeted tPNPs as well as free dyes. These results suggest greater drug delivery efficiency and selectivity for EpCAM-tPNPs to treat colorectal and other types of cancers overexpressing EpCAM on the cellular membrane [96].

2.5 Conclusion

In this study, we have developed tPNPs as a novel nanoparticle-based delivery formulation for CFZ to address pharmaceutical limitations of the proteasome inhibitor such as solubility, stability, and cytotoxicity against drug resistant colorectal cancer cells. tPNPs significantly improved entrapment yields, biostability, storage, and in vitro efficacy of CFZ as opposed to a CD-based formulation commercially available. Furthermore, tPNPs maintained nanoparticle integrity and stability regardless of drug entrapment and antibody conjugation. These promising results provide a strong basis for future investigation of tPNPs on their in vivo performance to treat various cancers resistant to proteasome inhibitors and other anticancer drugs that are substrates of P-gp.

CHAPTER 3. EFFECTS OF ORGANIC ACIDS ON DRUG RELEASE FROM TERNARY POLYPEPTIDE NANOPARTICLES ENTRAPPING CARFILZOMIB

Portions of this chapter is a modified adaptation from the manuscript previously published in [97]. Reproduced with permission from Elsevier. Copyright © (2021) American Pharmacists Association. Published by Elsevier Inc.

3.1 Introduction

We previously developed ternary polypeptide nanoparticles (tPNPs) as a new injection formulation for CFZ [32]. tPNPs are prepared by entrapping inclusion complexes of CFZ and heptakis(6-amino-6-deoxy)-β-cyclodextrin(hepta-hydrochloride) (HaβCD) in a self-assembling polyion complexes made of poly (ethylene glycol)-conjugated anionic polypeptides such as polyglutamate. CFZ-loaded tPNPs (CFZ-tPNPs) improved entrapment and aqueous solubility of CFZ while extending proteasome inhibition in cancer cells for greater efficacy than free drug and current CD-based formulations [32]. Despite these exciting results, CFZ-tPNPs still need further improvement in suppressing initial burst drug release and extending drug release half-life in an early stage of treatment (approximately 3 h). One possible solution to these problems is to stabilize the core of tPNPs without hampering drug release from the nanoparticles for fast yet prolonged drug responses. In one study, small molecule hydroxy organic acids show a remarkable effect on increasing the solubility of βCD (Figure 3.1) and consequently, its apparent complex stability [98]. We hypothesized that organic acids stabilize polyionic complexes of Haβ-CD and tPNPs and extend drug release half-life for CFZ while suppressing burst drug release (Figure 3.2). This study focuses on determining the effects of organic acids

commonly used in drug formulation design, such as citric acid (CA) and lactic acid (LA), on drug entrapment, drug release profiles, and overall particle stability of CFZ-tPNPs.

We aimed the minimum drug entrapment to be greater than 10 percentage by weight (wt%) for an active pharmaceutical ingredient (i.e. CFZ) with respect to other ingredients in the drug formulation (polymer, CD, and organic acids), which is 5 times greater than the current FDA-approved injection formulation of CFZ[99]. CFZ is a proteasome inhibitor that selectively causes cytotoxic effects on targeted cancer cells, and the drug is less likely to damage non-cancer cells that have low response to proteasome inhibition compared to proliferation cancer cells [40, 100, 101]. Thus, we anticipate that high drug entrapment of CFZ-tPNPs is beneficial to increase drug accumulation in targeted sites in the body such as tumor tissues with reduced toxicity to patients.

In this study, drug release profiles were analyzed to determine drug release half-life ($t_{1/2}$) in the initial stage and later stage ($t_{1/2, fast}$ and $t_{1/2, slow}$), which provide information on burst and sustained drug release, respectively. Small molecule drugs are generally cleared from the body quickly through renal filtration or hepatic degradation. The blood retention half-life of CFZ is between 4-39 minutes when injected intravenously using a CD formulation[53]. Our previous study showed that tPNPs extend $t_{1/2, fast}$ of CFZ up to 3 h[32], and thus tPNPs are expected to extend the blood retention half-life and duration of action for CFZ by protecting the proteasome inhibitor in the body. We expect that tPNPs stabilized by organic acids may further suppress the drug fast release half-life due to improved particle stability. CA and LA were selected as organic acids for testing the half-life in simulation because the toxicity profiles of these acids as excipients are reported minimal[102-105]. Particle stability is assessed in pH-controlled buffer solutions

mimicking in vivo conditions by measuring particle size before and after freeze drying of drug-loaded nanoparticles. We also monitored the particle stability in the presence and absence of drug to better investigate interactions between organic acids and drugs inside the nanoparticle. We determined particle stability after lyophilization of CFZ-tPNPs because freeze drying is important for long storage of drug-loaded nanoparticles for clinical applications[80, 106]. Freeze-dried CFZ-tPNPs were then reconstituted in a buffer solution to determine drug concentrations. All data was obtained from triplicate experiments and reported as mean values with standard deviations.

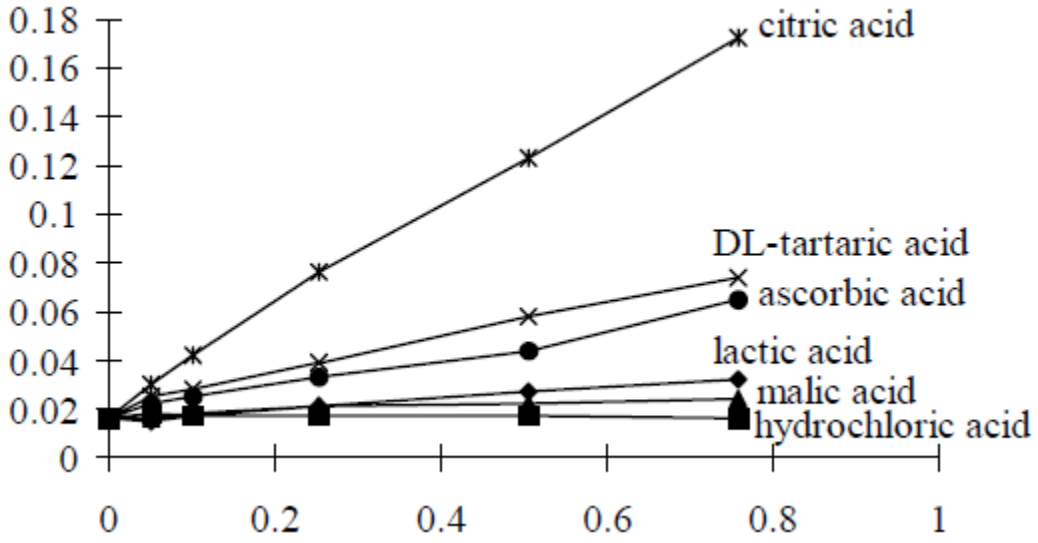

Figure 3.1. Solubility of βCD in solutions of hydroxy acids and HCL as a function of acid concentration. With permission from Fenyvesi E, Vikmon M, Szeman J, Redenti E, Delcanale M, Ventura P, Szejtli J. Interaction of hydroxy acids with β-cyclodextrin. *Journal of inclusion phenomena and macrocyclic chemistry*. 1999 Mar;33(3):339-44.

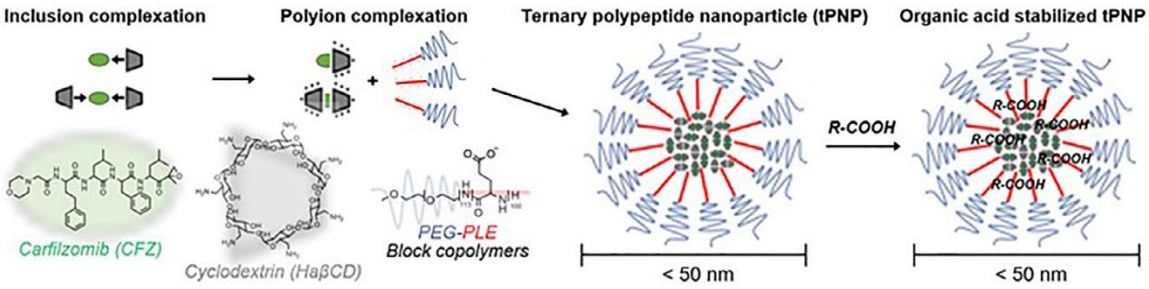

Figure 3.2. Preparation of organic acid stabilized tPNPs for improved particle stability and drug retention.

3.2 Materials and Methods

3.2.1 Materials

Carfilzomib (free base, >99%) was purchased from LC Laboratories (Woburn, MA). Poly (ethylene glycol)-block-poly (L-glutamic acid sodium salt) with 5 kDa PEG and 100 repeating units of glutamate (PEG-PLE) was purchased from Alamanda Polymers (Huntsville, AL). Heptakis (6-deoxy-6-amino)-beta-cyclodextrin heptahydrochloride (Haβ-CD) was purchased from Cyclolab R&D Laboratory Ltd. (Budapest, Hungary). Citric acid was purchased from EM Science (Gibbstown, NJ). LA was purchased from Spectrum (Gardena, CA). Slide-A-Lyzer MINI Dialysis Units 20,000 MWCO and HPLC grade water were purchased from Thermo Fisher Scientific (Rockford, IL).

3.2.2 Nanoparticle preparation

Nanoparticles were prepared by a modified nanoprecipitation method. For empty tPNPs, the starting procedure was as follows. Haβ -CD (4 mg) and PEG-PLE (2 mg) both dissolved in deionized water at a concentration of 10 mg/mL were mixed in a 1.5 mL conical tube. The resulting mixture was sonicated in a bath sonicator to form drug free tPNPs. For drug-loaded nanoparticles, 5 different CFZ/tPNPs were prepared following the method we previously reported [32]. Briefly, CFZ and Haβ-CD were dissolved in ethanol and water respectively, and the solutions were mixed in a 50 mL round bottom flask to form inclusion complexes at a drug to cyclodextrin mass ratio of 1:4. Organic acids (CA and LA) were added to the flask to stabilize the complexes. The mixing ratio of CA and LA was determined to neutralize the net charge in the nanoparticle core. The mixed

solution was evaporated using a rotary evaporator under reduced pressure at 60°C to remove ethanol. m-PEG-PLE (2 mg) was then added to the flask and sonicated for 2 minutes to form self-assembled CFZ/tPNPs. CFZ/tPNPs were transferred into 1.5 mL conical tubes. A 5% (w/v) trehalose solution was added to the tube followed by flash freezing in dry ice for 4 h. Frozen CFZ/tPNPs was lyophilized using a Labconco FreeZone freeze drying system. Freeze-dried CFZ/tPNPs were weighed and stored in a -20°C freezer until use. Lyophilization was employed to enhance the stability of CFZ/tPNPs. Our previous study showed that a 5% trehalose solution used as cryoprotectant performed best in maintaining the physiochemical properties of CFZ/tPNPs after freeze-drying compared to before [32]. Briefly, a 5% (w/v) trehalose solution was added to CFZ/tPNPs followed by flash freezing in dry ice (-78.5ºC) for 4 h. Frozen CFZ/tPNPs was lyophilized using a Labconco FreeZone freeze drying system. The samples were lyophilized overnight at a primary drying temperature of -50ºC and vacuum pressure of 0.02 mbar, followed by secondary drying phase of 25ºC for 24 hours and maximum vacuum. Freeze-dried CFZ/tPNPs were weighed and stored in a -20°C freezer until use.

3.2.3 Particle size measurement

The Zetasizer Nano ZS (Malvern, UK) was used to obtain particle characteristics. This instrument measures molecular size, molecular weight, particle size and zeta potential using dynamic light scattering (DLS). DLS was used for characterization of the nanoparticle in its liquid phase [107]. The freeze-dried tPNPs were reconstituted in PBS (10mM, pH 7.4) to a final concentration of 2 mg/mL to achieve this liquid phase. The

suspension was exposed to an electromagnetic wave causing the light beam to scatter. From this scattering, a diffusion coefficient of the particles is determined with an equation $f = kBT/ 6\pi\eta R_H$ to find the hydrostatic radius. The range of hydrostatic radius detected by DLS is between 0.3 nm to 10 µm, while parameters on the Zetasizer were set to 173º backscatter and 25ºC temperature. The reconstituted sample was placed in a DTS 1070 cuvette for particle size analysis. Each sample was measured in triplicate and data was recorded as mean ± S.D.

3.2.4 Drug loading quantification

Freeze-dried CFZ/tPNP were reconstituted in saline. High performance liquid chromatography (HPLC) was used to determine the amount of CFZ in the nanoparticle. The mobile phase of the HPLC was an isocratic mixture of acetonitrile and water (ACN: water = 55:45, 1% formic acid, 0.5 mL/min, Agent Eclipse XDB-C18 column). Drug peaks were integrated at a wavelength of 210 nm and elution time was around 3.4 minutes. A calibration curve of known concentrations of CFZ (0.03 - 1 mg/ml) was used to determine the amount of CFZ loaded in the freeze-dried tPNPs. Encapsulation efficiency was calculated as the percentage of drug encapsulated to the drug added in preparation. Drug loading efficiency was defined as the percentage of drug by weight of drug encapsulated to the weight of tPNP. All samples were measured in triplicate and data were summarized by mean ± S.D.

3.2.5 Effects of buffers on particle stability and drug release kinetics

Freeze-dried CFZ/tPNPs were reconstituted in different buffers and the dissolved nanoparticles were first observed visually to see how fast they aggregated over time. Buffers used for stability assessment were tris buffered saline (TBS), phosphate buffered saline (PBS), normal saline (NS) and citrate buffer (CB). Particle size was also measured with DLS as described above to determine stability in these buffers. In parallel, drug release kinetics were analyzed for of CFZ/tPNPs by using the dynamic dialysis method [108]. Briefly, freshly prepared tPNPs were reconstituted in potassium biphthalate sodium hydroxide buffer (pH 7.4, 5 mM) to a concentration of 10 mg/mL. Reconstituted CFZ/tPNPs were transferred to Thermo Scientific™ Slide-A-Lyzer™ MINI Dialysis Cups (20,000 MWCO) and placed in buffer (37°C, pH 7.4) to be dialyzed under sink conditions. At predetermined timepoints of 0, 0.5, 1, 3, 6, 24, 48, 72 h, samples were collected from the dialysis cups and drug remaining was determined by HPLC method described above. Drug remaining for each time point was normalized to the value obtained at t = 0 h. Drug release profiles were obtained by fitting the curve to an exponential decay using GraphPad Prism 9 software.

3.3 Results

3.3.1 Preparation of CFZ/tPNPs using organic acids

Zetasizer analysis of particle size showed tPNPs with less than 60 nm in diameter for all formulations with a size range between 33 nm and 55 nm. The average size of empty tPNPs was 46.1 ± 4.0 nm. CFZ precipitated after ethanol was evaporated without the inclusion of small molecule organic acids in our preparation. Therefore, organic acids were added to the formulations to prevent precipitation of CFZ from solution and enhance particle stability. Several organic acids were tested in preliminary studies, such as CA, LA, malic acid, maleic acid, succinic acid, and tartaric acid. Among these acids, CA, LA, and tartaric acid were successful in preventing precipitation during ethanol evaporation. However, tartaric acid required extensive sonication after freeze-drying to facilitate complete dissolution of particles. tPNPs prepared using CA and LA prevented precipitation of CFZ and dissolved readily with vortexing. The incorporation of CA and LA did not adversely affect particle size distribution for all combinations. Average particle size after the addition of these organic acids and CFZ was 41.1 ± 8.7nm. The distribution was unimodal with a Gaussian profile. Figure 3.3 shows the particle size distribution for tPNPs with various combinations of CA and LA.

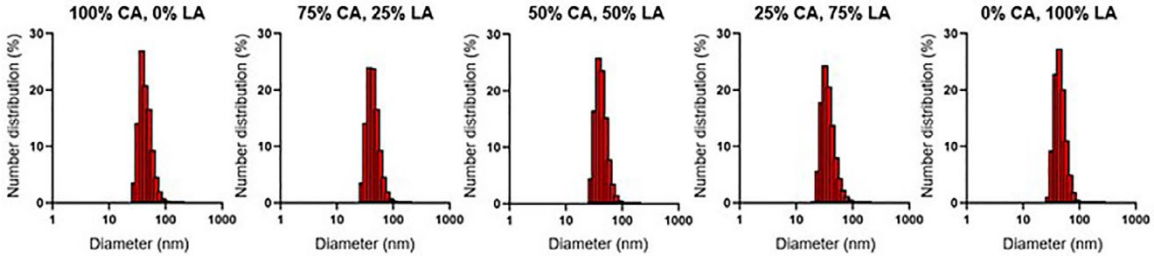

Figure 3.3. Particle size distribution of nanoparticles prepared using various combination of citric acid and lactic acid.

3.3.2 Effect of buffers on particle stability

CFZ/tPNPs were observed to see how fast they aggregated after reconstitution in various buffers. Tris buffer was unable to dissolve CFZ/tPNPs as indicated in its very large particle size (Figure 3.4). This is due to the amine groups in tris buffer disrupting the polyionic complex between Haβ-CD and PEG-PLE and breaking up the nanoparticles. PBS completely dissolved CFZ/tPNPs as no particles were seen in tube, but CFZ/tPNPs dissolved in PBS began to aggregate within 1 h after reconstitution and vortexing. Sonication was employed to enhance particle stability in PBS, but aggregation still occurred within 1 h. Citrate buffer and normal saline also completely dissolved CFZ/tPNPs. CFZ/tPNPs dissolved in citrate buffer and normal saline remained in solution for over 24 h.

3.3.3 Drug loading quantification

HPLC analysis revealed that CFZ was successfully entrapped in organic acid stabilized tPNPs. The calibration curve from known concentrations of CFZ was used to determine drug concentrations. CFZ/tPNPs for all combinations of CA and LA showed a drug loading average above 1 mg/mL indicating a high encapsulation efficiency. Drug loading efficiency of all CFZ/tPNPs was about 13 wt%. Physiochemical properties of tPNPs are summarized in Table 3.1.

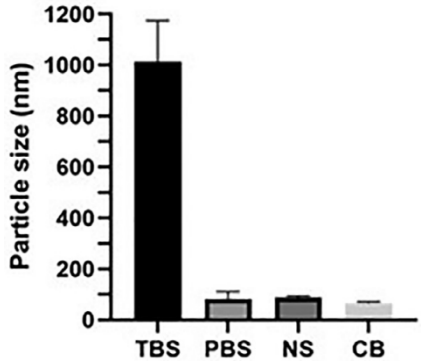

Figure 3.4. Particle stability in various buffers such as tris buffered saline (TBS), phosphate buffered saline (PBS), normal saline (NS) and citrate buffer (CB).

Table 3.1. Physiochemical properties of CFZ/tPNPs prepared by using different combinations of citric acid and lactic acid.

Formulation	CA (%): LA (%)	Particle size (nm)	PDI	Drug loading (mg/mL)
Empty tPNPs	-	46.1 ± 4.0	0.043	-
	100:0	33.7 ± 3.3	0.182	1.16 ± 0.23
	75:25	38.1 ± 5.8	0.313	0.94 ± 0.18
CFZ/tPNPs	50:50	55.8 ± 2.1	0.301	0.93 ± 0.05
	25:75	41.9 ± 7.9	0.364	1.06 ± 0.06
	0:100	36.1 ± 3.0	0.356	0.89 ± 0.16

3.3.4 Drug release

All tPNPs prepared showed a biphasic drug release profile with an initial burst followed by sustained release shown as $t_{1/2, fast}$ and $t_{1/2, slow}$, respectively (Figure 3.5). $t_{1/2, fast}$ for initial burst release was evaluated within the first 1 h, followed by determining $t_{1/2, slow}$ for slow drug release for 72 h. Figure 3.5 indicates that pure organic acids (100% CA or 100%LA) had the shortest burst release. The longest burst release was with 75% CA and 25% LA. Results with the inset displayed that using a ratio of organic acids produced greater efficacy in burst release reduction compared to pure organic acids. As summarized in Table 3.2, the half-life slow reduced as a function of CA proportion in tPNPs. Fast drug release was suppressed in all formulations except tPNPs with 100% LA, while half-life slow was delayed with the type or ratio of organic acids. tPNPs prepared with 100% CA had the longest half-life slow, and the formulation with 100% LA showed the shortest half-life slow.

3.3.5 Effect of mixing ratio on drug remaining after 24 h post incubation

The percent of drug remaining at 24 h was greater for tPNPs with mixed CA:LA than tPNPs with single acid. tPNPs with higher CA% contained more CFZ. The plateau of the tPNP with 75%CA:25%LA contained the highest amount of CFZ after 24 h, with 50%CA:50%LA and the 25%CA/75%LA formulations following respectively (Figure 3.6). Nanoparticles containing single organic acids reduced the initial burst release but did not have as much drug remaining after 24 h. tPNPs containing 100% CA and 100% LA

contained ~35% and ~57% respectively at 24 h. Although the burst release was lengthened, single organic acid tPNPs contained less than the ratioed organic acid tPNPs which contained between ~80-95% of drug after 1 h.

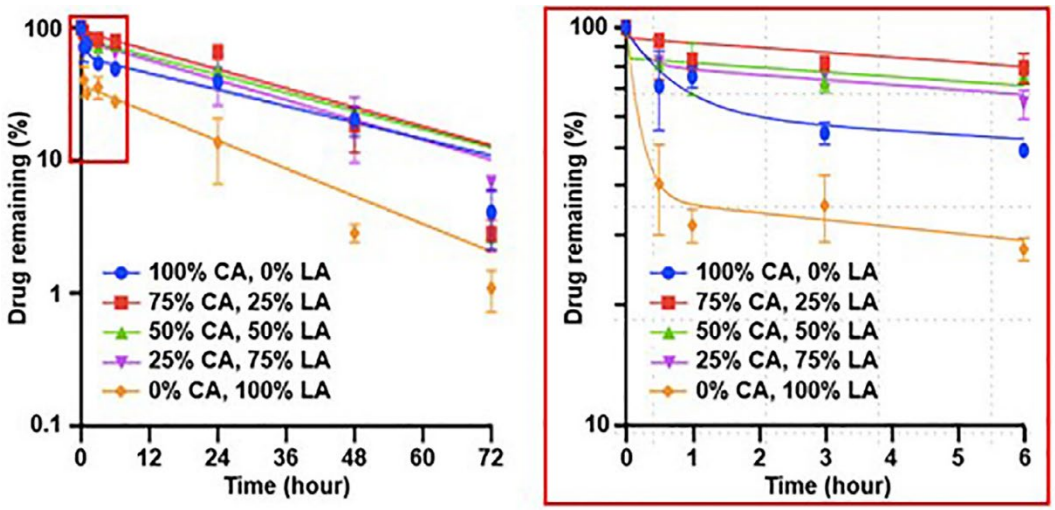

Figure 3.5. Drug release profiles for tPNPs with organic acids at various mixing ratios (enlarged view of inset for initial 6 h post incubation).

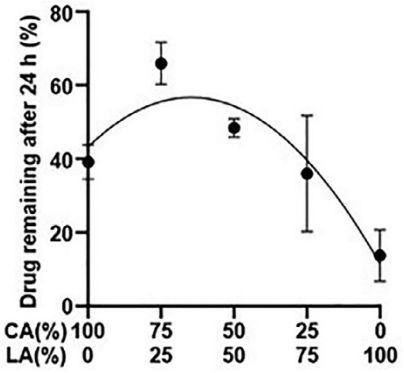

Figure 3.6. Drug entrapment assessment (% of CFZ remaining at t = 24 h)

Table 3.2. Kinetic parameters for CFZ release from tPNPs with organic acids at various mixing ratios.

Formulation	CA (%): LA (%)	K_{fast} (h^{-1})	K_{slow} (h^{-1})	$t_{1/2, fast}$ (h)	$t_{1/2, slow}$ (h)
	100:0	1.54	0.0239	0.45 ± 0.11	29.06 ± 6.18
	75:25	4.09	0.0249	0.15 ± 0.05	27.88 ± 4.34
CFZ/tPNPs	50:50	4.23	0.0275	0.18 ± 0.10	26.29 ± 5.61
	25:75	4.46	0.0325	0.16 ± 0.09	24.10 ± 3.81
	0:100	5.36	0.0402	0.13 ± 0.07	17.26 ± 3.90

3.4 Discussion

CFZ was approved by the FDA for the treatment of multiple myeloma due to the higher efficacy and lower toxicity than the first in class proteasome inhibitor Bortezomib[39]. Because of its success in multiple myeloma patients, CFZ has been further studied for the treatment of solid tumors and metastatic diseases. Despite promising pre-clinical data, CFZ achieved limited success in solid tumor treatment in the clinic potentially due to pharmaceutical limitations such as low solubility, poor biostability, and short release half-life, which lowered therapeutic outcomes[44-46]. Previous studies suggest that nanoparticle formulations can improve therapeutic efficacy of small molecule drugs by fine-tuning the in vivo drug release rates[109-115], which would better control tumor accumulation, body clearance, and toxicity of various anticancer drugs[116-121]. Unfortunately, few injection formulations are currently available that can safely increase drug retention in the body to maximize therapeutic potential and overcome clinical limitations of CFZ.

We previously reported that nanoparticle injection formulations made of tPNPs have great potential to address these problems because they can improve water solubility, biostability, and tumor accumulation of hydrophobic drugs including CFZ [32, 54, 57, 122-124]. In this study, we confirmed that organic acid stabilized CFZ/tPNPs can prevent rapid degradation of the epoxyketone pharmacophore of CFZ and degradation of its tetrapeptide chain, which is beneficial to increase therapeutic efficacy of CFZ. We particularly assessed the potential utility of tPNPs to improve the entrapment and drug release half-life of CFZ.

tPNPs were designed by supramolecular interactions, comprising the formation of inclusion complex between CFZ and HaβCD followed by ionic interactions between amine

groups of HaβCD and carboxylic groups of polyglutamate. By utilizing organic acids such as CA and LA, we aimed to improve particle stability and extend drug release half-life of CFZ from tPNP. In some studies, CA has been shown to be effective in stabilizing nanoformulations [125-128]. Three carboxylic acid groups of CA can stabilize the core of nanoparticles by surface adsorption and steric stabilization[126]. LA has previously garnered some attention in biomedical research due to its involvement in cellular metabolism in the human body, and its ability to mitigate adverse reactions[129].

Our findings indicate that CFZ/tPNPs for all combinations of CA and LA maintained a sub 50 nm particle size and inclusion of these additives did not adversely change particle size compared to drug free tPNPs. This shows efficient entrapment of CFZ within the core of HaβCD and stabilization with organic acids. Particle size is an important factor for nanoparticle biodistribution and circulation time in the body which determines therapeutic efficacy[130, 131]. Maintaining particle size below 50 nm is important because reports have shown that large nanoparticles (> 150 nm) are susceptible to plasma protein adsorption and opsonization leading to uptake by the liver [121, 132]. On the other hand, sub 50 nm particles have been shown to have reduced blood clearance by macrophages[133, 134].Our findings indicate that CFZ/tPNPs for all combinations of CA and LA maintained a sub 50 nm particle size and inclusion of these additives did not adversely change particle size compared to drug free tPNPs. Our findings indicate that CFZ/tPNPs for all combinations of CA and LA maintained a sub 50 nm particle size and inclusion of these additives did not adversely change particle size compared to drug free tPNPs. This shows efficient entrapment of CFZ within the core of HaβCD and stabilization with organic acids. Particle size is an important factor for nanoparticle biodistribution and

circulation time in the body which determines therapeutic efficacy [130, 131]. Maintaining particle size below 50 nm is important because reports have shown that large nanoparticles (> 150 nm) are susceptible to plasma protein adsorption and opsonization leading to uptake by the liver [121, 132]. On the other hand, sub 50 nm particles have been shown to have reduced blood clearance by macrophages [133, 134].Our findings indicate that CFZ/tPNPs for all combinations of CA and LA maintained a sub 50 nm particle size and inclusion of these additives did not adversely change particle size compared to drug free tPNPs. This shows efficient entrapment of CFZ within the core of HaβCD and stabilization with organic acids. Particle size is an important factor for nanoparticle biodistribution and circulation time in the body which determines therapeutic efficacy [130, 131]. Maintaining particle size below 50 nm is important because reports have shown that large nanoparticles (> 150 nm) are susceptible to plasma protein adsorption and opsonization leading to uptake by the liver [121, 132]. On the other hand, sub 50 nm particles have been shown to have reduced blood clearance by macrophages [133, 134].

Our results demonstrated a high drug loading of CFZ in tPNPs. All CFZ/tPNPs showed a drug loading approximately 1 mg/mL regardless of the CA to LA ratio. This translates to a very high encapsulation efficiency. Many nanoparticle systems have low to moderate encapsulation efficiency which limits the concentration of cytotoxic agents accumulating in tumors. CFZ/tPNPs have the potential to improve the accumulation of CFZ in solid tumors. The small size also allows it to have longer circulating time to offload its payload all together enhancing therapeutic efficacy.

We tested the stability of CFZ/tPNPs in different buffers. tPNPs were formed by the self-assembling process through ionic interactions between amine groups and

carboxylic acid groups. CFZ/tPNPs dissolved in TBS showed poor stability as indicated by particle size. This is due to the competition between the amine group of TBS and the amine group on the surface of HaβCD, which disrupts the formation of ionic interaction needed for tPNPs. PBS performed better than TBS, but we observed aggregation of CFZ/tPNPs within 3 h of reconstitution in buffer. This is likely due to counter ions present in PBS slowly infiltrating and disrupting ionic interactions in tPNPs. NS and CB performed optimally in stabilizing tPNPs and remained stable over 24 h.

Drug release profiles are important predictors of the stability and usefulness of drug delivery systems and how they modulate drug concentrations *in vivo* [135]. We aimed to improve the half-life of CFZ release from tPNPs. CA alone showed best performance in producing a sustained release of CFZ with a half-life of almost 30 h. This is a significant improvement over the current commercial CFZ formulation which has a half-life less than 1 h. Slow half-life reduced with increasing proportion of LA, and tPNPs made with 100% LA had the shortest slow half-life. However, CA and LA seemed to have a synergistic effect in reducing burst release. Using CA and LA at a 3 to1 ratio appeared to suppress the burst release 3-fold better than 100% CA. In addition, it has a comparable slow half-life (~ 28 h) to 100% CA. This 3 to 1 combination of CA to LA also showed the highest amount of drug remaining after 24 h. These results suggest that preparing CFZ/tPNPs with this combination of organic acids produced the most stable formulation.

3.5 Conclusion

tPNPs stabilized by CA and LA in mixture were found to improve the entrapment and drug release half-life for CFZ, which has few injection formulations for maximum therapeutic outcomes *in vivo*. The organic acid stabilized tPNPs formed sub-60 nm particles with > 1 mg/ml CFZ. The type and mixing ratio of organic acids appeared to mainly affect tPNP stability and drug release kinetics rather than charge density, which suggests that chemical structures of organic acids and drugs entrapped in the core of nanoparticle may play a major role in modulating entrapment and release of CFZ from tPNP. These findings are significant because organic acid-stabilized tPNPs having small particle size with high drug loading may expand the *in vivo* utility of CFZ and potentially other proteasome inhibitors from treating blood cancers to solid cancers.

CHAPTER 4. CARFILZOMIB-LOADED TERNARY POLYPEPTIDE NANOPARTICLES STABILIZED BY POLYCATIONIC COMPLEXATION

4.1 Introduction

As shown in the previous chapter, we developed CFZ loaded ternary polypeptide nanoparticles stabilized by small molecule organic acids such as citric acid and lactic acid [19]. However, CFZ/tPNPs need further stabilization to improve drug release half-life and further suppress burst drug release.

Many studies show that utilizing hydrophilic polymers in drug-cyclodextrin complexes increases the affinity of the drug for the hydrophobic cavity of cyclodextrins [136-140]. It does this by stabilizing the complex aggregates and as such increases drug solubility [141]. Additionally, from a manufacturing point of view, addition of hydrophilic polymers reduces the cost of production by minimizing the amount of cyclodextrin needed for drug solubilization [142].

In this study, we designed tPNPs comprised of amine substituted β-cyclodextrin, biocompatible and biodegradable polypeptides poly (L-glutamic acid) that self-assemble in solution (Figure 4.1). These nanoparticles have a well-defined structure with uniform particle size, high drug loading and stability. CFZ/tPNPs were further stabilized by cationic polymers with varying pKa values, which was intended to stabilize the core of tPNPs. Due to the acid-responsiveness of cationic polymer, we expect the release of CFZ from CFZ/tPNPs in cancer cells specifically in an intracellular pH-accelerated manner. Previously, acid-sensitive nanoparticles have garnered research attention due to the change in pH inherent in different cell layers. In systemic circulation, nanoparticles are exposed to pH 7.4. Once they are endocytosed into cells, the pH drops from 7.4 to 6.5 in

the early endosomes and 5.0 in the lysosome [143, 144]. Even more, extracellular regions such as tumor microenvironment have been shown to be slightly acidic (pH 6.4 - 6.8) [144]. Nanoparticles can be designed to be pH responsive by changing surface or core chemistry, and by so doing, drug payload can be released in response to pH changes [145]. Therefore, pH responsive nanoparticles provide an option to deliver therapeutics to tumor with specific stimuli that may be different from normal cells, increasing therapeutic efficacy and reducing toxicity.

In this study, three polycations were used as stabilizing agents for CFZ/tPNPs. We explored the use of methoxy-poly (ethylene glycol)-block-poly (L-lysine hydrochloride) (PLL) which is a highly hydrophilic graft copolymer as a molecule to improve CFZ/tPNP stability. PLL has been shown to decrease the large surface energy associated with nanoparticles [133, 146, 147]. Additionally, the use of PLL lies in its biocompatibility and its capability to reduce immunogenicity if used as a backbone for covalent linking to molecules on its amino groups [148]. Poly(L-histidine)-A-Ω-Bis-(Amino)-Terminated (PHis) was selected because of its strong endosomolytic property by its proton sponge effect [149]. Furthermore, PHis are a biocompatible material used for the construction of pH-responsive nanocarriers [150-152]. Although polyethyleneimine (PEI) is commonly used in nucleotide gene delivery, it also has wide application in stabilizing colloidal nanocarriers due to its high amine group density [153-156].

We expect that CFZ/tPNPs stabilized by polycations will show uniform physiochemical properties such as particle size, surface charge and drug loading. We also expect that polycations will produce improved drug release half-life in physiological pH, which will consequently enhance drug efficacy in proteasome inhibition.

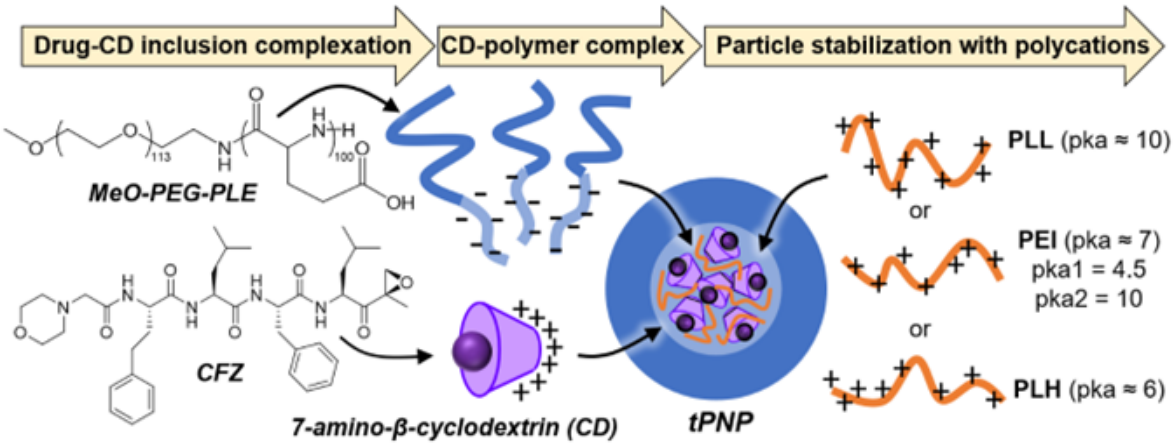

Figure 4.1. Design of CFZ-loaded tPNPs stabilized by polyion complexation

4.2 Materials and Methods

4.2.1 Materials

Potassium biphthalate sodium hydroxide buffer and HPLC grade water were obtained from Fisher Scientific (Fair-lawn, NJ). Slide-A-Lyzer Mini Dialysis Units (20,000 MWCO) was obtained from Thermo Scientific (Rockford, IL). Heptakis (6-amino-6-deoxy)-β-CD heptahydrochloride (HaβCD) was purchased from Cyclolab R&D Laboratory Ltd. (Budapest, Hungary). Citric acid was obtained from EM Science (Gibbstown, NJ). CFZ was purchased from LC laboratories (Woburn, MA). Methoxy-poly (ethylene glycol)-block-poly (L-glutamic acid sodium salt) (PLE), Methoxy-poly (ethylene glycol)-block-poly (L-lysine hydrochloride) (PLL) was purchased from Alamanda Polymers (Huntsville, AL). Poly(L-histidine)-A-Ω-Bis-(amino)-Terminated (PHis) was purchased from Polymer Source Inc (Montreal, Canada). Linear polyethyleneimine (PEI) was purchased from Polysciences Inc (Warrington, PA).

4.2.2 Cell culture

Human colorectal adenocarcinoma cell (DLD1) was cultured in RPMI-1640 medium supplemented with 10% fetal bovine serum, 1% sodium pyruvate and 1% penicillin-streptomycin at 37°C in a humidified incubator with 5% CO_2. The cells were maintained in an exponential growth phase by periodic sub-cultivation. For DLD1 CFZ/resistant cells, parent DLD1 cells were treated with increasing amount of CFZ for about 4 months until cells were resistant at a concentration of 1 μM.

4.2.3 Preparation of tPNPs

tPNPs were prepared by using a modified solvent evaporation method. Briefly, CFZ dissolved in ethanol was added to HaβCD solution at a 1:4 mass ratio in a 50 mL round bottom flask. Citric acid was added to the mixture to facilitate inclusion complex formation followed by sonication for 2 minutes. Ethanol in the solution was removed by using a rotary evaporation system at a reduced pressure and 60°C. Rotary evaporation was repeated followed by addition of m-PEG-PLL and m-PEG-PLE to make nanoparticles (Figure 4.1). The resultant CFZ/tPNPs were sonicated for 5 minutes and collected by freeze drying overnight (Labconco Freezone®) using sucrose as the cryoprotectant to obtain a fine powder of NPs which was then stored in a -20°C to protect from degradation. For freeze-drying, 2% (w/v) sucrose was added to CFZ/tPNPs followed by flash freezing in dry ice (-79°C) for 4 h. Subsequently, frozen CFZ/tPNPs was lyophilized overnight with a primary drying temperature of -50°C and vacuum pressure of 0.03 mTorr, followed by secondary drying at 25°C for 24 h. tPNPs were stabilized by three polymers such as PLL, PHis, and PEI, which have distinctive pKa values allowing for acid-responsiveness.

4.2.4 Particle size and zeta potential determination

The particle size and surface charge of tPNPs with and without CFZ were measured by dynamic light scattering (DLS, Zetasizer Nano ZS, Malvern, UK). Freeze-dried CFZ/tPNPs were resuspended in normal saline and sonicated to a concentration of 2 mg/mL. The resultant suspension was placed in a folded capillary cuvette and measurement

parameters were set to 173° backscatter and a temperature of 25°C for both particle size and zeta potential. PDI was also calculated with the accompanying software.

4.2.5 Drug loading and encapsulation efficiency

Drug loading of CFZ/tPNPs was determined by high performance liquid chromatography (HPLC; Agilent XDB-C18). The mobile phase consisted of water and acetonitrile with 0.1% formic acid. Using an isocratic method of 55:45 ACN: H_2O at a flow rate of 0.5 mL/min, CFZ was eluted at a retention time of 3.6 minutes. Drug concentrations were measured by integrating peaks at a wavelength of 210 nm and the area was compared to a calibration curve of known CFZ drug concentration. Drug loading efficiency was defined as the percentage of CFZ encapsulated to the weight of nanoparticles, and encapsulation efficiency was defined as the percentage of drug encapsulated to drug added. Data obtained are represented as mean ± SD.

4.2.6 Drug release confirmation

CFZ release kinetics was determined as previously reported [36]. Briefly, freeze-dried CFZ/PLL-tPNP, CFZ/PHis-tPNP, and CFZ/PEI-tPNP were dissolved in PBS (pH 7.4, 10 mM) at 10 mg/mL and placed in dialysis cups (MWCO 20kDa). The dialysis cups were then placed in 4 L PBS buffer at pH 7.4, 6.0 or 5.0 at 37°C, to simulate physiological and sink conditions. Nanoparticle solutions were retrieved at 0, 0.5, 1, 3, 6, 24, 48 and 72 h and drug remaining were measured using the HPLC method described above. Percent drug remaining at each time point was calculated as a normalized value of drug remaining

compared to drug concentration at t = 0 h. The release profiles were fitted to an exponential decay with GraphPad Prism 9 software.

4.2.7 Cell viability determination

CFZ-resistant DLD1 cells were cultured in the absence of drug for 9 days prior to starting the assay. On the ninth day, DLD1 cells were harvested and seeded in 96 well plate at a seeding density of 5,000 cells per well. Following attachment overnight, the cells were treated with serial dilutions of free CFZ, CFZ/PLL-tPNP, CFZ/PHis-tPNP, and CFZ/PEI-tPNP. The MTS assay (Promega) was used to determine cell viability and calculate IC_{50} values. Briefly, after cell incubation for 96 hours, 20 µL of MTS dyes was added to each well and the plates were placed in an incubator at 37°C and 5% CO_2 for 2 h. Absorbance was measured at 490 nm using a plate reader (Spectra Max M5). IC_{50} values were calculated by a non-linear regression method using GraphPad Prism 9 software.

4.2.8 Proteasome activity assay

DLD1 cells were grown in the presence of CFZ at 1 µM until drug resistance was gained. The cells were grown for 9 days without CFZ and then seeded at 150,000 cells/well in a 6-well plate for additional 24 h. The cells were treated with 0.5 µM of free CFZ, CFZ/PLL-tPNP, CFZ/PHis-tPNP, and CFZ/PEI-tPNP and incubated at 37°C with 5% CO_2. The cells were harvested at 6, 48, 72, and 96 h. Cell pellets were washed in DPBS and stored at -20°C until they were lysed with 1x Passive Lysis Buffer. The total protein was determined through a Bradford assay. When conducting the proteasome activity assay, 5 µg of protein was collected from each sample and the activity was measured following treatment with

100 μM of Suc-LLVY-AMC substrate. Fluorescence reading at a kinetic rate of 1 reading per minute was obtained at an excitation and emission wavelength of 360 and 460 nm respectively (Spectra Max M5). Proteasome activity was measured as the relative fluorescence compared to that of untreated cells.

4.3 Results

4.3.1 Physiochemical characterization of tPNPs

Cationic polymers were used to improve stability of ternary polypeptide nanoparticles [32]. Out of several polymers tested in preliminary studies, we selected PLL, PHis and PEI because they showed no precipitation of tPNPs after drug loading. All freeze-dried CFZ/tPNPs readily dissolved in aqueous solutions with simple vortexing and showed a unimodal particle size distribution (Figure 4.2). The particle size of empty and all CFZ/tPNPs was less than 100 nm (Table 4.1), which is suitable for tumor-specific drug delivery following intravenous injection [157]. The surface charge of all CFZ/tPNPs was neutral, which is favorable for prolonged survival in biological systems [90].

4.3.2 Drug loading and entrapment efficiency

The amount of CFZ loaded in tPNPs was calculated using the formulas described in the methods section. CFZ/PLL-tPNP, CFZ/PHis-tPNP and CFZ/PEI-tPNP had drug loading of 11.44%, 9.80% and 8.95% respectively. Correspondingly, the encapsulation efficiencies of CFZ/PLL-tPNP, CFZ/PHis-tPNP, CFZ/PEI-tPNP was 95.3%, 91.0% and 80.3% respectively. This indicates that incorporation of these polycations to the nanoparticle enhanced the hydrophobic interactions within the nanoparticle core, allowing a higher solubilization of CFZ.

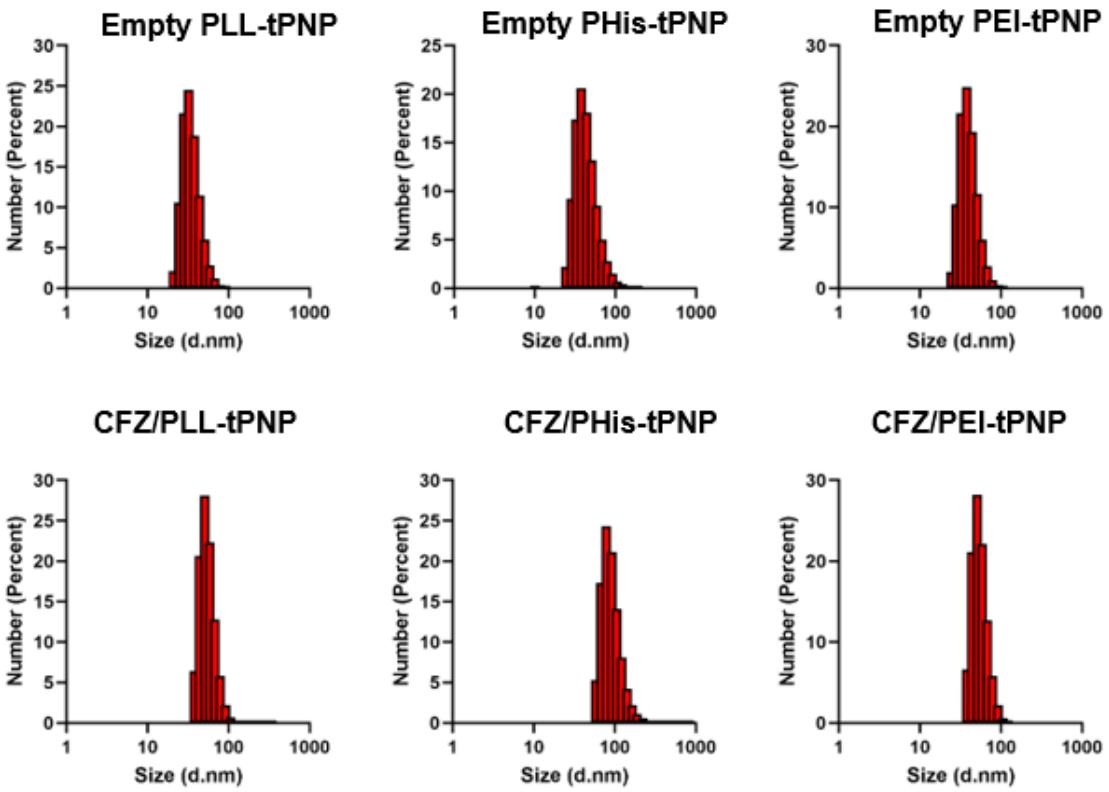

Figure 4.2. Histogram showing size distribution of polyion stabilized empty and CFZ/tPNPs

Table 4.1. Physiochemical properties of polyion stabilized tPNPs

Formulation	Particle size (nm)	PDI	Zeta potential (mV)	Drug loading capacity (%)	Entrapment efficiency (%)
Empty PLL-tPNP	34.9 ± 3.0	0.09 ± 0.03	-0.69 ± 0.40	-	-
CFZ/PLL-tPNP	54.2 ± 12.5	0.69 ±0.01	-1.02 ± 0.43	11.44 ± 0.48	95.3 ± 2.3
Empty PEI-tPNP	34.0 ± 3.3	0.20 ± 0.03	-1.07 ± 0.37	-	-
CFZ/PEI-tPNP	56.52 ± 9.8	0.48 ± 0.04	2.86 ± 0.49	8.95 ± 0.92	80.3 ± 4.5
Empty PLH-tPNP	41.8 ± 3.5	0.26 ± 0.01	-1.63 ± 0.40	-	-
CFZ/PLH-tPNP	91.9 ± 13.5	0.63 ± 0.05	-1.59 ± 0.29	9.80 ± 0.98	91.0 ± 3.2

4.3.3 Drug release of CFZ from tPNPs

Drug release from tPNPs was studied in PBS buffers at 37°C under three pH conditions mimicking the physiological (7.4), tumor tissue acidosis (6.0), and intracellular lysosomes (5.0). The release rate of all CFZ/tPNPs appeared pH dependent and generally increased as pH decreased (Figure 4.3). CFZ/PLL-tPNP showed no burst release and maintained a sustained release over the testing period of 72 h with CFZ/PLL-tPNP having an average slow-release half-life of 44 h (Table 4.2). Reduction of pH showed a bi-phasic release profile for CFZ/PLL-tPNP which is indicative of burst release. After burst release, a sustained release is achieved at pH 6.0 and 5.0 having corresponding slow half-lives of 25 h and 19 h respectively. CFZ/PHis-tPNP appeared less stable than CFZ/PLL-tPNP. At the physiological pH, CFZ/PHis-tPNP showed a burst release half-life less than 1 h. Following the initial burst release, CFZ/PHis-tPNP had a controlled release with slow half-life of 48 h. At pH 6.0 the fast half-life was 0.32 h which is similar to the fast half-life at pH 7.4, however, there is a clear pH dependent reduction in half-life (17.64 h) after the initial burst release. CFZ/PHis-tPNP was unstable when the pH was reduced to 5.0. The particles disintegrated rapidly causing the release of CFZ into media. CFZ/PEI-tPNP also showed a biphasic release profile for all three pH levels tested which indicates a burst release followed by sustained release. Compared to the other two formulations, CFZ/PEI-tPNP had the shortest slow half-life of 30 h at pH 7.4. With CFZ/PEI-tPNP there is also a pH dependent slow half-life of 16 h and 7.5 h at pH 6.0 and 5.0, respectively. Kinetic parameters of all formulations are summarized in Table 4.2.

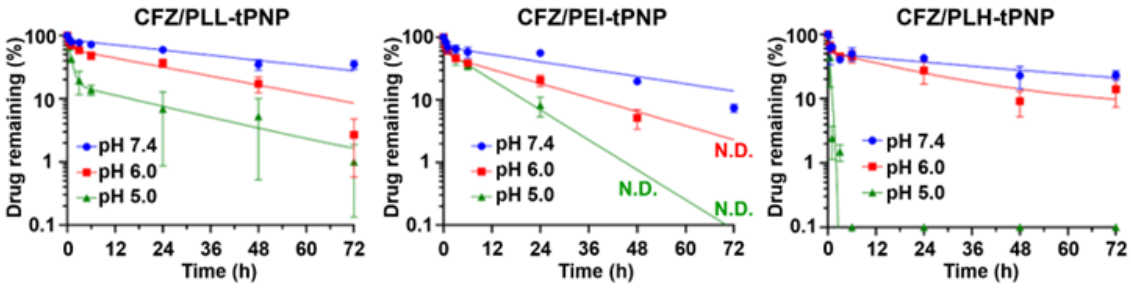

Figure 4.3. Effect of pH on the release of CFZ from polyion stabilized tPNPs

Table 4.2. Kinetic parameters of polyion stabilized tPNPs at different pH values.

Formulation	pH	t1/2 fast (h)	t1/2 slow (h)
CFZ/PLL-tPNP	7.4	N. D	44.04±5.25
CFZ/PLL-tPNP	6.0	0.54±0.12	25.27±2.70
CFZ/PLL-tPNP	5.0	0.63±0.08	19.98±11.5
CFZ/PHis-tPNP	7.4	0.30±0.01	48.73±1.01
CFZ/PHis-tPNP	6.0	0.32±0.12	17.64±4.54
CFZ/PHis-tPNP	5.0	0.34±0.11	0.34±0.06
CFZ/PEI-tPNP	7.4	0.39±0.23	30.72±5.63
CFZ/PEI-tPNP	6.0	0.49±0.05	16.09±1.31
CFZ/PEI-tPNP	5.0	0.45±0.17	7.54±1.63

4.3.4 Cell viability

The in vitro cytotoxic effect of free CFZ, CFZ/PLL-tPNP, CFZ/PHis-tPNP and CFZ/PEI-tPNP are shown in Figure 4.4. The results indicate that CFZ/PLL-tPNP inhibited DLD1 resistant cell growth at all concentrations. CFZ/PHis-tPNP had a comparable performance to free CFZ while CFZ/PEI-tPNP did not show much cytotoxic effect on cells. To measure the effectiveness of all formulations and free CFZ, we modeled the cell viability results to obtain a half-maximal inhibitory concentration (IC_{50}). CFZ/PLL-tPNP (3.9 ± 0.2 μM) had a lower IC_{50} compared to CFZ/PHis-tPNP (7.0 ± 0.5 μM) and about 3 ½- fold reduction compared to CFZ/PEI-tPNP (14 ± 0.9 μM).

4.3.5 Proteasome activity

Proteasome activity was determined by measuring the chymotrypsin-like activity of DLD1 cells after treatment and enzyme reaction. Figure 4.5 displays the reduction in proteasome activity in this cell line. At 6 h after treatment, both free CFZ and CFZ/PLL-tPNP reduced the proteasome activity by 50%. However, treatment with free drug produced a steady rise in proteasome activity at later time points up until 72 hours where there was a sharp recovery of proteasome activity. CFZ/PLL-tPNPs were able to produce sustained suppression of proteasome activity up until 72 hours. For CFZ/PHis-tPNP and CFZ/PEI-tPNP treatment, although they did not suppress proteasome activity more than 20% at 6-hour treatment, they reduced proteasome activity by 60% at 48 hours, after which there was a recovery in proteasome activity. CFZ/PLL-tPNP had the best combination of

proteasome activity reduction at early time point and a sustained suppression of proteasome activity.

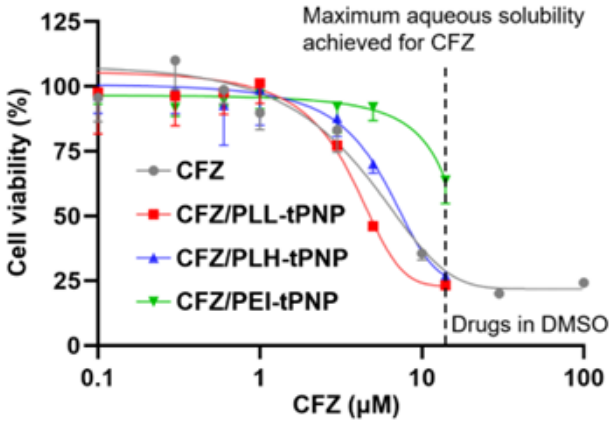

Figure 4.4. Cell Viability of DLD 1 CFZ resistant cells treated with CFZ or polyion stabilized CFZ/tPNPs

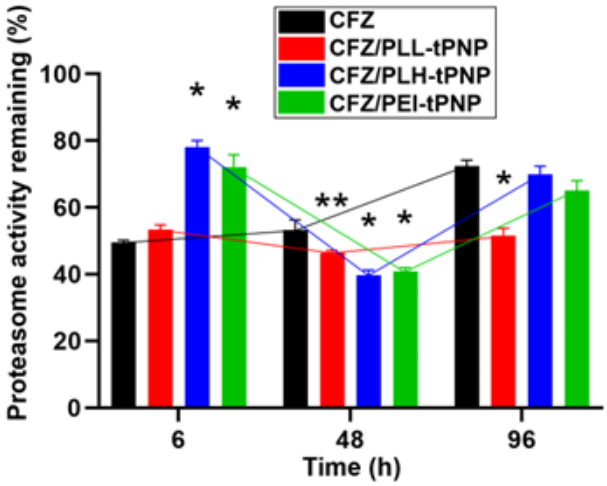

Figure 4.5. Proteasome activity of DLD 1 CFZ resistant cells treated with CFZ or polyion stabilized CFZ/tPNPs

4.4 Discussion

Following its success in the clinic in treating patients with relapsed/refractory multiple myeloma, CFZ has been under investigation as a potential therapy for other diseases [158-161]. CFZ has been explored in solid cancer treatment, however, these efforts have not yielded much success due to the prevalence of CFZ pharmaceutical limitations such as low solubility, poor biostability, enzyme degradation and short blood half-life [46]. To tackle these limitations, we previously developed tPNPs as drug carriers for CFZ [32, 97]. tPNPs have the advantage of low immunogenicity, better stability, versatile structures, and higher drug loading compared to other nano formulations like liposomes and micelles [54, 162]. When designed with optimized particle size and surface characteristics, these nanoparticles can increase in vivo blood circulation time, stealth, and drug accumulation in tumors.

The loading of hydrophobic molecules in nanostructures is mostly limited by their aqueous solubility [163]. Herein, we design a self-assembled pH sensitive nanoparticle with a high drug loading capacity and encapsulation for the highly hydrophobic CFZ. The core of our tPNPs is comprised of an inclusion complex of CFZ and HaβCD stabilized by water soluble cationic polymers. The nanostructure is completed by electrostatic interaction of the negatively charged poly-glutamic acid chains from m-PEG-PLE and the positively charged core. Besides the high loading capacity, the strong hydrophobic interaction between CFZ and the lipophilic core of HaβCD, loaded drug would have a controlled release resulting from the slow diffusion rate of CFZ from nanoparticle core. The cationic polymers produce a triggered release mechanism that allows travel through systemic circulation and drug delivery at disease sites where pH is different from physiological pH [164].

All tPNPs exhibited sub-100 nm particle size regardless of drug loading. This feature can facilitate delivery of our nanoparticles into tumor by taking advantage of their leaky vasculature and poor lymphatic drainage hence allowing nanoparticle tumor accumulation through enhanced permeation and retention effect [165-167]. tPNPs were optimized to have neutral surface charge which can prevent trafficking into macrophages of the reticuloendothelial system [168]. One of the limitations of many nanostructures is their low drug loading. This causes insufficient quantities of cytotoxic agents at disease sites ultimately reducing their efficacy [169, 170]. Our tPNPs had an encapsulation efficiency 80% or greater. This potentially can increase the efficacy of CFZ by delivering sufficient drug quantity to tumor site.

One of the major obstacles with nanoparticle delivery is significant drug release before reaching tumor sites. Nanoparticles travel through the bloodstream, delivering their payload with little control in peripheral tissues [171]. To this end, we developed our tPNPs with regard to the travel route to disease sites. After systemic drug delivery, nanoparticles travel through the blood which has a pH of 7.4 to various tissues in the body. At tumor sites, the pH reduces to around 6.0 and in lysosomes, the pH drops to around 4-5 [172, 173]. Our tPNPs show a clear pH dependent drug release profile. CFZ/PLL-tPNPs exhibit no burst release at physiological pH, they show a sustained release with half-life of about 44 hours. When the pH was reduced to 6.0 and 5.0, CFZ/PLL-tPNPs show a biphasic release profile with the initial burst release half-life less than one hour for both pH values followed by a slow-release half-life of about 25 hours at 6.0 and 19 hours at 5.0. These indicate the capability of CFZ/PLL-tPNPs to release drug faster in tumor microenvironment. As for CFZ/PHis-tPNPs, all pH values studied showed a biphasic

release profile, with fast half-life less than one hour. As we reduced pH, drug release from CFZ/PHis-tPNP increased. Interestingly, when pH was reduced to 5.0, drug was released from CFZ/PHis-tPNP almost instantaneously as indicated by half-life less than one hour. The nitrogen atom on imidazole ring of histidine side chain has a lone pair of electrons that is easily susceptible to protonation, especially when the pH is lower than the pKa of histidine which is 6.0 [174]. One possible reason for the instantaneous release of drug at pH 5.0 is the destabilization of nanoparticle core after complete ionization of histidine molecules. This weakening of the ionic interactions stabilizing nanoparticle core allows drug to diffuse freely into surrounding media. Similarly, CFZ/PEI-tPNPs also show a pH dependent release with the slowest release at pH 7.4 and the fastest release at pH 5.0. These three cationic polymer-stabilized nanoparticles can have utility dependent on disease site and delivery needs. Improving the efficacy and toxicity profile of drugs involves the application of formulations to allow the utility of potent drugs in overcoming resistance. Due to the prevalence of efflux pumps such as P-gp on many cancer cells, drugs such as CFZ which is a substrate of P-gp are transported outside cancer cells where they remain ineffective [175, 176]. CFZ/tPNPs allow drugs to be internalized into cells without P-gp detection. Inside cells, drug is released, inducing cytotoxic effect to cancer cells. CFZ/PLL-tPNPs showed the lowest IC_{50} followed by free CFZ, CFZ/PHis-tPNP and CFZ/LPE-tPNP. This may be attributed to the release rates of each nanoparticle. CFZ/PLL-tPNP showed the most controlled release which allows it to release CFZ in a sustained pattern to induce cytotoxic effect. On the other hand, CFZ/PEI-tPNP had the quickest release half-life. The effectiveness of free CFZ may be explained by the very high drug concentration which

saturates P-gp, allowing more drug internalization into cell. tPNPs can serve as an alternative to achieve drug efficacy while reducing potential toxicity.

Targeting the ubiquitin-proteasome pathway has garnered attention recently as a pathway for cancer treatment [177]. Suppression of proteasome activity has been shown to be effective for cancer treatment by facilitating cell cycle arrest and subsequently apoptosis [178]. By loading CFZ into tPNPs, they can evade P-gp on the surface of cell membranes, entering the cytoplasm where they can release their payload, and suppress proteasome activity. At early time points, free CFZ and CFZ/PLL-tPNP perform similarly proteasome activity suppression, however, CFZ/PHis-tPNP and CFZ/PEI-tPNP had minimal effect in reducing proteasome activity. This may be due to the release kinetics of CFZ from these tPNPs. CFZ/PLL-tPNP shows no biphasic release at physiological pH, which allows it to be internalized into the cell, unrecognized by P-gp. This sustained release allows it to deliver CFZ into cells where they can reduce proteasome activity. With CFZ/PHis-tPNP and CFZ/PEI-tPNP, the initial release may facilitate P-gp activation to reduce drug concentrations into the cells. Over longer period (>48 h), all three tPNPs suppress activity of proteasome followed by recovery. This is an improvement over free CFZ which fails to continue proteasome activity suppression after 6 hours. These results together serve as proof-of -concept for the utility of our pH triggered CFZ loaded tPNPs for improved drug efficacy.

4.5 Conclusions

We have developed tPNPs stabilized by polyion complexation using cationic polymers that modulate CFZ release from the nanoparticles in response to pH conditions, which may achieve triggered release of CFZ to allow drug accumulation in acidic tumor environment and cell compartments. CFZ/tPNPs showed uniform particle size and high drug loading while improving biostability and activity of CFZ against drug-resistant cancer cells. CFZ/tPNPs showed comparable or better efficacy against CFZ-resistant cells. These results demonstrate great potential of CFZ/tPNPs for their future in vivo studies and clinical applications.

CHAPTER 5. BIODISTRIBUTION OF TERNARY POLYPEPTIDE NANOPARTICLES USING FLUORESCENCE IMAGING: A QUALITATIVE AND QUANTITATIVE METHOD

5.1 Introduction

As stated in the previous chapters, polycation stabilized ternary polypeptide nanoparticles (tPNPs) were developed, characterized, and tested in vitro to assess their properties and efficacy against a drug resistant cell.

A prerequisite to understanding the effect of nanoparticles in biologically relevant systems is developing animal models [179]. In cancer studies, murine tumor models are used to bridge the gap between preclinical and clinical in vivo assessment of formulation biodistribution. Subcutaneous xenograft murine models are one of the most common tumor models used in the detection of angiogenesis in cancer and drug development for anti-cancer agents [180]. Development of subcutaneous xenografts requires the use of immunodeficient mice however, due to its relative simplicity, this murine model is often used as a first step in the analysis of nanoparticle biodistribution studies [181].

Traditionally, biodistribution in animals has been measured by using taking advantage of radioactivity associated drugs or by measuring drug metabolites using mass spectrometry (MS). The inherent danger associated with radioactivity possess a health risk for animals. Moreover, some isotopes with short half-lives decay quickly making them less quantifiable [182]. MS techniques pose less of a risk than radioactive measurements, however, MS assessment of biodistribution requires complete extraction and isolation of analytes from specimens for accurate measurements. Furthermore, MS allows the measurement of only endpoint outcomes, it lacks the ability to delineate the dynamic changes that occur as nanoparticles traverse the delivery route [182].

Fluorescent imaging has been used to assess the biodistribution of nanoparticles and other formulations in vivo. Its cost effectiveness and minimally invasive approach makes it very attractive for animal studies. Fluorescent probes can be conjugated to the surface of nanoparticles by facile chemistry. They can also be encapsulated within the core of nanoparticles by hydrophobic interactions or hydrogen bonding [183]. Selecting the right fluorophore is essential to visualize nanoparticle accumulation in different organs. Typically, fluorophores with an emission range in the red or near infra res wavelength (600 – 100 nm) are ideal for deep tissue imaging [184].

In this work, a subcutaneous tumor model is developed in nude mice. Following tumor growth, the biodistribution of polycation stabilized tPNPs are assessed after conjugation to a fluorophore using the subcutaneous mice model. To determine the effect of tumor size, mice bearing tumors of two different volumes were used for the biodistribution study. Epithelial cell adhesion molecule (EpCAM) antibody is used as a targeting ligand to confer targetability on tPNPs. The time dependent degree of nanoparticle distribution is measured. The accumulation of nanoparticles in different organs as well as tumor is measured by fluorescence imaging.

5.2 Materials and Methods

5.2.1 Materials

McCoy's 5A medium and trypsin-EDTA (0.25% trypsin and 2.21 mM EDTA) were purchased from Sigma (St. Louis, MO). Fetal bovine serum (FBS) and Gibco antibiotic-antimycotic were purchased from Thermo Fisher Scientific (Waltham, MA). HT29 cell line were purchased from ATCC (Manassas, VA). Heptakis (6-amino-6-deoxy)-βCD heptahydrochloride (HaβCD) was purchased from Cyclolab R&D Laboratory Ltd. (Budapest, Hungary). Azido-poly (ethylene glycol)-block-poly (L-glutamic acid sodium salt) (N_3-PEG-PLE) was purchased from Alamanda Polymers (Huntsville, AL). Alkyne-PEG-NHS (4 units of PEG modified with alkyne and N-hydroxysuccinimide at each end, 401.41 g/mol) was obtained from Thermo Fisher Scientific (Rockford, IL). Alexa-fluor 647-Dibenzocyclooctyne (AFDye 647 DBCO) was purchased from Click Chemistry Tools (Scottsdale, AZ). EpCAM antibody was purchased from Santa Cruz Biotechnology (Dallas, TX).

5.2.2 Preparation of fluorescent tPNPs

N_3-PEG-PLE was added to AFDye 647 DBCO dissolved in DMSO, and the mixture was left to react in the dark for 1 h. Free dye and DMSO were removed by dialyzing the mixture against deionized water. Dye-labeled polymers were collected by freeze drying. EpCAM antibody was modified with alkyne prior to complexation. Briefly, alkyne-PEG-NHS in DMSO was added at a 1.5 molar excess to an EpCAM antibody

solution in PBS. The reaction was allowed to proceed for 1 h and DMSO was removed by dialysis in PBS. The alkyne-modified EpCAM was reacted with N_3-PEG-PLE in PBS by copper-catalyzed [3+2] cycloaddition. The mixture was dialyzed in deionized water to remove free copper and other small molecule impurities. Polycation stabilized tPNP preparation is described in previous chapter. Fluorescent tPNPs (FL-PLL/tPNPs) is prepared in the same way except that a 1:1 mixture of dye labeled polymer and unlabeled polymer is used. Similarly, preparation of fluorescent EpCAM tPNPs (FL-PLL/EpCAM-tPNPs) required a 1:1 mixture of dye labeled polymer and EpCAM conjugated polymer

5.2.3 Subcutaneous tumor model development

All animal work was performed in accordance and approved by the University of Kentucky Institutional Animal Care and Use committee guidelines. Female athymic NCr nude mice (sp/sp) weighing 25 g were purchased from Taconic (Hudson, NY). Housing for these animals was a sterilized cage with HEPA filters and a 12 h light/12 h dark cycle. Mice were acclimated in their housing for 7 days. Following acclimatization, the animals were inoculated with HT29 cells. Briefly, 1 x 10^6 HT29 cells were subcutaneously injected into the left flank. Tumor length (L) and width (W) were measured every other day to determine tumor volume (V) using the formula:

$$V = \frac{1}{2} LW^2$$

Mice were divided into two groups and their tumors were allowed to grow to two different sizes, 100 mm^3 and 200 mm^3. Mice from the two groups were randomly divided

into 3 sub-groups representing different treatments (saline, FL-PLL/tPNPs or FL-PLL/EpCAM-tPNPs). These animals were then injected intravenously with 100 µL of formulation at a dose equivalent of 5 mg/kg CFZ

5.2.4 In vivo and ex vivo imaging

Following intravenous injection, mice were anesthetized, and non-invasive mice images were taken at 1 h, 3 h, 6 h and 24 h post injection using an in vivo Lago X imaging system (LAGO, USA). After the 24 h image, mice were by euthanized under 5% CO2 and heart, lungs, liver, kidney, spleen, and tumor were collected for ex vivo imaging (excitation 630 nm, emission 670 nm).

5.3 Results

5.3.1 In vivo imaging

We investigated the time dependent accumulation of tPNPs in tumor-bearing mice. Mice treated with saline were used as control. In vivo images showed that in animals bearing 100 mm^3 tumors, tPNPs are distributed through the entire body 1 h after administration, whereas no fluorescence was detected in control group. Primary accumulation appears to be in the liver, for both FL-PLL/tPNPs and FL-PLL/EpCAM-tPNPs. The circulation of these tPNPs is maintained even up to 24 hours post administration (Figure 5.1). For animals bearing bigger tumors (200 mm^3), distribution throughout the entire body is also observed for both treatment groups with the liver having primary accumulation (Figure 5.2). However, the liver accumulation as indicated by fluorescent intensity is lower in animals bearing 200 mm^3 tumors compared to the animals 100 mm^3 tumors. The biodistribution of tPNPs indicate prolonged blood circulation time in vivo.

5.3.2 Ex vivo imaging

Observation of organs 24 h post injection and dissection of animals confirmed the accumulation pattern of FL-PLL/tPNPs or FL-PLL/EpCAM-tPNPs in animals bearing tumors. As shown in Figure 5.3 and 5.4, primary accumulation of FL-PLL/tPNPs and FL-PLL/EpCAM-tPNPs in animals with 100 mm^3 tumors occurs in the liver with minimal accumulation in tumors. Similar trend occurs for animals with 200 mm^3 tumors as well

(Figure 5.5 and 5.6). Quantitative analysis of fluorescence intensity also showed that regardless of tumor size, animals treated FL-PLL/EpCAM-tPNPs did not have preferential accumulation compared to animals treated with just FL-PLL/tPNPs.

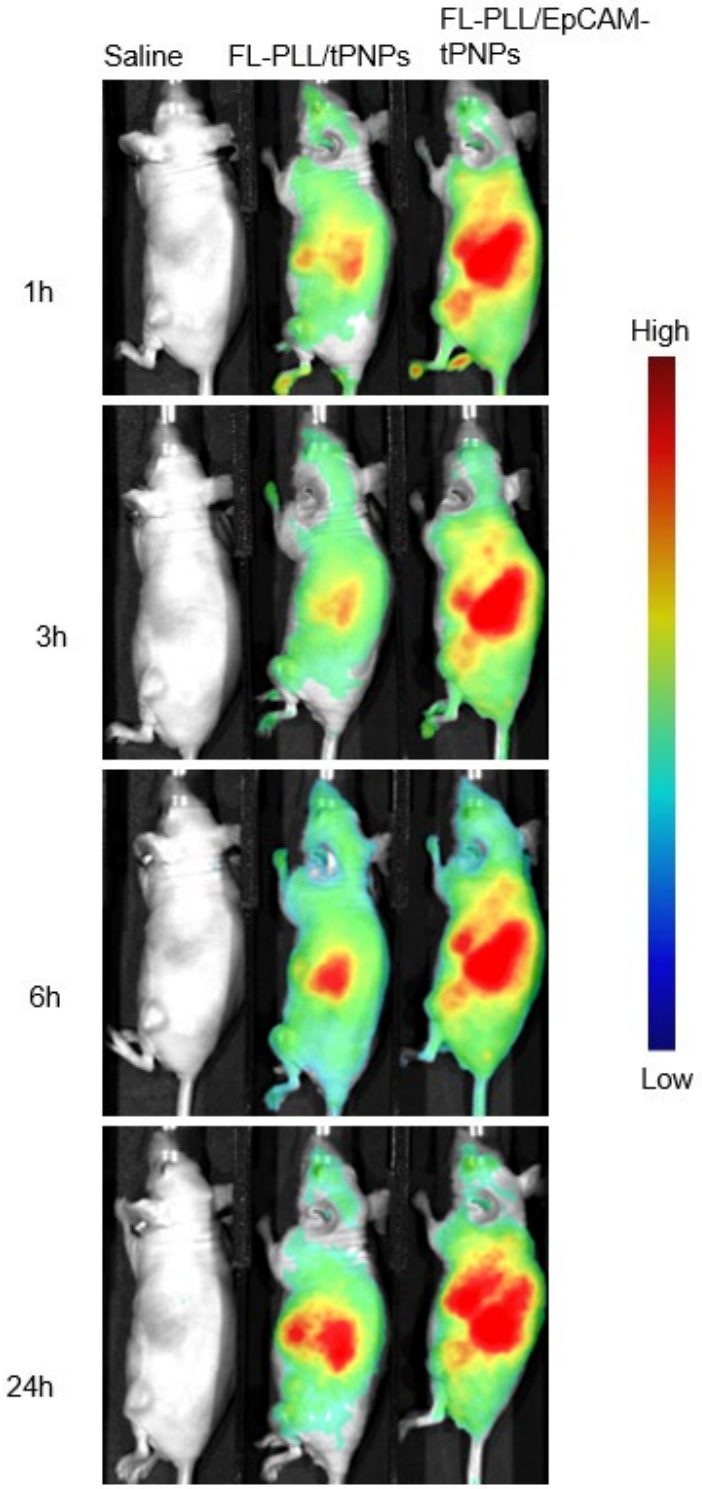

Figure 5.1. In vivo full body images of mice bearing 100 mm3 tumors treated with saline, FL-PLL/tPNPs or FL-PLL/EpCAM-tPNPs.

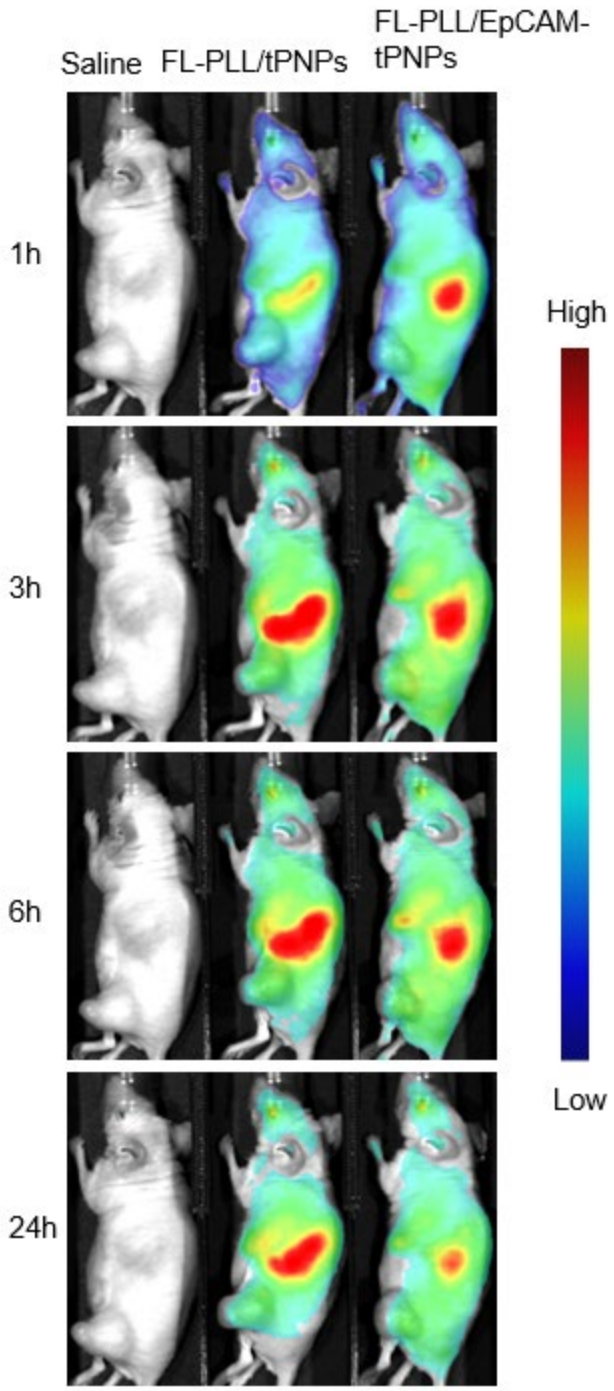

Figure 5.2. In vivo full body images of mice bearing 100 mm3 tumors treated with saline, FL-PLL/tPNPs or FL-PLL/EpCAM-tPNPs.

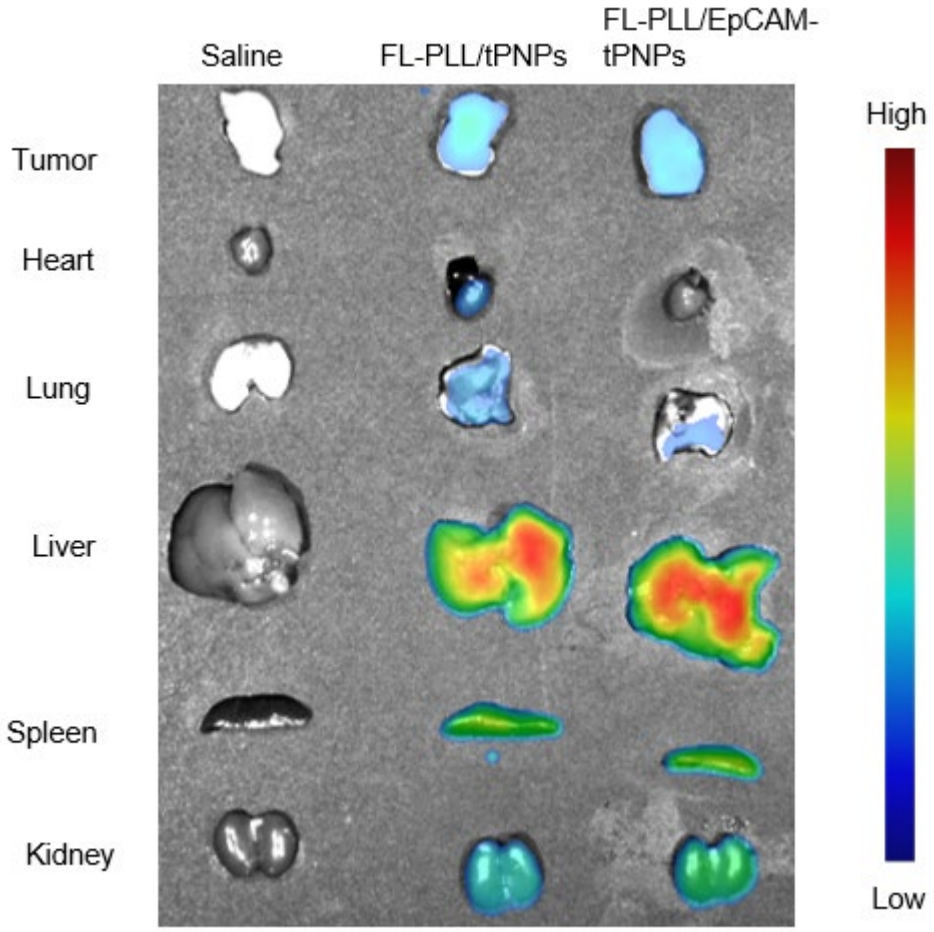

Figure 5.3. Ex vivo fluorescence images of organs and tumors obtained at 24 h post injection into 100 mm^3 tumor bearing mice

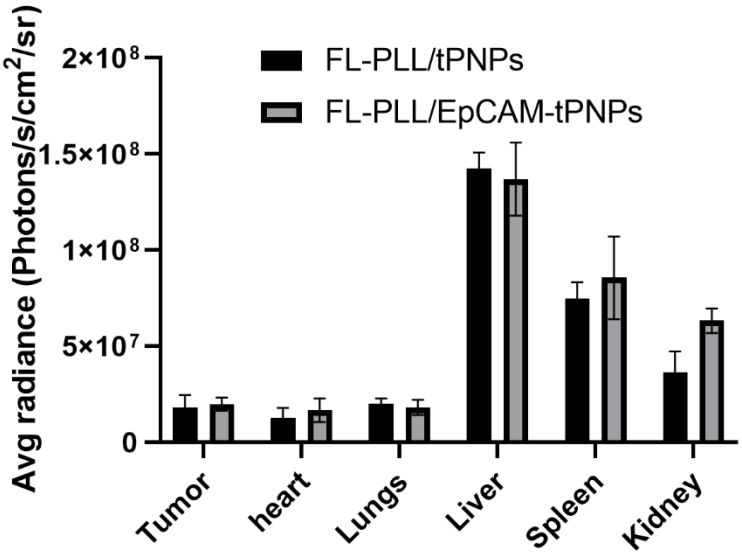

Figure 5.4. Semiquantitative analysis of fluorescence intensity for 100 mm^3 tumor bearing mice

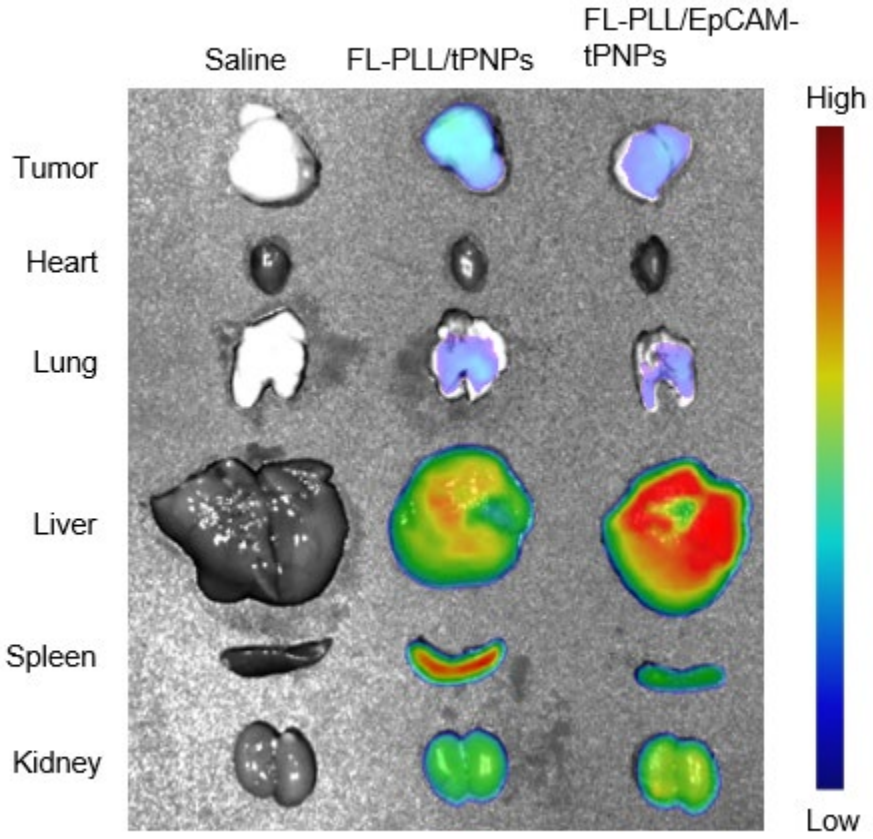

Figure 5.5. Ex vivo fluorescence images of organs and tumors obtained at 24 h post injection into 100 mm^3 tumor bearing mice

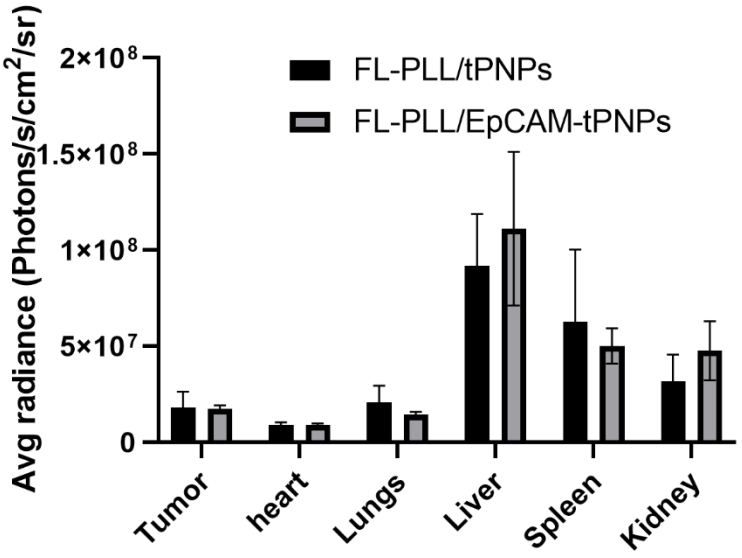

Figure 5.6. Semiquantitative analysis of fluorescence intensity for 100 mm^3 tumor bearing mice

5.4 Discussion

Active delivery of nanoparticles to malignant tumors has been imagined as a route to deliver drugs to minimize off site toxicity. However, a study of the literature has proved that less than 1% of administered nanoparticle actually gets delivers to tumors [185]. A challenging problem for active nanoparticle delivery is developing effective targeting ligands that can lead to preferential accumulation of nanoparticles in tumors [90]. In this work, EpCAM antibody was used a targeting moiety to probe active delivery. EpCAM is a transmembrane glycoprotein that is associated with proliferation and cell migration. These properties suggest that EpCAM is a molecule with pleiotropic properties that make it therapeutically useful. As such, EpCAM was conjugated on the surface of tPNPs to produce nanoparticles for tumor targeting.

Studying biodistribution of nanoparticles is a first step to evaluate their potential efficacy. Fluorescent imaging is very practical in initial studies to show the whole-body distribution. Only qualitative and semi-quantitative data can be achieved due to tissue heterogeneities. However, it is still informative to assess particle behavior in animal studies [182]. In vivo biodistribution studies were performed to determine the accumulation of tPNPs. A subcutaneous tumor xenograft model was developed and used for this study. This model was used due to its relative simplicity. It is however useful to give information on nanoparticle distribution. Mice were inoculated with colorectal cancer cell line HT29 and allowed to grow to 100 mm^3 or 200 mm^3.

Within minutes of administration, nanoparticles are circulated indiscriminately throughout the body by the circulatory system. Due to the small size of most tumors in comparison to the size of animals, tumors only receive a minute fraction of vascular output. Even more, uncoated nanoparticles are cleared within minutes to an hour [181]. Prolonging

blood circulation time is an effective strategy to promote access of therapeutics agents to tumors. Whole body images in this study show that after intravenous injection, nanoparticles are distributed throughout mice as early as 1 h. These results show that the liver is the primary site of accumulation of both FL-PLL/tPNPs and FL-PLL/EpCAM-tPNPs in both tumor sizes. These results also indicate that treating animals with FL-PLL/tPNPs or FL-PLL/EpCAM-tPNP showed comparable accumulation in tumors regardless of tumor size. We also observe prolonged blood circulation time of tPNPs in vivo which can lead to improved outcomes.

5.5 Conclusions

Biodistribution of tPNPs with and without EpCAM as a targeting ligand was studied in vivo. Primary accumulation of FL-PLL/tPNPs and FL-PLL/EpCAM-tPNPs in mice bearing smaller tumors was in the liver with minimal accumulation in tumor. Likewise, liver accumulation of FL-PLL/tPNPs and FL-PLL/EpCAM-tPNPs for larger tumors was also predominant compared to the accumulation in tumors. However, there was reduced accumulation of these nanoparticles in the liver of animals bearing the larger tumors compared to the ones with smaller tumors. These results provide the framework for further studies to develop more efficient targeting ligands and the exploration of more pertinent tumor models.

CHAPTER 6. SUMMARY AND FUTURE DIRECTION

The fight against cancer is centuries old. Efforts and strides continue to expand our knowledge on the pathology of cancer, but this knowledge also informs on how to pursue innovation to continue chipping away at this eternal adversary. Through successes and failure in attempts to develop innovative technology, progress continues to be made, slowly but surely. Nanotechnology has been of immense use in the fight against cancer. It has provided an avenue to make anti-cancer drugs more efficacious and abate their unwanted side effects.

This work has highlighted efforts to develop a novel nanoparticle formulation termed ternary polypeptide nanoparticle (tPNP) aimed at improving clinical and pharmaceutical limitations of chemotherapeutics. The core of tPNP is comprised of positively charged cyclodextrin. The model drug used in this work is CFZ. It was chosen for multiple reasons namely: It is a drug already approved by the FDA for use in patients experiencing relapsed or refractory multiple myeloma, it is a BCS class II drug that requires formulation and the preclinical evidence for its applicability in other forms of cancer. CFZ readily forms an inclusion complex with positively charged cyclodextrin. Polypeptides were used to create ionic complexes with the core guest-host complex to further stabilize the nanoparticle. Polypeptides have the advantage of their biocompatibility with biological environment but also, they can be modified to attach other targeting ligands.

The surface of tPNPs was modified with an antibody, EpCAM that has been shown to be overexpressed on many cancer cells of epithelial origin. All tPNPs had particle size below 100 nm with a neutral or slightly positive surface charge. They were also stable in serum proteins and their shelf-life was increased by lyophilization. Drug release studies

were performed to assess their release kinetics in medium simulating physiological conditions. It was observed that tPNPs encapsulating CFZ exhibited a biphasic release profile with an initial release indicative of burst release followed by a sustained release.

This biphasic release profile led to efforts to optimize tPNPs to mitigate burst release and improve its overall particle stability. In the first attempt at improving particle stability, organic acids were employed because of their ability to improve hydrophobic interactions within cyclodextrin core. Various combinations of citric acid and lactic acid were used in this new tPNP, and it was shown that particle size remained practically the same regardless of the ratio of citric acid to lactic acid. More importantly using combinations of the two acids appeared to reduce the burst release compared to tPNPs without organic acids. For single acid use, citric acid alone had a similar performance to acid combinations in reducing burst release; lactic acid did not reduce burst drug release. Despite the improvements achieved by using organic acids in improving particle stability, more work was done to further stabilize tPNPs.

For the next step in tPNP optimization, hydrophilic polycations were used to enhance particle stability. Small quantities of poly-lysine, poly-histidine and polyethylene imine were used in formulation preparation. Physiochemical properties of polycation stabilized tPNPs corresponded to the previous iterations of tPNPs. Drug release study showed that at physiological pH, PLL stabilized tPNPs had no burst release. The other two polycations used showed minimal burst release. It was also learned that there was a pH dependent release of CFZ. As pH decreased from 7.4 to 5.0, there was an increase in the release of CFZ from tPNPs.

Assessment of efficacy for the developed tPNPs was carried out using two important assays: cell viability and proteasome activity assays. Cell viability tells how efficacious a drug or formulation is against a particular cell line. The main cell line used for in vitro assays was a colorectal cancer cell line DLD-1. This cell line was trained to develop CFZ resistance at 1 μM. This was done to mimic drug resistance which is a hallmark of continuous chemotherapy. It was shown that both ordinary tPNPs and polycation stabilized tPNPs loaded with CFZ were more efficacious against this cell line than free CFZ as indicated by a lower IC_{50}. Proteasome activity is an important assay to probe drugs like CFZ that are proteasome inhibitors. Similarly, both tPNPs and polycation stabilized tPNPs suppressed the activity of the proteasome and showed longer suppression time than free CFZ.

Finally, in vivo biodistribution study was performed to assess the accumulation of tPNPs in organs and tumor. Although tPNPs accumulated in subcutaneous tumors, primary accumulation was found in the liver. There was also no apparent difference in tumor accumulation between tPNP treated mice versus EpCAM-tPNP treated mice. Although this is very informative, more insights could be attained by further probing the potential utility of tPNPs in other cell lines and animal models.

Beyond the scope of this work, tPNPs provide a basis for further studies. The methods developed herein allow for relatively easy modifications to treat other diseases or target other cancers. EpCAM was used as a targeting ligand against DLD-1 colorectal cancer. A pertinent question that needs answering is whether other targeting ligands may be more suitable for this cancer. Peptides and aptamers can also be attached to tPNPs and tested for their efficacy in other cancers and perhaps other diseases. Another avenue of

future pursuit is the exploration of a different and perhaps more biologically suitable tumor model. Subcutaneous tumor xenografts rarely metastasize from the original site even if the original patient tumors have metastatic origin. Therefore, it will be important to assess biodistribution and treatment using more relevant tumor models.

REFERENCES

1. Siegel, R.L., K.D. Miller, and A. Jemal, *Cancer statistics, 2019.* CA: a cancer journal for clinicians, 2019. **69**(1): p. 7-34.
2. Chu, E. and A. Sartorelli, *Cancer chemotherapy.* Lange's Basic and Clinical Pharmacology, 2018: p. 948-976.
3. Aslam, M.S., et al., *Side effects of chemotherapy in cancer patients and evaluation of patients opinion about starvation based differential chemotherapy.* Journal of Cancer Therapy, 2014. **2014**.
4. Monsuez, J.-J., et al., *Cardiac side-effects of cancer chemotherapy.* International journal of cardiology, 2010. **144**(1): p. 3-15.
5. Mansoori, B., et al., *The different mechanisms of cancer drug resistance: a brief review.* Advanced pharmaceutical bulletin, 2017. **7**(3): p. 339.
6. Lipinski, C.A., et al., *Experimental and computational approaches to estimate solubility and permeability in drug discovery and development settings.* Advanced drug delivery reviews, 1997. **23**(1-3): p. 3-25.
7. Lipinski, C.A., *Drug-like properties and the causes of poor solubility and poor permeability.* Journal of pharmacological and toxicological methods, 2000. **44**(1): p. 235-249.
8. Loftsson, T., M.E. Brewster, and M. Masson, *Role of cyclodextrins in improving oral drug delivery.* American Journal of Drug Delivery, 2004. **2**(4): p. 261-275.
9. Alexis, F., et al. *New frontiers in nanotechnology for cancer treatment*. in *Urologic Oncology: Seminars and Original Investigations*. 2008. Elsevier.

10. Torchilin, V., *Tumor delivery of macromolecular drugs based on the EPR effect.* Advanced drug delivery reviews, 2011. **63**(3): p. 131-135.

11. Van Eerdenbrugh, B., et al., *Solubility increases associated with crystalline drug nanoparticles: methodologies and significance.* Molecular pharmaceutics, 2010. **7**(5): p. 1858-1870.

12. Sun, C., et al., *Applications of antibiofouling PEG-coating in electrochemical biosensors for determination of glucose in whole blood.* Electrochimica Acta, 2013. **89**: p. 549-554.

13. Huang, J. and A. Heise, *Stimuli responsive synthetic polypeptides derived from N-carboxyanhydride (NCA) polymerisation.* Chemical Society Reviews, 2013. **42**(17): p. 7373-7390.

14. Deng, C., et al., *Functional polypeptide and hybrid materials: Precision synthesis via α-amino acid N-carboxyanhydride polymerization and emerging biomedical applications.* Progress in Polymer Science, 2014. **39**(2): p. 330-364.

15. Liu, H., et al., *Reversible thermo-sensitivity induced from varying the hydrogen bonding between the side residues of rationally designed polypeptides.* Chemical Communications, 2015. **51**(50): p. 10174-10177.

16. Song, Z., et al., *Polypeptide vesicles with densely packed multilayer membranes.* Soft Matter, 2015. **11**(20): p. 4091-4098.

17. Meier, C., et al., *Self-assembly of high molecular weight polypeptide copolymers studied via diffusion limited aggregation.* Biomacromolecules, 2014. **15**(1): p. 219-227.

18. Cai, C., L. Wang, and J. Lin, *Self-assembly of polypeptide-based copolymers into diverse aggregates.* Chemical Communications, 2011. **47**(40): p. 11189-11203.

19. Carlsen, A., *S. b. Lecommandoux.* Curr. Opin. Colloid Interface Sci, 2009. **14**: p. 329-339.

20. Pratesi, G., et al., *Poly-L-aspartic acid as a carrier for doxorubicin: a comparative in vivo study of free and polymer-bound drug.* British journal of cancer, 1985. **52**(6): p. 841-848.

21. Sela, M. and E. Katchalski, *Biological properties of poly-α-amino acids*, in *Advances in protein chemistry*. 1959, Elsevier. p. 391-478.

22. Zhang, Y., et al., *Polypeptides–drug conjugates for anticancer therapy.* Advanced Healthcare Materials, 2021. **10**(11): p. 2001974.

23. Hadjichristidis, N., et al., *Synthesis of well-defined polypeptide-based materials via the ring-opening polymerization of α-amino acid N-carboxyanhydrides.* Chemical reviews, 2009. **109**(11): p. 5528-5578.

24. Aliferis, T., H. Iatrou, and N. Hadjichristidis, *Living polypeptides.* Biomacromolecules, 2004. **5**(5): p. 1653-1656.

25. Gitsas, A., et al., *Effect of chain topology on the self-organization and dynamics of block copolypeptides: from diblock copolymers to stars.* Biomacromolecules, 2008. **9**(7): p. 1959-1966.

26. Zagorodko, O., et al., *Polypeptide-Based Conjugates as Therapeutics: Opportunities and Challenges.* Macromolecular Bioscience, 2017. **17**(1): p. 1600316.

27. Langer, R. and M. Moses, *Biocompatible controlled release polymers for delivery of polypeptides and growth factors.* Journal of cellular biochemistry, 1991. **45**(4): p. 340-345.

28. Perrett, S., et al., *Importance of electrostatic interactions in the rapid binding of polypeptides to GroEL.* Journal of molecular biology, 1997. **269**(5): p. 892-901.

29. Liu, L., et al., *The role of self-assembling polypeptides in building nanomaterials.* Physical Chemistry Chemical Physics, 2011. **13**(39): p. 17435-17444.

30. Eckman, A.M., et al., *Drug release patterns and cytotoxicity of PEG-poly (aspartate) block copolymer micelles in cancer cells.* Pharmaceutical research, 2012. **29**(7): p. 1755-1767.

31. Wu, Y., et al., *Fabrication of elastin-like polypeptide nanoparticles for drug delivery by electrospraying.* Biomacromolecules, 2008. **10**(1): p. 19-24.

32. Agbana, P., et al., *Ternary Polypeptide Nanoparticles with Improved Encapsulation, Sustained Release, and Enhanced In Vitro Efficacy of Carfilzomib.* Pharmaceutical Research, 2020. **37**(11): p. 1-12.

33. Yang, Y., et al., *Optimizing the refolding conditions of self-assembling polypeptide nanoparticles that serve as repetitive antigen display systems.* Journal of structural biology, 2012. **177**(1): p. 168-176.

34. Matsumura, Y. and H. Maeda, *A new concept for macromolecular therapeutics in cancer chemotherapy: mechanism of tumoritropic accumulation of proteins and the antitumor agent smancs.* Cancer research, 1986. **46**(12_Part_1): p. 6387-6392.

35. Kane, R.C., et al., *Velcade: US FDA approval for the treatment of multiple myeloma progressing on prior therapy.* The oncologist, 2003. **8**(6): p. 508-513.

36. Hanada, M., et al., *Epoxomicin, a new antitumor agent of microbial origin.* The Journal of antibiotics, 1992. **45**(11): p. 1746-1752.

37. Meng, L., et al., *Epoxomicin, a potent and selective proteasome inhibitor, exhibits in vivo antiinflammatory activity.* Proceedings of the National Academy of Sciences, 1999. **96**(18): p. 10403-10408.

38. Lonial, S., C.S. Mitsiades, and P.G. Richardson, *Treatment options for relapsed and refractory multiple myeloma.* Clinical Cancer Research, 2011. **17**(6): p. 1264-1277.

39. Stewart, A.K., et al., *Carfilzomib, lenalidomide, and dexamethasone for relapsed multiple myeloma.* New England Journal of Medicine, 2015. **372**(2): p. 142-152.

40. Jagannath, S., et al., *An open-label single-arm pilot phase II study (PX-171-003-A0) of low-dose, single-agent carfilzomib in patients with relapsed and refractory multiple myeloma.* Clinical Lymphoma Myeloma and Leukemia, 2012. **12**(5): p. 310-318.

41. Jakubowiak, A.J., et al., *A phase 1/2 study of carfilzomib in combination with lenalidomide and low-dose dexamethasone as a frontline treatment for multiple myeloma.* Blood, 2012: p. blood-2012-04-422683.

42. Lub, S., et al., *Novel strategies to target the ubiquitin proteasome system in multiple myeloma.* Oncotarget, 2016. **7**(6): p. 6521.

43. Kortuem, K.M. and A.K. Stewart, *Carfilzomib.* Blood, The Journal of the American Society of Hematology, 2013. **121**(6): p. 893-897.

44. Yang, W., et al., *Proteasome inhibition induces both pro-and anti-cell death pathways in prostate cancer cells.* Cancer letters, 2006. **243**(2): p. 217-227.

45. Ao, L., et al., *Development of peptide-based reversing agents for p-glycoprotein-mediated resistance to carfilzomib.* Molecular pharmaceutics, 2012. **9**(8): p. 2197-2205.

46. Papadopoulos, K.P., et al., *A phase I/II study of carfilzomib 2–10-min infusion in patients with advanced solid tumors.* Cancer chemotherapy and pharmacology, 2013. **72**(4): p. 861-868.

47. Yang, J., et al., *Pharmacokinetics, pharmacodynamics, metabolism, distribution, and excretion of carfilzomib in rats.* Drug metabolism and disposition, 2011. **39**(10): p. 1873-1882.

48. Gutman, D., A.A. Morales, and L.H. Boise, *Acquisition of a multidrug-resistant phenotype with a proteasome inhibitor in multiple myeloma.* Leukemia, 2009. **23**(11): p. 2181-2183.

49. Ivancsits, D., et al., *The Proteasome Inhibitor PR-171 Inhibits Cell Growth, Induces Apoptosis, and Overcomes De Novo and Acquired Drug Resistance in Human Multiple Myeloma Cells*. 2005, American Society of Hematology.

50. Verbrugge, S.E., et al., *Inactivating PSMB5 mutations and P-glycoprotein (multidrug resistance-associated protein/ATP-binding cassette B1) mediate resistance to proteasome inhibitors: ex vivo efficacy of (immuno) proteasome inhibitors in mononuclear blood cells from patients with rheumatoid arthritis.* Journal of Pharmacology and Experimental Therapeutics, 2012. **341**(1): p. 174-182.

51. Park, J.E., et al., *Expanding therapeutic utility of carfilzomib for breast cancer therapy by novel albumin-coated nanocrystal formulation.* Journal of Controlled Release, 2019. **302**: p. 148-159.

52. Lewis, E., et al., *Cyclodextrin complexation methods for formulating peptide proteasome inhibitors*. 2015, Google Patents.

53. Wang, Z., et al., *Clinical pharmacokinetics, metabolism, and drug-drug interaction of carfilzomib.* Drug Metabolism and Disposition, 2013. **41**(1): p. 230-237.

54. Ao, L., et al., *Polymer micelle formulations of proteasome inhibitor carfilzomib for improved metabolic stability and anticancer efficacy in human multiple myeloma and lung cancer cell lines.* Journal of Pharmacology and Experimental Therapeutics, 2015. **355**(2): p. 168-173.

55. Park, J.E., et al., *Polymer micelle formulation for the proteasome inhibitor drug carfilzomib: Anticancer efficacy and pharmacokinetic studies in mice.* PloS one, 2017. **12**(3).

56. Park, J.E., et al., *Novel Polymer Micelle and Nanocrystal Formulations for the Proteasome Inhibitor Drug Carfilzomib: Pharmacokinetic and Pharmacodynamic Studies in Human Lung and Breast Cancer Models.* The FASEB Journal, 2017. **31**(1_supplement): p. 822.6-822.6.

57. Reichel, D., et al., *Tethered polymer nanoassemblies for sustained carfilzomib release and prolonged suppression of proteasome activity.* Therapeutic delivery, 2016. **7**(10): p. 665-681.

58. Ashley, J.D., et al., *Liposomal carfilzomib nanoparticles effectively target multiple myeloma cells and demonstrate enhanced efficacy in vivo.* Journal of Controlled Release, 2014. **196**: p. 113-121.

59. Ashley, J.D., et al., *Dual carfilzomib and doxorubicin–loaded liposomal nanoparticles for synergistic efficacy in multiple myeloma.* Molecular cancer therapeutics, 2016. **15**(7): p. 1452-1459.

60. Trzpis, M., et al., *Epithelial cell adhesion molecule: more than a carcinoma marker and adhesion molecule.* The American journal of pathology, 2007. **171**(2): p. 386-395.

61. Maetzel, D., et al., *Nuclear signalling by tumour-associated antigen EpCAM.* Nature cell biology, 2009. **11**(2): p. 162-171.

62. Patriarca, C., et al., *Epithelial cell adhesion molecule expression (CD326) in cancer: a short review.* Cancer treatment reviews, 2012. **38**(1): p. 68-75.

63. Seimetz, D., H. Lindhofer, and C. Bokemeyer, *Development and approval of the trifunctional antibody catumaxomab (anti-EpCAM× anti-CD3) as a targeted cancer immunotherapy.* Cancer treatment reviews, 2010. **36**(6): p. 458-467.

64. Armstrong, A. and S.L. Eck, *EpCAM: a new therapeutic target for an old cancer antigen.* Cancer biology & therapy, 2003. **2**(4): p. 320-325.

65. Lugli, A., et al., *Prognostic impact of the expression of putative cancer stem cell markers CD133, CD166, CD44s, EpCAM, and ALDH1 in colorectal cancer.* British journal of cancer, 2010. **103**(3): p. 382-390.

66. Reichel, D., P. Rychahou, and Y. Bae, *Polymer nanoassemblies with solvato-and halo-fluorochromism for drug release monitoring and metastasis imaging.* Therapeutic delivery, 2015. **6**(10): p. 1221-1237.

67. Reichel, D. and Y. Bae, *Comparison of dialysis-and Solvatofluorochromism-based methods to determine drug release rates from polymer Nanoassemblies.* Pharmaceutical research, 2017. **34**(2): p. 394-407.

68. Malich, G., B. Markovic, and C. Winder, *The sensitivity and specificity of the MTS tetrazolium assay for detecting the in vitro cytotoxicity of 20 chemicals using human cell lines.* Toxicology, 1997. **124**(3): p. 179-192.

69. Bae, Y. and K. Kataoka, *Intelligent polymeric micelles from functional poly (ethylene glycol)-poly (amino acid) block copolymers.* Advanced drug delivery reviews, 2009. **61**(10): p. 768-784.

70. McCormack, P.L., *Carfilzomib.* Drugs, 2012. **72**(15): p. 2023-2032.

71. Siegel, D.S., et al., *A phase 2 study of single-agent carfilzomib (PX-171-003-A1) in patients with relapsed and refractory multiple myeloma.* Blood, The Journal of the American Society of Hematology, 2012. **120**(14): p. 2817-2825.

72. Dimopoulos, M.A., et al., *Carfilzomib and dexamethasone versus bortezomib and dexamethasone for patients with relapsed or refractory multiple myeloma (ENDEAVOR): a randomised, phase 3, open-label, multicentre study.* The Lancet Oncology, 2016. **17**(1): p. 27-38.

73. Moreau, P., et al., *Impact of prior treatment on patients with relapsed multiple myeloma treated with carfilzomib and dexamethasone vs bortezomib and*

dexamethasone in the phase 3 ENDEAVOR study. Leukemia, 2017. **31**(1): p. 115-122.

74. Khan, M.L. and A.K. Stewart, *Carfilzomib: a novel second-generation proteasome inhibitor.* Future oncology, 2011. **7**(5): p. 607-612.

75. Demo, S.D., et al., *Antitumor activity of PR-171, a novel irreversible inhibitor of the proteasome.* Cancer research, 2007. **67**(13): p. 6383-6391.

76. Pawarode, A., et al., *Phase 1 Study of Carfilzomib for the Prevention of Relapse and Graft-Versus-Host Disease in Allogeneic Hematopoietic Cell Transplantation for High-Risk Hematologic Malignancies*. 2015, American Society of Hematology Washington, DC.

77. Nishiyama, N. and K. Kataoka, *Current state, achievements, and future prospects of polymeric micelles as nanocarriers for drug and gene delivery.* Pharmacology & therapeutics, 2006. **112**(3): p. 630-648.

78. Abdelwahed, W., et al., *Freeze-drying of nanoparticles: formulation, process and storage considerations.* Advanced drug delivery reviews, 2006. **58**(15): p. 1688-1713.

79. Chaubal, M.V. and C. Popescu, *Conversion of nanosuspensions into dry powders by spray drying: a case study.* Pharmaceutical research, 2008. **25**(10): p. 2302-2308.

80. Wang, L., et al., *Cryoprotectant choice and analyses of freeze-drying drug suspension of nanoparticles with functional stabilisers.* Journal of microencapsulation, 2018. **35**(3): p. 241-248.

81. Alihosseini, F., et al., *Freeze-drying of ampicillin solid lipid nanoparticles using mannitol as cryoprotectant.* Brazilian journal of pharmaceutical sciences, 2015. **51**(4): p. 797-802.

82. Fonte, P., et al., *Stability study perspective of the effect of freeze-drying using cryoprotectants on the structure of insulin loaded into PLGA nanoparticles.* Biomacromolecules, 2014. **15**(10): p. 3753-3765.

83. Sonner, C., Y.F. Maa, and G. Lee, *Spray-freeze-drying for protein powder preparation: Particle characterization and a case study with trypsinogen stability.* Journal of pharmaceutical sciences, 2002. **91**(10): p. 2122-2139.

84. Lee, M.K., et al., *Cryoprotectants for freeze drying of drug nano-suspensions: effect of freezing rate.* Journal of pharmaceutical sciences, 2009. **98**(12): p. 4808-4817.

85. Abdelwahed, W., G. Degobert, and H. Fessi, *Investigation of nanocapsules stabilization by amorphous excipients during freeze-drying and storage.* European journal of pharmaceutics and biopharmaceutics, 2006. **63**(2): p. 87-94.

86. Hirsjärvi, S., et al., *Freeze-drying of low molecular weight poly (L-lactic acid) nanoparticles: effect of cryo-and lyoprotectants.* Journal of nanoscience and nanotechnology, 2006. **6**(9-10): p. 3110-3117.

87. De Jaeghere, F., et al., *Formulation and lyoprotection of poly (lactic acid-co-ethylene oxide) nanoparticles: influence on physical stability and in vitro cell uptake.* Pharmaceutical research, 1999. **16**(6): p. 859-866.

88. Fàbregas, A., et al., *Impact of physical parameters on particle size and reaction yield when using the ionic gelation method to obtain cationic polymeric chitosan–*

tripolyphosphate nanoparticles. International journal of pharmaceutics, 2013. **446**(1-2): p. 199-204.

89. Barenholz, Y.C., *Doxil®—the first FDA-approved nano-drug: lessons learned.* Journal of controlled release, 2012. **160**(2): p. 117-134.

90. Rychahou, P., et al., *Colorectal cancer lung metastasis treatment with polymer–drug nanoparticles.* Journal of controlled release, 2018. **275**: p. 85-91.

91. Fang, J., H. Nakamura, and H. Maeda, *The EPR effect: unique features of tumor blood vessels for drug delivery, factors involved, and limitations and augmentation of the effect.* Advanced drug delivery reviews, 2011. **63**(3): p. 136-151.

92. Danhier, F., *To exploit the tumor microenvironment: Since the EPR effect fails in the clinic, what is the future of nanomedicine?* Journal of Controlled Release, 2016. **244**: p. 108-121.

93. Song, W., et al., *Magnetic nanobubbles with potential for targeted drug delivery and trimodal imaging in breast cancer: an in vitro study.* Nanomedicine, 2017. **12**(9): p. 991-1009.

94. Lamprecht, A., et al., *Biodegradable nanoparticles for targeted drug delivery in treatment of inflammatory bowel disease.* Journal of Pharmacology and Experimental Therapeutics, 2001. **299**(2): p. 775-781.

95. Mou, X., et al., *Applications of magnetic nanoparticles in targeted drug delivery system.* Journal of nanoscience and nanotechnology, 2015. **15**(1): p. 54-62.

96. Went, P., et al., *Frequent high-level expression of the immunotherapeutic target Ep-CAM in colon, stomach, prostate and lung cancers.* British journal of cancer, 2006. **94**(1): p. 128-135.

97. Jackson, S., et al., *Effects of Organic Acids on Drug Release From Ternary Polypeptide Nanoparticles Entrapping Carfilzomib.* Journal of Pharmaceutical Sciences, 2022. **111**(4): p. 1172-1177.

98. Fenyvesi, E., et al., *Interaction of hydroxy acids with β-cyclodextrin.* Journal of inclusion phenomena and macrocyclic chemistry, 1999. **33**(3): p. 339-344.

99. Lewis, E., et al., *Cyclodextrin complexation methods for formulating peptide proteasome inhibitors*. 2018, Google Patents.

100. Jakubowiak, A.J., et al., *A phase 1/2 study of carfilzomib in combination with lenalidomide and low-dose dexamethasone as a frontline treatment for multiple myeloma.* Blood, The Journal of the American Society of Hematology, 2012. **120**(9): p. 1801-1809.

101. Vij, R., et al., *An open-label, single-arm, phase 2 (PX-171-004) study of single-agent carfilzomib in bortezomib-naive patients with relapsed and/or refractory multiple myeloma.* Blood, The Journal of the American Society of Hematology, 2012. **119**(24): p. 5661-5670.

102. Garcia-Fernandez, M.J., et al., *New multifunctional pharmaceutical excipient in tablet formulation based on citric acid-cyclodextrin polymer.* International journal of pharmaceutics, 2016. **511**(2): p. 913-920.

103. Metz, J.K., et al., *Safety assessment of excipients (SAFE) for orally inhaled drug products.* 2020.

104. Rayaprolu, B.M., J.J. Strawser, and G. Anyarambhatla, *Excipients in parenteral formulations: selection considerations and effective utilization with small*

molecules and biologics. Drug development and industrial pharmacy, 2018. **44**(10): p. 1565-1571.

105. Pifferi, G. and P. Restani, *The safety of pharmaceutical excipients.* Il Farmaco, 2003. **58**(8): p. 541-550.

106. Alihosseini, F., et al., *Freeze-drying of ampicillin solid lipid nanoparticles using mannitol as cryoprotectant.* Brazilian journal of pharmaceutical sciences, 2015. **51**: p. 797-802.

107. Lim, J., et al., *Characterization of magnetic nanoparticle by dynamic light scattering.* Nanoscale research letters, 2013. **8**(1): p. 1-14.

108. Ponta, A., et al., *Release, partitioning, and conjugation stability of doxorubicin in polymer micelles determined by mechanistic modeling.* Pharmaceutical research, 2015. **32**(5): p. 1752-1763.

109. Parveen, S., R. Misra, and S.K. Sahoo, *Nanoparticles: a boon to drug delivery, therapeutics, diagnostics and imaging.* Nanomedicine: Nanotechnology, Biology and Medicine, 2012. **8**(2): p. 147-166.

110. Singh, R. and J.W. Lillard Jr, *Nanoparticle-based targeted drug delivery.* Experimental and molecular pathology, 2009. **86**(3): p. 215-223.

111. Mody, N., et al., *Dendrimer, liposomes, carbon nanotubes and PLGA nanoparticles: one platform assessment of drug delivery potential.* Aaps Pharmscitech, 2014. **15**(2): p. 388-399.

112. Parsian, M., et al., *Loading of Gemcitabine on chitosan magnetic nanoparticles increases the anti-cancer efficacy of the drug.* European journal of pharmacology, 2016. **784**: p. 121-128.

113. Feng, C., et al., *Preparation and optimization of poly (lactic acid) nanoparticles loaded with fisetin to improve anti-cancer therapy.* International journal of biological macromolecules, 2019. **125**: p. 700-710.

114. Sahana, D., et al., *PLGA nanoparticles for oral delivery of hydrophobic drugs: influence of organic solvent on nanoparticle formation and release behavior in vitro and in vivo using estradiol as a model drug.* Journal of pharmaceutical sciences, 2008. **97**(4): p. 1530-1542.

115. Yang, T., et al., *Preparation of andrographolide-loaded solid lipid nanoparticles and their in vitro and in vivo evaluations: characteristics, release, absorption, transports, pharmacokinetics, and antihyperlipidemic activity.* Journal of pharmaceutical sciences, 2013. **102**(12): p. 4414-4425.

116. Mattu, C., et al., *Alternating block copolymer-based nanoparticles as tools to modulate the loading of multiple chemotherapeutics and imaging probes.* Acta biomaterialia, 2018. **80**: p. 341-351.

117. Yallapu, M.M., et al., *Fabrication of curcumin encapsulated PLGA nanoparticles for improved therapeutic effects in metastatic cancer cells.* Journal of colloid and interface science, 2010. **351**(1): p. 19-29.

118. Van Vlerken, L.E. and M.M. Amiji, *Multi-functional polymeric nanoparticles for tumour-targeted drug delivery.* Expert opinion on drug delivery, 2006. **3**(2): p. 205-216.

119. Yadav, K.S., et al., *Effect of size on the biodistribution and blood clearance of etoposide-loaded PLGA nanoparticles.* PDA J Pharm Sci Technol, 2011. **65**(2): p. 131-139.

120. Zhao, J., et al., *Zwitterionic stealth peptide-protected gold nanoparticles enable long circulation without the accelerated blood clearance phenomenon.* Biomaterials science, 2018. **6**(1): p. 200-206.

121. Hoshyar, N., et al., *The effect of nanoparticle size on in vivo pharmacokinetics and cellular interaction.* Nanomedicine, 2016. **11**(6): p. 673-692.

122. Park, J.E., et al., *Polymer micelle formulation for the proteasome inhibitor drug carfilzomib: Anticancer efficacy and pharmacokinetic studies in mice.* PloS one, 2017. **12**(3): p. e0173247.

123. Lee, M.J., et al., *Development of novel epoxyketone-based proteasome inhibitors as a strategy to overcome cancer resistance to carfilzomib and bortezomib.* Journal of medicinal chemistry, 2019. **62**(9): p. 4444-4455.

124. Ao, L., et al., *Nanoformulations of Carfilzomib for Improved Metabolic Stability and Anti-Cancer Efficacy.* The FASEB Journal, 2015. **29**: p. 620.1.

125. De Sousa, M.E., et al., *Stability and relaxation mechanisms of citric acid coated magnetite nanoparticles for magnetic hyperthermia.* The Journal of Physical Chemistry C, 2013. **117**(10): p. 5436-5445.

126. Shinohara, S., et al., *The Role of citric acid in the stabilization of nanoparticles and colloidal particles in the environment: measurement of surface forces between hafnium oxide surfaces in the presence of citric acid.* Langmuir, 2018. **34**(8): p. 2595-2605.

127. Dheyab, M.A., et al., *Simple rapid stabilization method through citric acid modification for magnetite nanoparticles.* Scientific reports, 2020. **10**(1): p. 1-8.

128. Miskeen, S., et al., *Fabrication of citric acid-modified starch nanoparticles to improve their thermal stability and hydrophobicity.* Carbohydrate Polymers, 2021. **253**: p. 117242.

129. Casalini, T., et al., *A perspective on polylactic acid-based polymers use for nanoparticles synthesis and applications.* Frontiers in bioengineering and biotechnology, 2019. **7**: p. 259.

130. Aggarwal, P., et al., *Nanoparticle interaction with plasma proteins as it relates to particle biodistribution, biocompatibility and therapeutic efficacy.* Advanced drug delivery reviews, 2009. **61**(6): p. 428-437.

131. He, C., et al., *Effects of particle size and surface charge on cellular uptake and biodistribution of polymeric nanoparticles.* Biomaterials, 2010. **31**(13): p. 3657-3666.

132. Zhang, Y.-N., et al., *Nanoparticle–liver interactions: cellular uptake and hepatobiliary elimination.* Journal of controlled release, 2016. **240**: p. 332-348.

133. Walkey, C.D., et al., *Nanoparticle size and surface chemistry determine serum protein adsorption and macrophage uptake.* Journal of the American Chemical Society, 2012. **134**(4): p. 2139-2147.

134. Niidome, T., et al., *PEG-modified gold nanorods with a stealth character for in vivo applications.* Journal of Controlled Release, 2006. **114**(3): p. 343-347.

135. Huang, X. and C.S. Brazel, *On the importance and mechanisms of burst release in matrix-controlled drug delivery systems.* Journal of controlled release, 2001. **73**(2-3): p. 121-136.

136. Alshehri, S., et al., *Formulation of piperine ternary inclusion complex using β CD and HPMC: physicochemical characterization, molecular docking, and antimicrobial testing.* Processes, 2020. **8**(11): p. 1450.

137. Patel, A.R. and P.R. Vavia, *Preparation and evaluation of taste masked famotidine formulation using drug/β-cyclodextrin/polymer ternary complexation approach.* Aaps Pharmscitech, 2008. **9**(2): p. 544-550.

138. Mane, P.T., B.S. Wakure, and P.S. Wakte, *Ternary inclusion complex of docetaxel using β-cyclodextrin and hydrophilic polymer: Physicochemical characterization and in-vitro anticancer activity.* Journal of Applied Pharmaceutical Science, 2022. **12**(12): p. 150-161.

139. Lateh, L., et al., *Enhancing the water-solubility of curcuminoids-rich extract using a ternary inclusion complex system: Preparation, characterization, and anti-cancer activity.* Food Chemistry, 2022. **368**: p. 130827.

140. Pandya, P., et al., *Formulation and characterization of ternary complex of poorly soluble duloxetine hydrochloride.* Journal of Applied Pharmaceutical Science, 2015. **5**(6): p. 088-096.

141. Messner, M., et al., *Self-assembled cyclodextrin aggregates and nanoparticles.* International journal of pharmaceutics, 2010. **387**(1-2): p. 199-208.

142. Savolainen, J., et al. *Coadministration of a water-soluble polymer increases the usefulness of cyclodextrins in solid oral dosage forms*. in *Proceedings of the Ninth International Symposium on Cyclodextrins*. 1999. Springer.

143. Such, G.K., et al., *Interfacing materials science and biology for drug carrier design.* Advanced Materials, 2015. **27**(14): p. 2278-2297.

144. Deirram, N., et al., *pH-responsive polymer nanoparticles for drug delivery.* Macromolecular rapid communications, 2019. **40**(10): p. 1800917.

145. Yan, Y. and H. Ding, *pH-responsive nanoparticles for cancer immunotherapy: a brief review.* Nanomaterials, 2020. **10**(8): p. 1613.

146. Monopoli, M.P., et al., *Biomolecular coronas provide the biological identity of nanosized materials.* Nature nanotechnology, 2012. **7**(12): p. 779-786.

147. Dumur, F., et al., *Controlled spontaneous generation of gold nanoparticles assisted by dual reducing and capping agents.* Gold bulletin, 2011. **44**(2): p. 119-137.

148. Bogdanov Jr, A., et al., *A new macromolecule as a contrast agent for MR angiography: preparation, properties, and animal studies.* Radiology, 1993. **187**(3): p. 701-706.

149. Benns, J.M., et al., *pH-sensitive cationic polymer gene delivery vehicle: N-Ac-poly (L-histidine)-graft-poly (L-lysine) comb shaped polymer.* Bioconjugate chemistry, 2000. **11**(5): p. 637-645.

150. Lee, E.S., et al., *Poly (l-histidine)–PEG block copolymer micelles and pH-induced destabilization.* Journal of Controlled Release, 2003. **90**(3): p. 363-374.

151. Kim, G.M., Y.H. Bae, and W.H. Jo, *pH-induced Micelle Formation of Poly (histidine-co-phenylalanine)-block-Poly (ethylene glycol) in Aqueous Media.* Macromolecular bioscience, 2005. **5**(11): p. 1118-1124.

152. Lee, E.S., K. Na, and Y.H. Bae, *Doxorubicin loaded pH-sensitive polymeric micelles for reversal of resistant MCF-7 tumor.* Journal of controlled release, 2005. **103**(2): p. 405-418.

153. Liu, L., et al., *The assembly of polyethyleneimine-entrapped gold nanoparticles onto filter paper for catalytic applications.* RSC advances, 2015. **5**(126): p. 104239-104244.

154. Aymonier, C., et al., *Hybrids of silver nanoparticles with amphiphilic hyperbranched macromolecules exhibiting antimicrobial properties.* Chemical Communications, 2002(24): p. 3018-3019.

155. Cai, H., et al., *Facile hydrothermal synthesis and surface functionalization of polyethyleneimine-coated iron oxide nanoparticles for biomedical applications.* ACS applied materials & interfaces, 2013. **5**(5): p. 1722-1731.

156. Kong, L., et al., *Polyethyleneimine-stabilized hydroxyapatite nanoparticles modified with hyaluronic acid for targeted drug delivery.* RSC advances, 2016. **6**(104): p. 101790-101799.

157. Hao, Y., et al., *The evaluation of cellular uptake efficiency and tumor-targeting ability of MPEG–PDLLA micelles: effect of particle size.* RSC advances, 2016. **6**(17): p. 13698-13709.

158. Jeitany, M., et al., *Novel carfilzomib-based combinations as potential therapeutic strategies for liposarcomas.* Cellular and Molecular Life Sciences, 2021. **78**(4): p. 1837-1851.

159. Longhitano, L., et al., *Proteasome inhibitors as a possible therapy for SARS-CoV-2.* International Journal of Molecular Sciences, 2020. **21**(10): p. 3622.

160. Jiang, C., et al., *Sorafenib and Carfilzomib Synergistically Inhibit the Proliferation, Survival, and Metastasis of Hepatocellular CarcinomaCombination of Sorafenib*

and Carfilzomib against HCC. Molecular cancer therapeutics, 2018. **17**(12): p. 2610-2621.

161. Gao, M., et al., *Therapeutic potential and functional interaction of carfilzomib and vorinostat in T-cell leukemia/lymphoma.* Oncotarget, 2016. **7**(20): p. 29102.

162. Varela-Moreira, A., et al., *Polymeric micelles loaded with carfilzomib increase tolerability in a humanized bone marrow-like scaffold mouse model.* International Journal of Pharmaceutics: X, 2020. **2**: p. 100049.

163. Liu, Y., et al., *Stable polymer nanoparticles with exceptionally high drug loading by sequential nanoprecipitation.* Angewandte Chemie, 2020. **132**(12): p. 4750-4758.

164. Tyagi, P. and J.A. Subramony, *Nanotherapeutics in oral and parenteral drug delivery: Key learnings and future outlooks as we think small.* Journal of Controlled Release, 2018. **272**: p. 159-168.

165. Kalyane, D., et al., *Employment of enhanced permeability and retention effect (EPR): Nanoparticle-based precision tools for targeting of therapeutic and diagnostic agent in cancer.* Materials Science and Engineering: C, 2019. **98**: p. 1252-1276.

166. Tahmasbi Rad, A., et al., *Combinational effects of active targeting, shape, and enhanced permeability and retention for cancer theranostic nanocarriers.* ACS applied materials & interfaces, 2019. **11**(11): p. 10505-10519.

167. Shi, Y., et al., *The EPR effect and beyond: Strategies to improve tumor targeting and cancer nanomedicine treatment efficacy.* Theranostics, 2020. **10**(17): p. 7921.

168. Di, J., et al., *Size, shape, charge and "stealthy" surface: Carrier properties affect the drug circulation time in vivo.* Asian journal of pharmaceutical sciences, 2021. **16**(4): p. 444-458.

169. Seynhaeve, A., et al., *Hyperthermia and smart drug delivery systems for solid tumor therapy.* Advanced Drug Delivery Reviews, 2020. **163**: p. 125-144.

170. Xu, F., et al., *A size-changeable collagenase-modified nanoscavenger for increasing penetration and retention of nanomedicine in deep tumor tissue.* Advanced Materials, 2020. **32**(16): p. 1906745.

171. Arisoy, S., et al., *In vitro and in vivo evaluation of levodopa-loaded nanoparticles for nose to brain delivery.* Pharmaceutical Development and Technology, 2020. **25**(6): p. 735-747.

172. Thews, O. and A. Riemann, *Tumor pH and metastasis: a malignant process beyond hypoxia.* Cancer and Metastasis Reviews, 2019. **38**(1): p. 113-129.

173. Cardone, R.A., V. Casavola, and S.J. Reshkin, *The role of disturbed pH dynamics and the Na+/H+ exchanger in metastasis.* Nature reviews cancer, 2005. **5**(10): p. 786-795.

174. Wu, H., L. Zhu, and V.P. Torchilin, *pH-sensitive poly (histidine)-PEG/DSPE-PEG co-polymer micelles for cytosolic drug delivery.* Biomaterials, 2013. **34**(4): p. 1213-1222.

175. Lee, M.J., et al., *H727 cells are inherently resistant to the proteasome inhibitor carfilzomib, yet require proteasome activity for cell survival and growth.* Scientific reports, 2019. **9**(1): p. 1-9.

176. Besse, A., et al., *Carfilzomib resistance due to ABCB1/MDR1 overexpression is overcome by nelfinavir and lopinavir in multiple myeloma.* Leukemia, 2018. **32**(2): p. 391-401.

177. Myung, J., K.B. Kim, and C.M. Crews, *The ubiquitin-proteasome pathway and proteasome inhibitors.* Medicinal research reviews, 2001. **21**(4): p. 245-273.

178. Mani, A. and E.P. Gelmann, *The ubiquitin-proteasome pathway and its role in cancer.* Journal of clinical oncology, 2005. **23**(21): p. 4776-4789.

179. Richmond, A. and Y. Su, *Mouse xenograft models vs GEM models for human cancer therapeutics*. 2008, The Company of Biologists Limited. p. 78-82.

180. Zhang, W., et al., *Comparative study of subcutaneous and orthotopic mouse models of prostate cancer: vascular perfusion, vasculature density, hypoxic burden and BB2r-Targeting Efficacy.* Scientific reports, 2019. **9**(1): p. 1-10.

181. Nichols, J.W. and Y.H. Bae, *Odyssey of a cancer nanoparticle: from injection site to site of action.* Nano today, 2012. **7**(6): p. 606-618.

182. Liu, Y., Y.-c. Tseng, and L. Huang, *Biodistribution studies of nanoparticles using fluorescence imaging: a qualitative or quantitative method?* Pharmaceutical research, 2012. **29**(12): p. 3273-3277.

183. Frangioni, J.V., *In vivo near-infrared fluorescence imaging.* Current opinion in chemical biology, 2003. **7**(5): p. 626-634.

184. Hilderbrand, S.A. and R. Weissleder, *Near-infrared fluorescence: application to in vivo molecular imaging.* Current opinion in chemical biology, 2010. **14**(1): p. 71-79.

185. Wilhelm, S., et al., *Analysis of nanoparticle delivery to tumours.* Nature reviews materials, 2016. **1**(5): p. 1-12.

VITA

Preye Agbana

EDUCATION

A.S in engineering studies August 2013 – May 2015

Brescia University, Owensboro, KY

B.S. in Chemistry August 2013 – May 2017

Brescia University, Owensboro, KY

Graduate Student in Pharmaceutical Sciences August 2018 – Present

University of Kentucky, Lexington, KY

Advisor: Dr. Younsoo Bae

PROFESSIONAL EXPERIENCE

Graduate Research Assistant August 2018 - Present

University of Kentucky, Lexington, KY

Graduate Teaching Assistant August 2018 – May 2019

University of Kentucky, Lexington, KY

R&D Pilot Lab Technician May 2017 – May 2018

Daramic, LLC, Owensboro, KY

Internship Fellow May 2016 – August 2016

Lab Assistant August 2014 – May 2016

Brescia University, Owensboro, KY

PEER REVIEWED PUBLICATIONS

- **Agbana, Preye**, Min Jae Lee, Piotr Rychahou, Kyung-Bo Kim, and Younsoo Bae. "Ternary Polypeptide Nanoparticles with Improved Encapsulation, Sustained Release, and Enhanced In Vitro Efficacy of Carfilzomib." Pharmaceutical Research 37, no. 11 (2020): 1-12.

- Jackson, Sharonda, **Preye Agbana**, Kyung-Bo Kim, and Younsoo Bae. "Effects of Organic Acids on Drug Release from Ternary Polypeptide Nanoparticles Entrapping Carfilzomib." Journal of Pharmaceutical Sciences 111, no. 4 (2022): 1172-1177

- Kenneally, Allison M., **Preye Agbana**, Brian Gardner, Younsoo Bae, Trenika Mitchell, and Elizabeth J. Beckman. "Compatibility of calcium chloride with milrinone, epinephrine, vasopressin, and heparin via in vitro testing and simulated Y-site administration." American Journal of Health-System Pharmacy (2022).

PUBLICATIONS IN PREPARATION

- **Agbana, Preye**, Ji Eun Park, Kaysi Lee, Kyung-Bo Kim, and Younsoo Bae. "Carfilzomib-loaded Ternary Polypeptide Nanoparticles Stabilized by Polycationic Complexation." (In writing)

- **Agbana, Preye**, Piotr Rychahou, and Younsoo Bae. "Anti-SSTR2 octreotide-polypeptide nanoparticles for neuroendocrine tumor liver metastasis therapy." (In writing)

PRESENTATIONS

- Ternary polypeptide nanoparticles with improved encapsulation, sustained release and enhanced in vitro efficacy of carfilzomib (Poster). Presented at 2022 Globalization for Pharmaceutics Education Network (GPEN) conference, Minneapolis, Minnesota

- Ternary polypeptide nanoparticles with improved encapsulation, sustained release and enhanced in vitro efficacy of carfilzomib (Poster). Presented at 2022 Center for Clinical and Translational Science Spring Conference, University of Kentucky

- Ternary polypeptide nanoparticles with improved encapsulation, sustained release and enhanced in vitro efficacy of carfilzomib (Poster). Presented at 2021 Merck Emerging Talent Symposium

- Ternary polypeptide nanoparticles with improved encapsulation, sustained release and enhanced in vitro efficacy of carfilzomib (Poster). Presented at 2021 AAPS PharmSci 360 conference, Philadelphia, Pennsylvania

- Ternary polypeptide nanoparticles with improved encapsulation, sustained release and enhanced in vitro efficacy of carfilzomib (Oral). Presented at 2021 Pharmaceutical sciences departmental seminar

- Ternary polypeptide nanoparticles with improved encapsulation, sustained release and enhanced in vitro efficacy of carfilzomib (Oral). Presented at 2021 annual ISPE research pane

- Ternary polypeptide nanoparticles with improved encapsulation, sustained release and enhanced in vitro efficacy of carfilzomib (Poster). Presented at 2021 annual Rho Chi research day

- Effect of stabilizers on drug loading and particle size of alginic acid hydrogels (Oral)

- Development of core-stabilized alginic acid hydrogels for enhanced entrapment and sustained release of proteasome inhibitor drug carfilzomib (Oral)

- Development of polypeptide nanoparticles (PNPs) for targeted delivery of phosphoinositide-3-kinase (PI3K) inhibitor SN-38 (Oral)

- Design of ternary polypeptide nanoparticles with improved encapsulation, sustained release and enhanced in vitro efficacy of carfilzomib (Oral)

- 2020 Participant in the NIH virtual student fair

- 2019 Participant in the Therapeutics, Outcome, Discovery, and Delivery (TODD) annual drug use disorder symposium elevator speech competition

AWARDS

University of Kentucky

- Pharmaceutical Sciences Excellence in Graduate Achievement Fellowship 2021 – 2022
- Pharmaceutical Sciences Graduate Student Program Travel Award 2021 – 2022
- First place, Annual Rho Chi Research Day Poster Presentation 2021
- Joseph V. Swintosky PhD Travel Scholarship Award 2021
- Lyman T. Johnson Diversity Fellowship 2018 - 2020

Brescia University

- "Spirit of Angela Merici" Award (representing the image of the Brescia institution) 2017
- High Scholastic Achievement in Science 2017
- St. Sebastian Scholar Athlete (Athlete with the highest GPA) 2015 – 2017
- Leadership Award – Captain of the Men's Soccer Program 2016 – 2017
- American Chemical Society (ACS) Outstanding Achievement in Chemistry 2016
- First place, Kentucky Academy of Science (KAS) Biochemistry Poster Presentation 2016
- Joint Award in Physics and Engineering 2015
- NAIA Scholar Athlete 2015 – 2016
- NAIA Champion of Character 2016

PROFESSIONAL INVOLVEMENT

- Vice President, International Society of Pharmaceutical Engineers (ISPE) 2020 – 2022

- Member, American Association of Pharmaceutical Scientists (AAPS) 2020 – Present

- Member, Alpha Chi Honors Society 2014 – 2017

- Vice President, Brescia University Black Students Union 2015 – 2016

- Secretary and Student Representative, Brescia University International Club 2014 – 2015

- Athlete, National Association of Intercollegiate Athletics (NAIA) 2013 - 2017